NAVAL POSTGRADUATE SCHOOL
Monterey , California

DTIC
ELECTE
S JUL 13 1992 D

THESIS

ON-LINE IDENTIFICATION OF THE SPEED,
STEERING AND DIVING RESPONSE PARAMETERS
OF AN AUTONOMOUS UNDERWATER VEHICLE
FROM EXPERIMENTAL DATA

by

Fredric G. Bahrke

March, 1992

Thesis Advisor: Anthony J. Healey

Approved for public release; distribution is unlimited.

92-18185

92

REPORT DOCUMENTATION PAGE	Form Approved OMB No 0704-0188

1a REPORT SECURITY CLASSIFICATION UNCLASSIIED	1b RESTRICTIVE MARKINGS
2a SECURITY CLASSIFICATION AUTHORITY	3 DISTRIBUTION/AVAILABILITY OF REPORT
2b DECLASSIFICATION/DOWNGRADING SCHEDULE	Approved for public release; distribution is unlimited

4 PERFORMING ORGANIZATION REPORT NUMBER(S)	5 MONITORING ORGANIZATION REPORT NUMBER(S)

6a NAME OF PERFORMING ORGANIZATION Naval Postgraduate School	6b OFFICE SYMBOL (If applicable) Code ME	7a NAME OF MONITORING ORGANIZATION Naval Postgraduate School
6c ADDRESS (City, State, and ZIP Code) Monterey, California 93943-5000		7b ADDRESS (City, State, and ZIP Code) Monterey, California 93943-5000

8a NAME OF FUNDING/SPONSORING ORGANIZATION	8b OFFICE SYMBOL (If applicable)	9 PROCUREMENT INSTRUMENT IDENTIFICATION NUMBER
8c ADDRESS (City, State, and ZIP Code)		10 SOURCE OF FUNDING NUMBERS

PROGRAM ELEMENT NO	PROJECT NO	TASK NO	WORK UNIT ACCESSION NO

11 TITLE (Include Security Classification) ON-LINE IDENTIFICATION OF THE SPEED, STEERING AND DIVING RESPONSE PARAMETERS OF AN AUTONOMOUS UNDERWATER VEHICLE FROM EXPERIMENTAL DATA

12 PERSONAL AUTHOR(S) Bahrke, Fredric G.

13a TYPE OF REPORT Master's Thesis	13b TIME COVERED FROM _____ TO _____	14 DATE OF REPORT (Year, Month, Day) 1992 March	15 PAGE COUNT 180

16 SUPPLEMENTARY NOTATION The views expressed are those of the author and do not reflect the official policy or position of the Department of Defense or the U.S. Government

17 COSATI CODES			18 SUBJECT TERMS (Continue on reverse if necessary and identify by block number)
FIELD	GROUP	SUB-GROUP	System Identification; Sliding Mode Control; Autopilot/Guidance of Autonomous Underwater Vehicles

19 ABSTRACT (Continue on reverse if necessary and identify by block number)

The experimental response data from autonomous maneuvering using the NPS AUV II vehicle has been analyzed with a view to defining Kalman filters to provide on-line estimates of system parameters and their variability. Kalman filters, designed for parameter estimation are expected to be the first step in the development of autonomous fault detection systems for underwater vehicles. Secondly, extraction of vehicle hydrodynamic coefficients from these parameters can help to develop vehicle dynamic simulators. Thirdly, knowledge of these parameters will allow the design of improved autopilot and guidance laws.

20 DISTRIBUTION/AVAILABILITY OF ABSTRACT ☒ UNCLASSIFIED/UNLIMITED ☐ SAME AS RPT ☐ DTIC USERS	21 ABSTRACT SECURITY CLASSIFICATION Unclassified
22a NAME OF RESPONSIBLE INDIVIDUAL Prof. A.J. Healey	22b TELEPHONE (Include Area Code) (408) 646-2586 22c OFFICE SYMBOL Code ME/HY

DD Form 1473, JUN 86   Previous editions are obsolete   SECURITY CLASSIFICATION OF THIS PAGE

S/N 0102-LF-014-6603   UNCLASSIFIED

On-Line Identification of the Speed,Steering and
Diving Response Parameters of an Autonomous
Underwater Vehicle from Experimental Data

by

Fredric G. Bahrke
Lieutenant, United States Navy
B.S., University of Wisconsin, 1983

Submitted in partial fulfillment
of the requirements for the degree of

MASTER OF SCIENCE IN MECHANICAL ENGINEERING
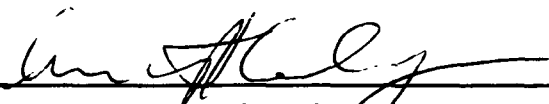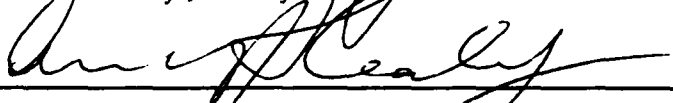and MECHANICAL ENGINEER

from the

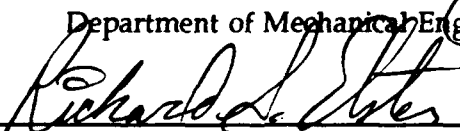NAVAL POSTGRADUATE SCHOOL
MARCH 1992

Author: _____
Fredric G. Bahrke

Approved by: _____
Anthony J.Healey, Thesis Advisor

_____
Anthony J. Healey, Chairman
Department of Mechanical Engineering

_____
Richard S. Elster,
Dean of Instruction

ii

ABSTRACT

The experimental response data from autonomous maneuvering using the NPS AUV II vehicle has been analyzed with a view to defining Kalman filters to provide on-line estimates of system parameters and their variability. Kalman filters, designed for parameter estimation are expected to be the first step in the development of autonomous fault detection systems for underwater vehicles. Secondly, extraction of vehicle hydrodynamic coefficients from these parameters can help to develop vehicle dynamic simulators. Thirdly, knowledge of these parameters will allow the design of improved autopilot and guidance laws.

Accession For	
NTIS GRA&I	☑
DTIC TAB	☐
Unannounced	☐
Justification	
By	
Distribution/	
Availability Codes	
Dist	Avail and/or Special
A-1	

iii

TABLE OF CONTENTS

LIST OF TABLES

LIST OF FIGURES

PRIMARY NOMENCLATURE

Variable	Description
X,Y,Z	Global Position of vehicle
x,y,z	Distance along the vehicle principal axes
u,v,w	Velocity components of body axis system relative to fluid along body axes
p,q,r	Angular velocity components of body relative to inertial reference system along body axes
$X_{(.)}, Y_{(.)}, Z_{(.)}$	Hydrodynamic force components along body axes with respect to (.) motion component
$K_{(.)}, M_{(.)}, N_{(.)}$	Hydrodynamic moment components along body axes with respect to (.) motion component
Ψ, θ, ϕ	Yaw, pitch, and roll angles (Euler angles)
m	Mass of the AUV II (including the fluid in the floodable sonar dome)
W	Weight of the AUV II (=gm)
∇	Displacement volume of the AUV II
B	Buoyancy force acting on the AUV II (=gρ∇)
x_G, y_G, z_G	Coordinates of the Center of Gravity in the body axis system. These depend on the mass distribution of the vehicle
x_B, y_B, z_B	Coordinates of the Center of Buoyancy in the body axis system. These are independent of the mass distribution of the vehicle
I_x, I_y, I_z	Moments of inertia about the body system axes
ρ	Mass density water
l	Reference length used to nondimensionalize the hydrodynamic coefficients
δ_b, δ_s	Bow and Stern plane deflection angles in radians
δ_{rb}, δ_{rs}	Bow and Stern rudder deflection angles in radians

ACKNOWLEDGEMENTS

It is with deep gratification I would like to thank Dr. Anthony Healey, Dr. Fotis Papoulias and David Marco for their energy and patience in working with me on this thesis. Without their help and inspiration, this document would not have been possible. I contribute much of my education here at the Naval Postgraduate School to Dr Healey. With his unending patience and dedication to teaching, he was able to help me understand and use exceedingly difficult concepts in this thesis. He has also given me the tools necessary to read and understand highly technical material in relation to marine vehicle dynamics.

Finally, and most importantly, I would like to thank my wife Mary, for her unending support and encouragement throughout my graduate education and thesis research.

I. INTRODUCTION

A. GENERAL BACKGROUND

Autonomous Underwater Vehicles (AUV's) are unmanned and fall in the special class of vehicles which are autonomous with respect to power and control. For example, torpedoes are self contained with respect to power and control (unless guided by wire or fiber optic connection to the mother ship), but remotely operated vehicles (ROV's), used for diving support, usually derive their power and control functions from a manned surface asset. Torpedoes and naval mobile targets, however, are separated from AUV's because of their special missions, higher speed range and singularity of purpose. A broad class of AUV's is receiving interest for both naval and ocean science activity that have speed ranges up to 8-12 knots, autonomous power and control, and sufficient computer intelligence on board to permit intermittent, low bandwidth (< 5K baud) communication. Missions include search, survey package recovery, mobile sensor placements, sensory data gathering, as well as, submarine and surface ship off board sensing capability. Clearly, unmanned vehicles are to be used to extend human presence into hostile and unsafe areas.

1

The full range of control capability required is enormous, spanning vehicle cruise control, hover mode capability, acoustic positioning, coordinated management of manipulators, and vehicle health status monitoring and fault tolerant control.

This thesis addresses a small part of the autonomous control problem dealing with automatic on line identification of vehicle response parameters that will be required firstly to provide information necessary to the design of advanced autopilot controllers, and secondly to provide diagnostic assessments of dynamic response changes that may indicate degraded performance or failure.

It is contended here that a Kalman filter based parameter identification scheme is useful to both vehicle autopilot control design and adaptation, understanding the relation between vehicle design principles and resulting motion performance and providing input to automatic failure diagnostic systems.

B. PREVIOUS LITERATURE

Previous literature pertinent to this problem comes from many sources. These include the areas of underwater vehicle maneuvering design principles and practice, system dynamic response parameter identification, signal processing and filtering, and the design of feedback controllers for uncertain and highly variable systems.

2

The behavior of submersible vehicles in motion control scenarios has been discussed by Abkowitz (1969), Young (1969), Gertler and Hagen (1967), Humphries (1981), Dobeck (1982), Lewis and Lipscomb (1984), and as described in Lewis ("Principles of Naval Architecture", 1989), is highly dependent on values for the hydrodynamic coefficients that are analogous to the stability derivatives in aircraft design. Motion control of ROV's, without particular hydrodynamic shape (open frame vehicles on which control and sensing packages are attached), has been described by Yoerger and Slotine (1985, 1986), where the robustness of sliding mode control design procedures have been utilized to overcome hydrodynamic coefficient variability and uncertainty. However, in spite of the potential, its implementation on ROV's has provided control that could be still improved if the thruster dynamics were precisely known (Yoerger, 1991). Fossen (1991) has described a parameter adaptive control that is essentially the same as that discussed by Slotine (1987), but how this works in practice is still not known. The work of Fossen and Slotine assume that the system motion response can be expressed in terms of a linear differential equation, linear in the values of the differential equation coefficients. Kalman filtering or the use of batch least squares minimization of errors may be used to find values for these model coefficients but these have no direct relationship to the vehicle's hydrodynamic coefficients. Abkowitz (1980) in a large experiment with a

3

tanker vehicle, indicated that the hydrodynamic coefficients important to the steering response of that vehicle could be identified using extended Kalman filtering (discussed at length in Gelb, 1988), a common technique in system state and parameter estimation. The prevailing opinion in the discussion of Abkowitz's work was that determination of hydrodynamic coefficients prior to shipbuilding is more important than determination after the event so that problem designs can be modified prior to construction. While this is true, it is still important to build a knowledge base that lends confidence to vehicle maneuvering predictive power. Additionally, a new requirement - partly solvable with Kalman filters - is to detect changes in dynamic response behavior indicating probable failures in an automatic way.

Automatic failure diagnostics, surveyed by Wilsky (1976), Isermann (1984), and Gertler (1986), have indicated that Kalman filters are essential to the detection of dynamic failures. Static failures, such as the complete loss of a signal, can be easily identified automatically via simple logical rules (Himmelblau, 1978). More recently, for dynamic failures, DeBenito (1990), discusses the use of banks of filters, each tuned to a particular output sensor, coupled with a maximum likelihood check that would indicate the most probable failure. Deitz (1989) has discussed the use of Neural Networks for rocket engine failure prediction, a technology

that will be combined with Kalman filtering to provide ease in the design of failure diagnostic systems of AUV's (Healey, 1992).

C. MOTIVATION AND ENGINEERING SIGNIFICANCE OF THIS STUDY

The motivation of this work is derived from the background statement taken in context with the current state of the art. To explore the ability of present predictive techniques for vehicle motion behavior, the NPS AUV II vehicle was constructed (Healey, Good, 1992) and has been the subject of extensive experimentation during the last year. Figure 1.1 shows the NPS AUV II. Data from certain key experiments are analyzed and pertinent parameters are identified using Kalman filtering. These results produce a set of coefficient values useful for reproducing the maneuvering response of the NPS AUV II in speed, steering and diving control that would be considered to lie within the range of normal operation.

D. SCOPE OF THIS WORK

The thrust of this thesis is threefold: 1) Earlier work was performed by Warner (1991) based on first principles to predict the response data recorded by the NPS AUV II during test trials in the Naval Postgraduate School swimming pool. The work in this thesis uses system identification techniques to verify and refine the six degrees of freedom computer model for the NPS AUV II. 2) The development of an on line real time

5
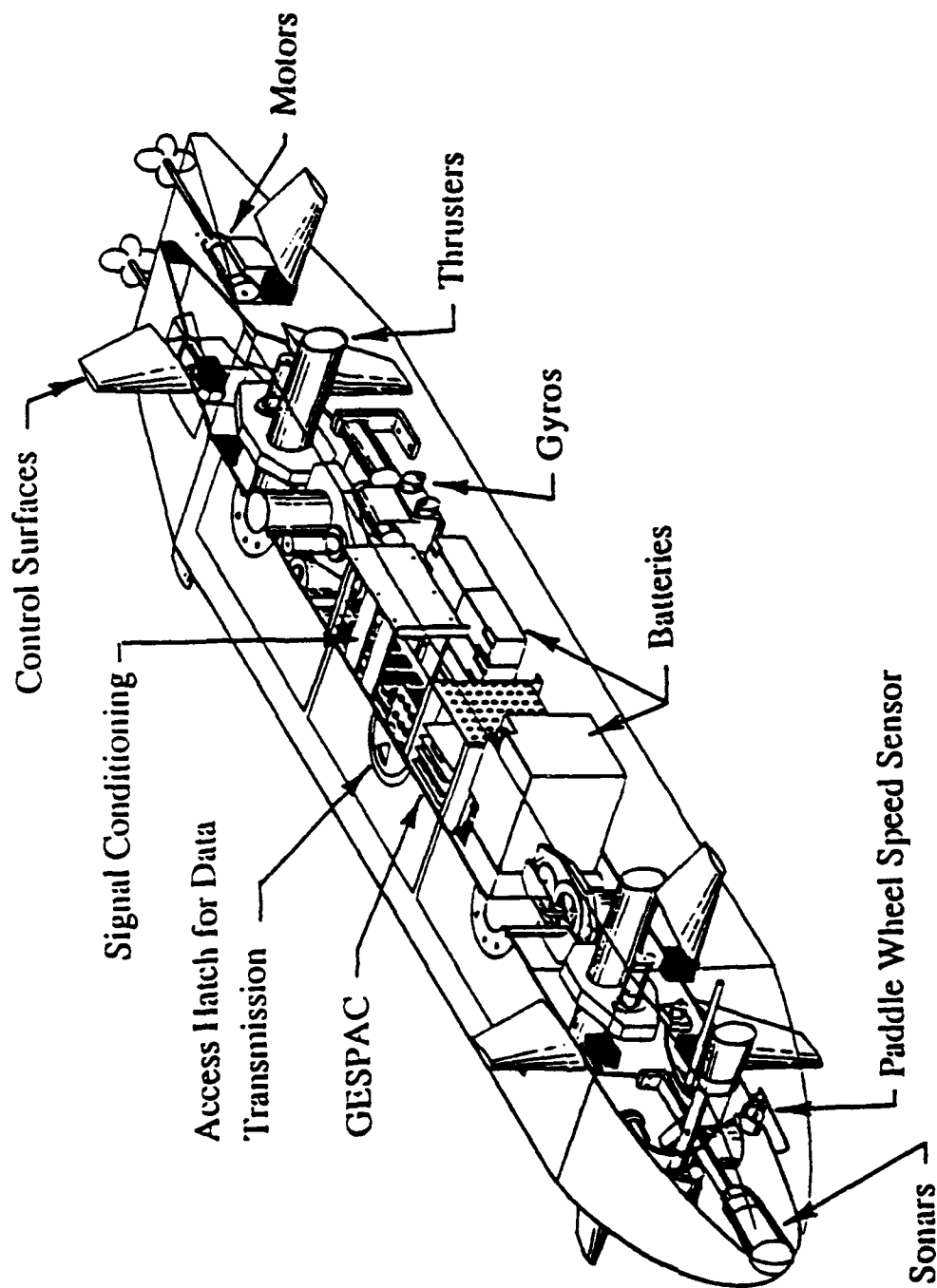
Figure 1.1 Naval Postgraduate School Autonomous Underwater Vehicle II

diagnostics tool in the form of a system parameter identifier.
3) Develop and test sliding mode speed, steering and diving controllers for the autopilot of the NPS AUV II.

Chapter II focuses on the development of the theory necessary to use a Kalman filter for both parameter identification and for optimal state estimation. In addition Sliding mode control theory is presented for the development of the control laws in the following chapters based on the system parameters identified through the Kalman filtering techniques.

Chapter III provides a thorough presentation of the automatic identification technique of the Kalman filter as a parameter estimator. The resulting estimates are then used to develop a sliding mode controller for speed. Results on the performance of the controller are then discussed.

Chapter IV provides a thorough presentation on the automatic identification technique of the Kalman filter for the steering system parameters. A sensitivity analysis is performed on the identified parameters and a final choice of representative parameters is given. The final steering system parameters are used to construct a Kalman state estimator which provides the vehicle's unmeasured sway velocity to the navigation system. Finally, the parameters are used to develop a sliding mode steering controller. The comparison of the sliding mode controller to the PD controller of similar design characteristics is made.

Chapter V uses the same techniques described above to identify the diving system parameters and to provide optimal estimates of the state variables for use by the sliding mode diving controller.

II. SYSTEM IDENTIFICATION AND SLIDING MODE CONTROL

A. INTRODUCTION

The objective of this chapter is to describe the theory and methods available for system identification and the theory of sliding mode control. For any control system to function properly the dynamics of the system being controlled must be understood and reasonably modeled mathematically. The mathematical model should be reasonably accurate, although discrepancies will always be present. The robustness of the control system is measured by the performance of the control system acting on the actual system with the ever present unmodeled effects. The sliding mode control theory is described in detail in section C of this chapter.

Prior to the application of the sliding mode control theory the system model must be constructed and the appropriate modeling coefficients identified. System identification techniques available are discussed in section B of this chapter. The method deemed most desirable uses the Kalman filter modified to be a parameter estimator. As an added benefit this parameter estimator was found to be readily adaptable to an on line fault monitor coded into the operating system of the NPS AUV II continually monitoring the value of

9

the system parameters and giving fault warnings when the bounds of the parameters are exceeded.

The six equations of motion for a submerged vehicle: (Smith, 1978) surge, sway, heave, yaw, pitch, and roll were incorporated into the computer code developed by Boncal (1987) in constructing a generic submerged vehicle analytical model. This permitted the maximum flexibility in determining the level of model sophistication. The computer program has the capability to simulate a submerged vehicle using knowledge of all hydrodynamic coefficients. In developing the AUV II model, Warner (1991) used a number of simplifying assumptions. These assumptions and known physical characteristics of the AUV II are summarized below:

1. The AUV II is neutrally buoyant: $W=B$

2. The AUV II is symmetrically loaded in the transverse direction ($y_G=0$ and $y_B=0$), and the vertical center of buoyancy is midway between the top and bottom of AUV II ($z_B=0$).

3. The counter-rotating propellers produce no yaw moment ($N_{prop}=0$).

4. The products of inertia about the body system are zero because the AUV II possesses two axes of symmetry.

5. The AUV II acceleration and deceleration rates are small enough so that propeller slip can be neglected.

6. The effect of cross-coupled hydrodynamic coefficients can be neglected in most cases, again because of the AUV II geometric symmetry.

The resulting equations of motion are presented below.

SURGE EQUATION

$$m\dot{u} + mz_G\dot{q} - X_{\dot{u}}\dot{u} =$$

$$mvr - mwq + mx_Gq^2 + mx_Gr^2 - mz_Gpr + X_{rr}r^2 + X_{vv}v^2$$

$$+ u^2(X_{\delta s\delta s}\delta_s^2 + X_{\delta b\delta b}\delta_b^2 + X_{\delta_n\delta_n}\delta_{rb}^2 + X_{\delta_n\delta_n}\delta_{rs}^2) \qquad \textbf{(2.1)}$$

$$+ X_{res}u^2 + X_{prop}n^2$$

SWAY EQUATION

$$m\dot{v} + mx_G\dot{r} - mz_G\dot{p} - Y_{\dot{r}}\dot{r} - Y_{\dot{v}}\dot{v} =$$

$$mwp - mur - mx_Gpq$$

$$- mz_Gqr + Y_rur + Y_vuv + u^2(Y_{\delta_n}\delta_{rb} + Y_{\delta_n}\delta_{rs}) \qquad \textbf{(2.2)}$$

$$- \int_{x_{tail}}^{x_{nose}} [C_{Dy}h(x)(v+xr)^2 + C_{Dz}b(x)(w-xq)^2]\frac{(v+xr)}{U_{cf}(x)}dx$$

HEAVE EQUATION

$$m\dot{w} - mx_G\dot{q} - Z_{\dot{q}}\dot{q} - Z_{\dot{w}}\dot{w} =$$

$$muq - mvp - mx_Gpr + mz_G(p^2 + q^2)$$

$$+ Z_quq + Z_wuw + u^2(Z_{\delta s}\delta_s + Z_{\delta b}\delta_b) \qquad \textbf{(2.3)}$$

$$- \int_{x_{tail}}^{x_{nose}} [C_{Dy}h(x)(v+xr)^2 + C_{Dz}b(x)(w-xq)^2]\frac{(w-xq)}{U_{cf}(x)}dx$$

ROLL EQUATION

$$I_x\dot{p} - mz_G\dot{v} - K_{\dot{p}}\dot{p} =$$

$$(I_y - I_z)qr + mz_Gur - mz_Gwp + K_pup - (z_GW - z_BB)\cos\theta\sin\phi \qquad \textbf{(2.4)}$$

11

YAW EQUATION

$$I_z \dot{r} + mx_G \dot{v} - N_{\dot{r}} \dot{r} - N_{\dot{v}} \dot{v} =$$

$$(I_x - I_y) pq - mx_G ur + mx_G wp + N_r ur + N_v uv$$

$$+ u^2 (N_{\delta_{r_n}} \delta_{rb} + N_{\delta_{r_n}} \delta_{rs}) + (x_G W - x_B B) \cos\theta \sin\phi \quad (2.5)$$

$$- \int_{x_{tail}}^{x_{nose}} [C_{Dy} h(x) (v+xr)^2 + C_{Dz} b(x) (w-xq)^2] \frac{(v+xr)}{U_{cf}(x)} x \, dx$$

PITCH EQUATION

$$I_y \dot{q} - mx_G \dot{w} + mz_G \dot{u} - M_{\dot{q}} \dot{q} - M_{\dot{w}} \dot{w} =$$

$$(I_z - I_x) pr - mx_G uq + mx_G vp + mz_G vr - mz_G wq +$$

$$+ M_q uq + M_w uw + u^2 (M_{\delta_s} \delta_s + M_{\delta_b} \delta_b) - (z_G W - z_B B) \sin\theta \quad (2.6)$$

$$- \int_{x_{tail}}^{x_{nose}} [C_{Dy} h(x) (v+xr)^2 + C_{Dz} b(x) (w-xq)^2] \frac{(w-xq)}{U_{cf}(x)} x \, dx$$

where $U_{cf}(x) = [(v+xr)^2 + (w - xq)^2]^{1/2}$

In addition to these equations, the six-degree-of-freedom computer model includes equations for the euler angle rates (ψ, ϕ, θ) and inertial position rates ($\dot{X}$, $\dot{Y}$, $\dot{Z}$). These equations are contained in Smith (1978).

Table 2.1 provides the nominal values of the dominant hydrodynamic coefficients and vehicle characteristics developed by Warner (1991). The initial focus of this thesis is to verify or refine the nominal hydrodynamic coefficients based on actual experimental data recorded during test trials of the NPS AUV II in the Naval Postgraduate School swimming pool. These refined hydrodynamic coefficients are then placed

into the generic submerged vehicle simulation code to provide an accurate analytical model of the NPS AUV II. This analytical model may then be used as a simulation testing code for actual planned missions of the NPS AUV II. Based on these refined hydrodynamic coefficients, a sliding mode controller is designed for the speed, steering and diving systems of the NPS AUV II.

TABLE 2.1 NOMINAL HYDRODYNAMIC COEFFICIENTS

Coefficient	Value	Coefficient	Value
X_{rr}	-0.01735	M_q	-0.03565
X_u	-0.00282	M_w	0.05122
X_{vv}	-0.04019	$M_{\delta s}$	$-0.377*L*Z_{\delta s}$
$X_{\delta s \delta s}$	-0.02345	$M_{\delta b}$	$0.283*L*Z_{\delta b}$
$X_{\delta b \delta b}$	-0.02345	N_r	-0.00047
$X_{\delta r \delta r}$	-0.02345	N_v	-0.00178
X_{prop} (C_{DO})	0.015	N_r	-0.01022
Y_r	-0.00178	N_v	-0.00769
Y_v	-0.03430	$N_{\delta rs}$	$-0.377*L*Y_{\delta rs}$
Y_r	0.01187	$N_{\delta rb}$	$0.283*L*Y_{\delta rb}$
Y_v	-0.03896	I_x (ft^4)	2.7
$Y_{\delta rs}$	0.02345	I_y (ft^4)	42.0
$Y_{\delta rb}$	0.02345	I_z (ft^4)	45.0
Z_q	-0.00253	X_{rs}	$-0.377*L$
Z_w	-0.09340	X_{rb}	$0.283*L$
Z_q	-0.07013	Weight (lbs)	435
Z_w	-0.15687	Length (ft)	7.3
$Z_{\delta s}$	-0.02345	ρ (slugs/ft^3)	1.94
$Z_{\delta b}$	-0.02345	X_G	0.0104
K_p	-0.00024	Z_G	0.0892
K_p	-0.00540	X_B	0.0104
M_q	-0.00625	C_{DY}	0.5
M_w	-0.00253	C_{DZ}	0.6

B. SYSTEM IDENTIFICATION METHODS

There are many methods in use today to identify
appropriate values for unknown parameters that make a system
dynamics model 'fit' experimental response. In the context of
underwater vehicle motion control, one approach is to generate
a nominal model using equations of motion with initial
estimates for the coefficients, and to compare model
simulations using a range of different values for the
parameters to corresponding measured input output data.
This approach is based on open loop simulation and is good for
studying the sensitivity of the system to changes or
estimation errors in the parameters. This approach is called
'parameter tweaking' in this thesis and is modeled in Figure
2.1.

A second approach is to automate the adjustment of
parameters through minimization of some performance index or
quality of fit measure. Two popular indexes in use are the
minimization of mean square error (least squares fit) or the
use of a probabilistic maximum likelihood measure. A good
exposition of modern system identification methods is given in
Astrom (1990). Many methods are based on an input/output model
that is linear in parameters, and if a dynamics model for the
parameter variation with time is included, Kalman filter
equations can be used. Kalman filters are commonly used for
either state estimation based on noisy measurements, or
parameter estimation based on noisy measurements.

15
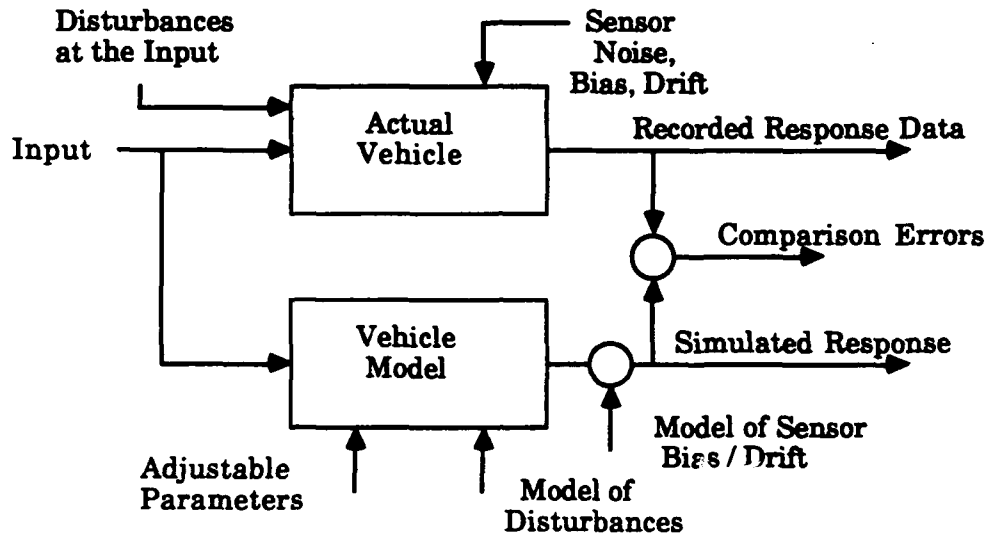
Figure 2.1   Model and Vehicle Data Comparison

1.   Identification Through Kalman Filtering

The discrete time Kalman filter equations from Gelb (1988) are stated below:

The Filter State Equations

$$\hat{x}(k+1|k) = \Phi\hat{x}(k|k) + \Gamma_1 u(k)$$

$$\hat{y}(k+1|k) = C\hat{x}(k+1|k)$$

$$\hat{x}(k+1|k+1) = \hat{x}(k+1|k) + G(k+1)[y(k+1) - \hat{y}(k+1|k)]$$

The Gain Equations

$$P(k+1|k) = \Phi P(k|k) \Phi^T + \Gamma_2 W \Gamma_2^T$$

$$G(k+1) = P(k+1|K) C^T \left[C P(k+1|k) C^T + V \right]^{-1}$$

$$P(k+1|k+1) = [I - G(k+1)C] P(k+1|k)$$

To implement these equations the following is required:

1. State space model

2. Plant noise covariance

3. Measurement noise covariance

4. Initial state estimate

5. Initial estimation error covariance

a. State Filter

The form of these filter equations may be modified and have been arranged here for state estimation first, followed by rearrangement for parameter estimation. The continuous time state space model is of the form:

$$\dot{x} = Ax + B_1 u + B_2 w$$
$$y = Cx + D_1 u + D_2 v$$

where:

x   is the state vector

y   is the measurement vector

w   is the system noise (assumed white)

v   is the measurement noise (assumed white)

A   is the system dynamics matrix

17

$B_{1,2}$ is the system input matrix

C is the system measurement matrix

$D_{1,2}$ is the measurement input matrix

The continuous system is discretized to the following:

$$x(k+1) = \Phi x(k) + \Gamma_1 u(k) + \Gamma_2 w$$

$$y(k) = C x(k) + D_1 u(k) + D_2 v$$

$$\text{where} \quad \Phi = e^{AT} \quad \text{and} \quad \Gamma_i = \int_0^T e^{AT} B_i \, d\tau$$

Using this form of the state equation the Kalman filter is an optimal state estimator and is to be used to provide relatively noise free signals to the sliding mode controllers.

b. Parameter Filter

To use the filter for parameter identification, the form of the equations must be rearranged. It is assumed that from experimental data the inputs $u(k)$ are known and the states of the system $x(k)$ measured. We can rearrange the state space equation by first expanding the right hand side of the system equation, for example a two state system is as follows:

$$\begin{Bmatrix} \dot{x}_1 \\ \dot{x}_2 \end{Bmatrix} = \begin{bmatrix} a_{11} x_1 & a_{12} x_2 & b_1 u \\ a_{21} x_1 & a_{22} x_2 & b_2 u \end{bmatrix} + \begin{Bmatrix} w_1 \\ w_2 \end{Bmatrix}$$

Each row of the expanded system is now in the form of a measurement equation for a Kalman Parameter Filter. By taking

18

each row as an independent measurement equation, the row can be written with the parameter as the state as follows:

$$\dot{x}_1 = \begin{bmatrix} x_1 & x_2 & u \end{bmatrix} \begin{Bmatrix} a_{11} \\ a_{12} \\ b_1 \end{Bmatrix} + w_1$$

The parameters of a_{11}, a_{12}, and b_1 are treated as states of a normal Kalman State Filter where the inputs and the measured states are known and the filter is now an optimal parameter estimator. This is the basis of the measurement equation for the Kalman Parameter Filter where each row of the normal system is now a measurement equation for the filter.

The system equation for the parameters is created with the assumption that the parameters being identified are not time varying. This causes the parameter dynamics matrix to be a square matrix of zeros and the input matrix to the parameter dynamics to be the weighing matrix for the parameter noise Q estimated on each parameter as follows:

$$\dot{\theta} = A\theta + BQ$$
$$or \quad \dot{\theta} = BQ$$

Where θ is the vector of parameters being identified, Q is the parameter noise and B is the parameter noise input matrix which can be weighed to place more or less noise on any individual parameter. This is the system equation used for the Kalman Parameter filter.

19

C. CONTROL VIA VARIABLE STRUCTURE AND SLIDING MODES

1. Development of the Sliding Mode Control Law

The objective of a tracking control for any linearized SIMO subsystem of the form:

$$\dot{x}(t) = Ax(t) + Bu(t) + \delta f(t)$$
$$\tilde{x}(t) = x(t) - x_d(t)$$

(2.1)

where:

x(t) is the state vector

$x_d(t)$ is the desired value of the state vector

$\tilde{x}(t)$ is the state error vector

u(t) is the single input to the system

A is the dynamics matrix linearized about the nominal operating point

B is the input matrix linearized about the nominal operating point and

$\delta f(t)$ is the vector of unmodeled and nonlinear coupling terms of the system which is unknown precisely but bounded;

is to find a control law for u(t) that will drive the state error $\tilde{x}(t)$ to zero. With a sliding mode control, $\tilde{x}(t)$ is driven to zero by ensuring that the value of a sliding surface, σ, (a function of the errors) is driven to zero. Provided that the corresponding error dynamics are stable, the tracking errors will then also go to zero.

20

The sliding surface is defined as:

$$\sigma(t) = s^T \tilde{x}(t) \qquad \textbf{(2.2)}$$

Defining the Lyapunov function as:

$$V(\tilde{x}) = \frac{1}{2}[\sigma(\tilde{x})]^2$$

we guarantee that the sliding surface $\sigma(\tilde{x}) = 0$ is reached in a finite amount of time by the condition:

$$\sigma\dot{\sigma} = -\eta_0^2(\tilde{x})|\sigma(\tilde{x})| \quad \text{or} \quad \dot{\sigma} = -\eta_0^2(\tilde{x})\,\text{sign}(\sigma(\tilde{x}))$$

In order to minimize the chatter on the control signal from the $\text{sign}(\sigma(\tilde{x}))$ term when the system deviates slightly on *either side of the sliding surface the hyperbolic tangent function* is used in its place:

$$\dot{\sigma}(t) = -\eta_0^2\,\text{sign}(\sigma) \quad \text{or} \quad -\eta_0^2\tanh\left(\frac{\sigma}{\phi}\right) \qquad \textbf{(2.3)}$$

where ϕ is the 'boundary layer' thickness and controls the slope of the hyperbolic tangent function passing through the origin. The hyperbolic tangent function provides a smooth transition from one side of the sliding surface to the other and the boundary layer thickness ϕ allows control of the chatter on the controllers nonlinear switching term.

21

Substituting 2.1 and 2.2 into 2.3 gives:

$$s^T(A\tilde{x}(t) + Bu(t) + \delta f(t) - \dot{x}_d(t)) = -\eta_0^2 \tanh(s^T(\tilde{x})) \quad (2.4)$$

solving Equation 2.4 for **u(t)** gives:

$$u(t) = - [s^TB]^{-1}s^TA\tilde{x}(t) - [s^TB]^{-1}\delta f(t)$$
$$+ [s^TB]^{-1}\dot{x}_d(t) - [s^TB]\eta_0^2 \tanh(s^T(\tilde{x}))$$

which is the complete control law for the sliding mode controller. However, $\delta f(t)$ is unknown exactly and only a bound on $\delta f(t)$ may be estimated. Therefore the control law to be used cannot include the $\delta f(t)$ term and is given as follows:

$$u(t) = - [s^TB]^{-1}s^TA\tilde{x}(t) + [s^TB]^{-1}\dot{x}_d(t)$$
$$- [s^TB]^{-1}\eta_0^2 \tanh(s^T(\tilde{x})) \quad (2.5)$$

2. Determination of error dynamics through pole placement

Special notice is given to the control law in equation 2.5 which can be written in simplified form as:

$$u(t) = \hat{u} + u_r + \overline{u}$$

where:

$\hat{u} = -[s^TB]^{-1}s^TAx(t)$ is the linear feedback law

$u_r = [s^TB]^{-1}\dot{x}_d(t)$ is the linear desired rate command feed

forward

22

$\overline{u} = -[s^{T}B]^{-1} \eta\tanh(s^{T}\tilde{x}(t))$ is the nonlinear switching term to drive the system to the sliding surface.

When the system is on the sliding surface $\sigma = s^{T}\tilde{x}(t)$ = 0 and $\overline{u}$ = 0 and when the desired rate of the state vector is zero (u_{r} = 0) then:

$$u(t) = \hat{u} = -[s^{T}B]^{-1}s^{T}A\tilde{x}(t) \qquad (2.6)$$

since the closed loop dynamics must be stable, Equation 2.6 is used as the basis for selecting s^{T} so that system errors will be stable on the sliding surface. Closed loop errors are governed by:

$$\dot{\tilde{x}} = [A - B[s^{T}B]^{-1}s^{T}A]\tilde{x}$$

which is analogous to :

$$\dot{\tilde{x}} = (A - Bk)\tilde{x} \qquad \text{where} \qquad k = [s^{T}B]^{-1}s^{T}A \qquad (2.7)$$

The closed loop error dynamics are described as $A_{c} = A - Bk$ with the eigenvalues of A_{c} defining the closed loop system response of the system when the system is on the sliding surface. It is noted that one of the system poles must be placed at zero to allow the decomposition of the control law given in equation 2.5. The gains k can be found through standard pole placement techniques with desired settling times and percent overshoot using equation 2.7 and $A_{c} = A - Bk = 0$ solve for s:

23

$$s^T Bk = s^T A \quad \rightarrow \quad s^T(A - Bk) = 0$$

Therefore **s** is the right eigenvector of $(A - Bk)^T$ which corresponds to the zero eigenvalue.

3. Sliding Mode Gain Determination

The closed loop system is described by substituting equation 2.5 into equation 2.1 as follows:

$$\dot{\tilde{x}}(t) = A\tilde{x}(t)$$
$$+ B\{-[s^T B]^{-1}s^T A\tilde{x}(t) + [s^T B]^{-1}\dot{x}_d(t) - [s^T B]^{-1}\eta_0^2 \tanh(s^T \tilde{x})\}$$
$$+ \delta f(t)$$

for stability we need $\sigma\dot{\sigma} < 0$ to keep the state on the sliding surface and $\sigma = s^T x(t)$. Multiplying the above equation by s^T and rearranging yields:

$$\dot{\sigma} = s^T \dot{\tilde{x}}(t) = -\eta_0^2 \tanh(s^T \tilde{x}) + \delta f(t) < 0$$

therefore for stability

$$-\eta_0^2 \tanh(s^T \tilde{x}(t)) + \delta f(t) < 0$$

The tanh function is bounded between ± 1.0 and therefore:

$$\eta_0^2 > |\delta f(t)|$$

and global asymptotic stability is guaranteed if the nonlinear switching term gain is greater than the bounded value of the unknown nonlinear coupled term.

D. METHODS USED IN THIS WORK

The Kalman State Filter is used in each of the three control systems to optimally predict the full state model of each subsystem. This state observer provides relatively clean sensor signals to the system controllers and also provides an estimate of v (sway velocity) and w (heave velocity) which is required by the dead reckoning navigation system.

The Kalman Parameter Filter is used as an initial parameter identifier for the system model. Once the parameter filter was tuned to the desired characteristics the parameter filter is used as an on line parameter estimator/fault monitor to detect radical changes in the vehicle performance. Following initial parameter identification, the resulting system was tweaked to provide a more complete analytical model of the vehicle using additional coefficients which are known to exist but were beyond the capacity of the Kalman Parameter Filter to identify.

Sliding mode controllers are designed for each of the three subsystems: speed, steering and diving, based on the refined subsystem models. The sliding mode controllers use filtered inputs from the Kalman State Filters to control the propeller rpm and the control surface deflections. Figure 2.2 shows a functional block diagram of the NPS AUV II autopilot system, inclusive of a dead reckoning navigation system and the Kalman Parameter estimators providing inputs to the subsystems fault monitors.
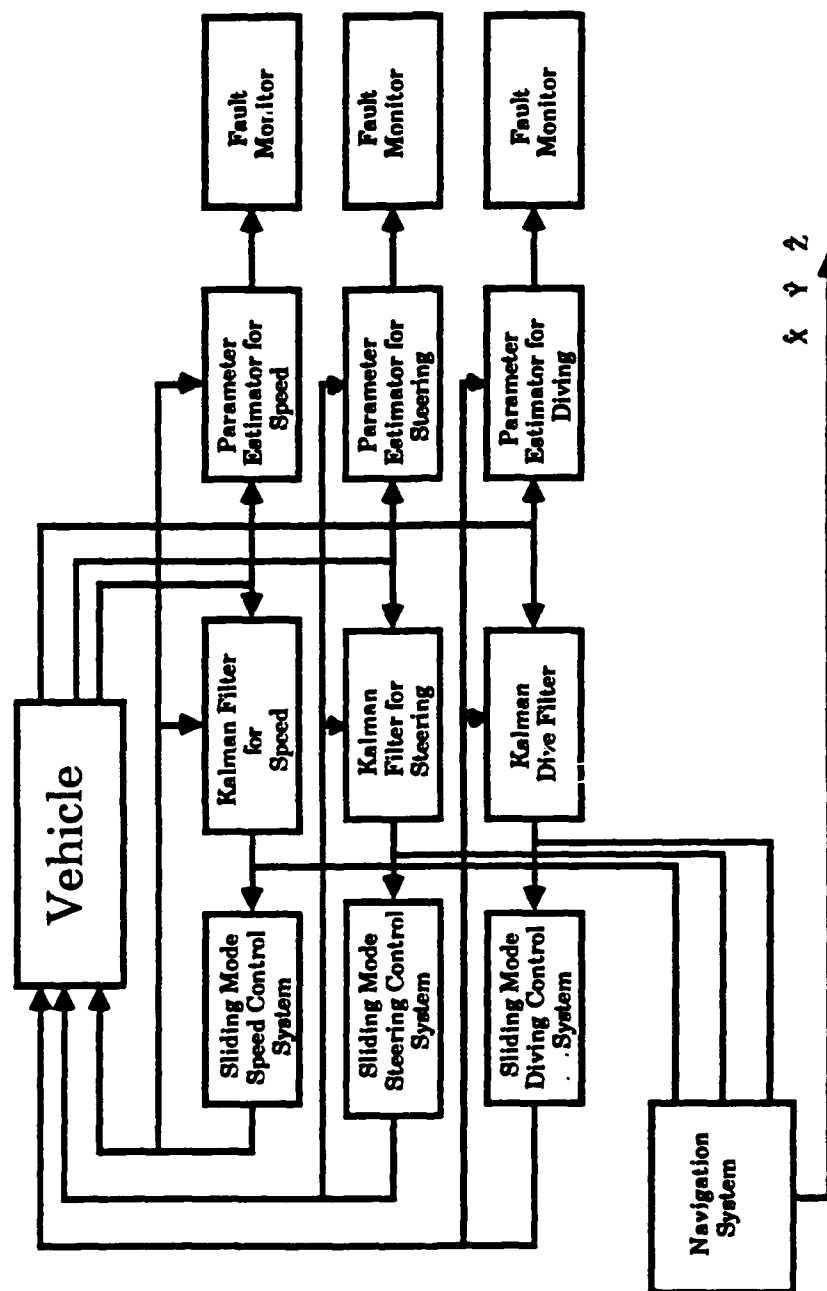
Figure 2.2 **Functional Block Diagram of the NPS AUV II Autopilot, Navigation and Fault Monitor**

III.   PROPULSION SYSTEM CONTROL

A.   INTRODUCTION

The focus of this chapter is to develop an analytical model of the propulsion system of the NPS AUV II and to verify this analytical model by comparison to experimental data recorded during trial runs of the NPS AUV II in the Naval Postgraduate swimming pool. The initial analytical model is a first order model with only three terms to describe the longitudinal motion of the NPS AUV II. The follow on model includes terms which are small in straight line forward motion of the NPS AUV II but are large in a turning maneuver. With the expanded model, it was desired to increase the accuracy of the model in a turn. Following the identification of a reasonable model of the propulsion system a sliding mode controller was designed and tested to control the longitudinal speed of the NPS AUV II.

B.   OUTLINE OF THE PROPULSION SYSTEM

The propulsion system of the NPS AUV II consists of two 4 inch propellers each driven by a separate 24 volt electric motor as shown in Figure 3.1. The motors drive the two independent counter rotating propeller shafts. Additional propulsion system hardware consists of a shaft speed sensor on each propeller shaft (rpm), a motor controller which regulates
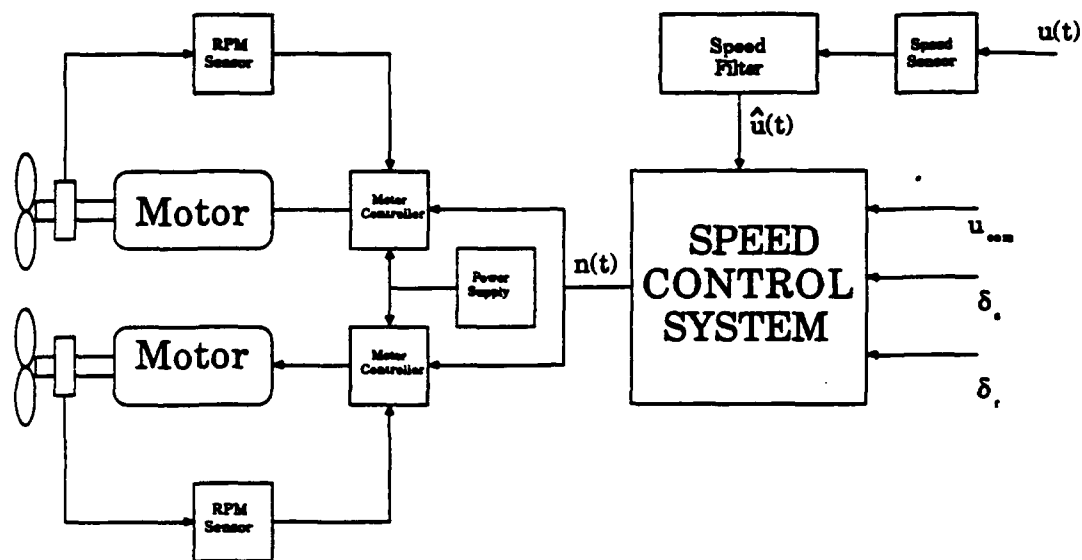
Figure 3.1 Functional Diagram of Propulsion System

the voltage supplied to each motor, a paddle wheel speed
sensor to measure vehicle speed (ft/sec) and a speed
controller which accepts inputs from the paddle wheel speed
sensor, the rudder and plane commands and the commanded
vehicle speed from the mission planner to send the commanded
rpm signal to the motor controllers.

The speed of the propellers is controlled by the motor
controllers operating on the error between the actual shaft
rpm and the commanded shaft rpm received from the speed
controller regulating the voltage supplied to the propulsion
motors between 0 and 24 volts. The motor controller works well
up to the point of the physical limitations of the system. The
right propulsion motor experiences a greater amount of
friction between the propeller shaft and the water tight seal

than the left propeller shaft. This is important to keep in mind at high commanded rpm's because the right propeller shaft may be physically limited to reaching the commanded rpm.
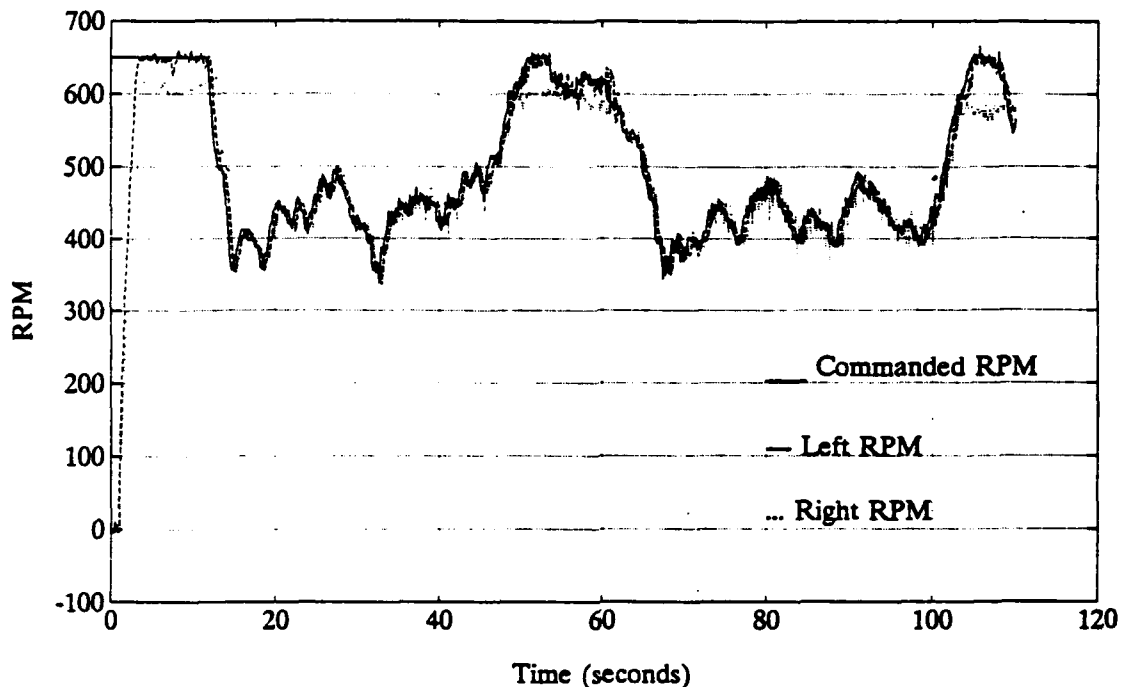
Figure 3.2   Commanded, Right and Left Motor RPM

Figure 3.2 shows that the motor controller responds very rapidly to minimize the error between the commanded rpm and the actual rpm with the exception of the right propeller rpm being limited at high commanded rpm's due to the excess friction involved with the right propeller shaft.

The propulsion system is governed by Equation 2.1 the Surge Equation of Motion. Simplifying the surge equation with the following assumptions, provides a basic starting point for the identification of the propulsion parameters.

1. The vehicle is in straight line motion ψ, r and $v = 0$.

2. The vehicle is in level flight θ, ϕ, p, q and $w = 0$.

The resulting simplified equation is as follows:

$$(m - X_{\dot{u}}) \dot{u} = X_{res} u|u| + X_{prop} n|n|$$
$$+ u|u| (X_{\delta_s \delta_s} \delta_s^2 + X_{\delta_b \delta_b} \delta_b^2 + \dot{X}_{\delta_{rb} \delta_{rb}} \delta_{rb}^2 + X_{\delta_{rs} \delta_{rs}} \delta_{rs}^2)$$

Operation of the NPS AUV II presently has the deflection of the bow rudder equal in magnitude but opposite in direction to the stern rudder and likewise for the dive planes. Therefore $\delta_{rb} = -\delta_{rs}$ and $\delta_b = -\delta_s$. The rudder control surfaces are identical in size and shape to the dive plane control surfaces therefore $X_{\delta_{rb} \delta_{rb}} = X_{\delta_{rs} \delta_{rs}} = X_{\delta_b \delta_b} = X_{\delta_s \delta_s}$. Dividing through by the inertia term and using the above rudder and plane relations yields:

$$\dot{u} = \frac{X_{res}}{(m - X_{\dot{u}})} u|u| + \frac{X_{prop}}{(m - X_{\dot{u}})} n|n| + \frac{2 X_{\delta_s \delta_s}}{(m - X_{\dot{u}})} u|u| (\delta_s^2 + \delta_r^2)$$

The simplified nonlinear equation of motion used for the propulsion system is given as Equation 3.1. This form of the equation is linear in parameters α, β and γ while the state of the system and the inputs are quadratic.

$$\dot{u} = \alpha u|u| + \beta n|n| + \gamma u|u|\delta^2 + [\delta_u] \tag{3.1}$$

30

Where:

u   is the state of the system (surge (ft/sec))

n   is a input to the system (rpm)

$\delta^2 = (\delta_s^2 + \delta_r^2)$ is a input to the system (radian of plane or

rudder deflection)

$$\alpha = \frac{X_{res}}{(m-X_u)} = \frac{-C_{DO}\frac{1}{2}\rho L^2}{(m-\frac{1}{2}\rho L^3 \dot{X}_u)} \qquad \text{is the longitudinal body drag}$$

coefficient

$$\beta = \frac{X_{prop}}{(m-X_u)} = \frac{C_{DO}\frac{1}{2}\rho L^2 \left(\frac{u_0}{n_0}\right)^2}{(m-\frac{1}{2}\rho L^3 \dot{X}_u)} \qquad \text{is the longitudinal propulsion}$$

thrust coefficient

$$\gamma = \frac{2X_{\delta s \delta s}}{(m-X_u)} = \frac{-2\dot{X}_{\delta s \delta s}\frac{1}{2}\rho L^2}{(m-\frac{1}{2}\rho L^3 \dot{X}_u)} \qquad \text{is the longitudinal rudder and plane}$$

drag coefficient

$[\delta_a]$ is the lumped unmodeled terms

The values of α, β and γ were first determined
analytically by Warner (1991) based on geometric scaling of
the SDV to the AUV II. The state and inputs are measured by
sensors on board the AUV II leaving only, $[\delta_a]$, a noise term
which is not known but is bounded. It is assumed that the $[\delta_a]$
term can be modeled as Gaussian white noise with zero mean and
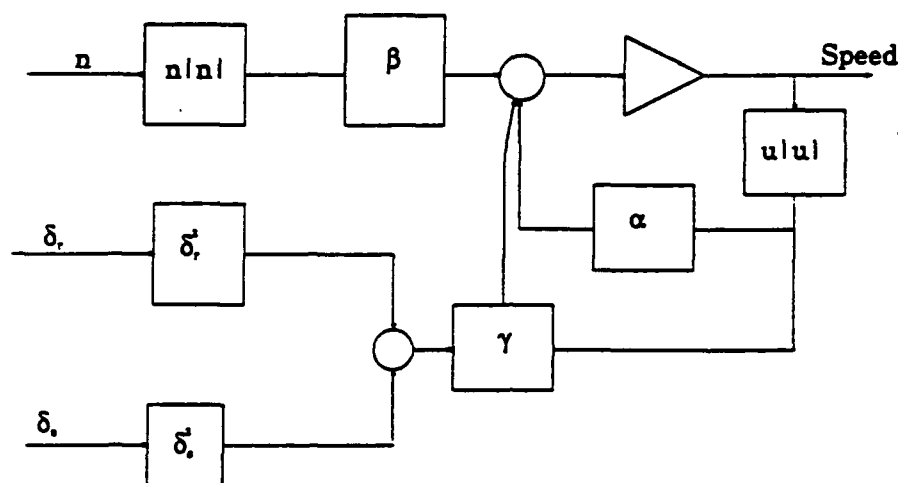
Figure 3.3   Block Diagram of Equation 3.1

an estimated variance. The block diagram corresponding to Equation 3.1 is shown in Figure 3.3.

C.   EXPERIMENTAL WORK WITH NPS AUV II

Numerous trials have been run on the NPS AUV II in the swimming pool at the Naval Postgraduate School. The data records from these trials are available for post mission analysis. The data of interest for the propulsion system identification are the recorded vehicle speed (u), the commanded rpm, actual right and left shaft rpm's and the rudder and plane angle deflections. Recorded data of the above mentioned variables from the 'zig-zag' mission are shown in Figure 3.4. This recorded data was used for the following discussion of the propulsion system parameter identification.

32
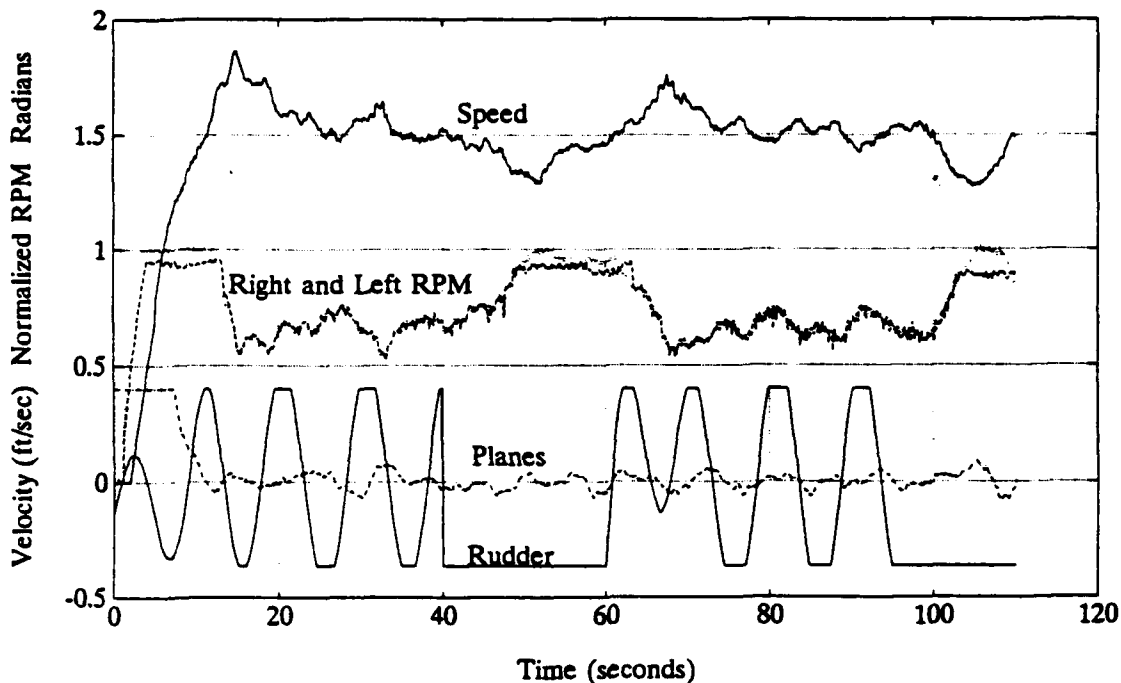
Figure 3.4 'Zig-Zag' Mission Recorded Data

D. PARAMETER IDENTIFICATION: 3 PARAMETER MODEL

The Kalman filter was used as a parameter identification tool for two major reasons 1) the work of Abkowitz (1980) showed the power of the Kalman filter in providing ship maneuvering parameter identification as well as state estimation and 2) the Kalman filter can be implemented as an on line parameter estimator/fault monitor.

The use of a Kalman filter as described earlier in Chapter II requires the following ingredients for operation:

1. State space model
2. Plant noise covariance
3. Measurement noise covariance
4. Initial state estimate
5. Initial estimation error covariance

33

1. State Space Model

The state space model is derived from Equation 3.1 by arranging the measurement (output) equation as follows:

$$\dot{u} = \begin{bmatrix} u|u| & n|n| & \delta^2 u|u| \end{bmatrix} \begin{Bmatrix} \alpha \\ \beta \\ \gamma \end{Bmatrix} + [\delta_a] \qquad (3.2)$$

This places the propulsion system equation in the form of a measurement equation for the Kalman filter where the system parameters are now treated as the states of a typical Kalman state filter. The $[\delta_a]$ term is now considered as the measurement noise. This filter is referred to here as the 'Kalman Parameter Filter'. The parameter dynamics equations for the identification routine are:

$$\frac{d}{dt} \begin{Bmatrix} \alpha \\ \beta \\ \gamma \end{Bmatrix} = \begin{bmatrix} & A & \end{bmatrix} \begin{Bmatrix} \alpha \\ \beta \\ \gamma \end{Bmatrix} + \begin{bmatrix} & B & \end{bmatrix} Q \qquad (3.3)$$

Where the expected rates of change of the system parameters are zero, i.e. the parameters should be constant. Therefore the **A** matrix (parameter dynamics) in this case is a 3x3 matrix of zeros and the **B** matrix (parameter noise input) is a 3x3 diagonal matrix of weighing values as to which parameter is subject to what portion of parameter noise **Q**.

2. Plant Noise Covariance

The covariance of the parameter system noise Q is not known and is estimated. The ideal value of Q is zero corresponding to perfectly constant parameters, however since our analytical model is not precise the variations in the model are absorbed by changes in the system parameters driven by white noises Q. The B matrix of the above parameter system equation allows the various parameters to be weighted differently thereby placing more or less of the system noise on individual parameters. The overall amount of parameter noise injected into the system is controlled by the value of Q. The larger the value of Q the faster the filter responds and essentially places more variability on each of the identified system parameters. Figure 3.5 shows the response of α for three different values of Q it is seen that the filter converges faster for a larger value of Q but the noise on the parameter is also increased and the bound on the parameter is more difficult to predict. For smaller values of Q the parameter converges slower and less noise is injected into the parameter identification. At this point it is the choice of the filter designer to choose a value of Q which allows the filter to respond rapidly enough but also does not carry with it excessive amounts of system noise. For our filter, three values of Q were chosen for further study of parameter identification.

35
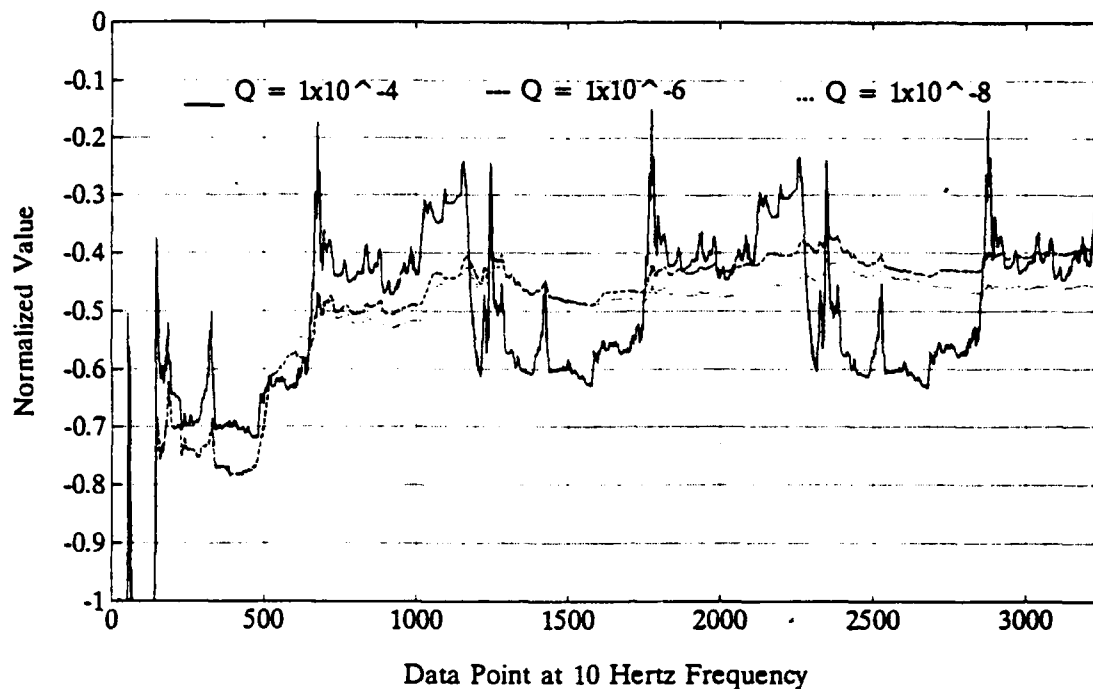
Figure 3.5   Response of Filter for values of Q

3.   Measurement Noise Covariance

The measurement noise covariance needed to be calculated. The $[\delta_a]$ term is the measurement noise in the rearrangement of Equation 3.1 to the Kalman Parameter Filter. The covariance of the $[\delta_a]$ term is determined as the square of the standard deviation of the difference between the measured rate of surge and the calculated rate of surge from the nominal analytical model. If the $[\delta_a]$ term is white this indicates that the system identification is precise. However, if the $[\delta_a]$ term has a non-zero mean or shows obvious trends

36

of oscillation, then the $[\delta_a]$ term is not white. Additional terms are then required to model the system precisely.

With the present model, the maximum, average and standard deviation of the $[\delta_a]$ term are measurable. This measurement of the $[\delta_a]$ term is also necessary to determine the minimal nonlinear switching term gain for the sliding mode controller. Using the nominal model parameters developed by Warner (1991), an analytical model simulation was run and the difference in measured surge rate and analytical surge rate is displayed in Figure 3.6. Analysis of the plotted data provides a mean, standard deviation and a variance. The variance of $[\delta_a]$ is used in the Kalman parameter filter as the measurement error covariance.

4. Initial State Estimate

The initial parameter estimates are taken directly from the work of Warner (1991) as the starting point for the operation of the Kalman parameter filter.

5. Initial Estimation Error Covariance

The initial estimation error covariance is unknown and is set equal to 1.0 for each of the parameters being identified. The nature of the Kalman filter as a dynamic optimal estimator allows the initial estimation error
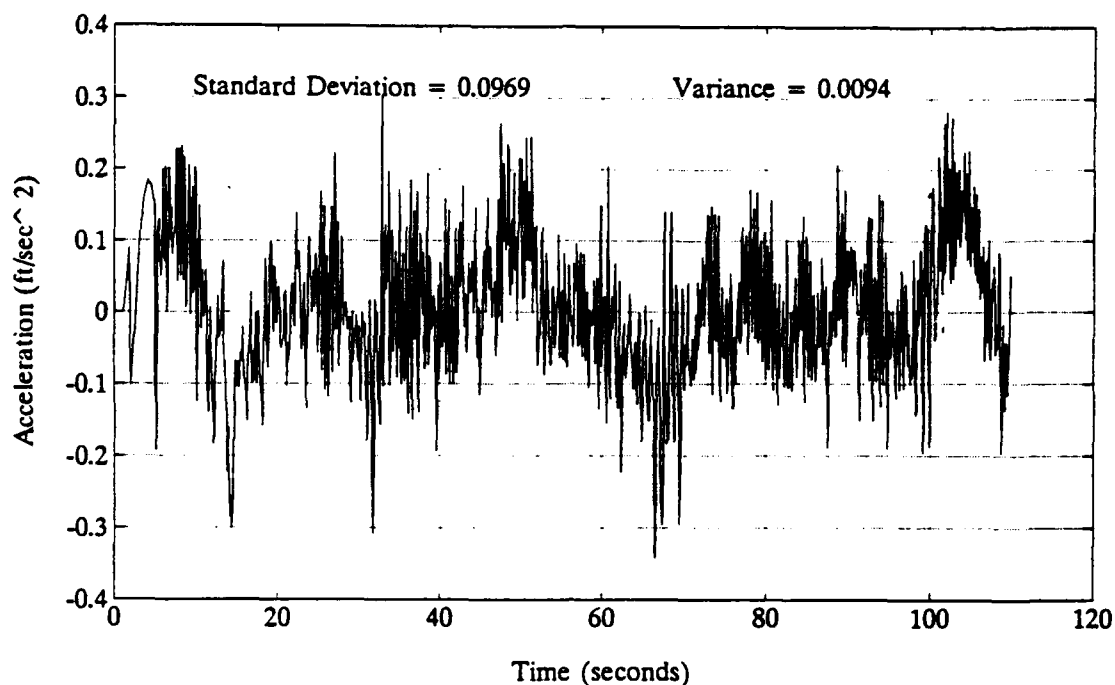
Figure 3.6 Plot of [δ_u] From Nominal System Parameters Developed by Warner

covariances to converge to the actual values of the estimation error covariance. It was found that, by allowing the filter to run on the data set and at the end of the run taking the final parameter estimates and the final estimation error covariances as new initial conditions, the filter could be run again with the updated initial conditions. The filter was found to converge to a steady state value of estimation error covariance for each of the parameters after about four data passes and the parameter estimates converged to a steady state value after about five data passes. This allowed the estimation error covariances to begin at a value of 1.0, run the filter about four or five times, updating the initial estimation error covariances with the final values of the

38

estimation error covariances from the previous run until the steady state estimation error covariances were identified. With the steady state estimation error covariance now known, the Kalman Parameter Filter is now ready for use as a parameter identifier.

E. KALMAN PARAMETER FILTER RESULTS

The weighing of the **B** matrix was also investigated. Both investigations of **B** matrix weighing were compared at each of the three selected values of parameter noise **Q**. The first investigation used unequal weighing and weighed the α and β parameters at 0.1 and the γ parameter at 1.0. This placed one tenth the amount of the system noise on the α and β parameters as on the γ parameter. The response is shown in Figure 3.7 with the covariance of **Q** equal to 1×10^{-8}. The second investigation weighed all the parameters equally at 1.0. This placed an equal amount of system noise on each of the parameters. The results of the equal weighing are shown in Figure 3.8 with the covariance of **Q** equal to 1×10^{-8}. This investigation shows that the Kalman Parameter Filter can be tuned to give a desired speed of response with the trade off that a faster filter induces more noise into the identified parameter and that the parameters may be weighed to allow the parameters of less confidence to take up more of the system noise and allow better identification of the remaining parameters.
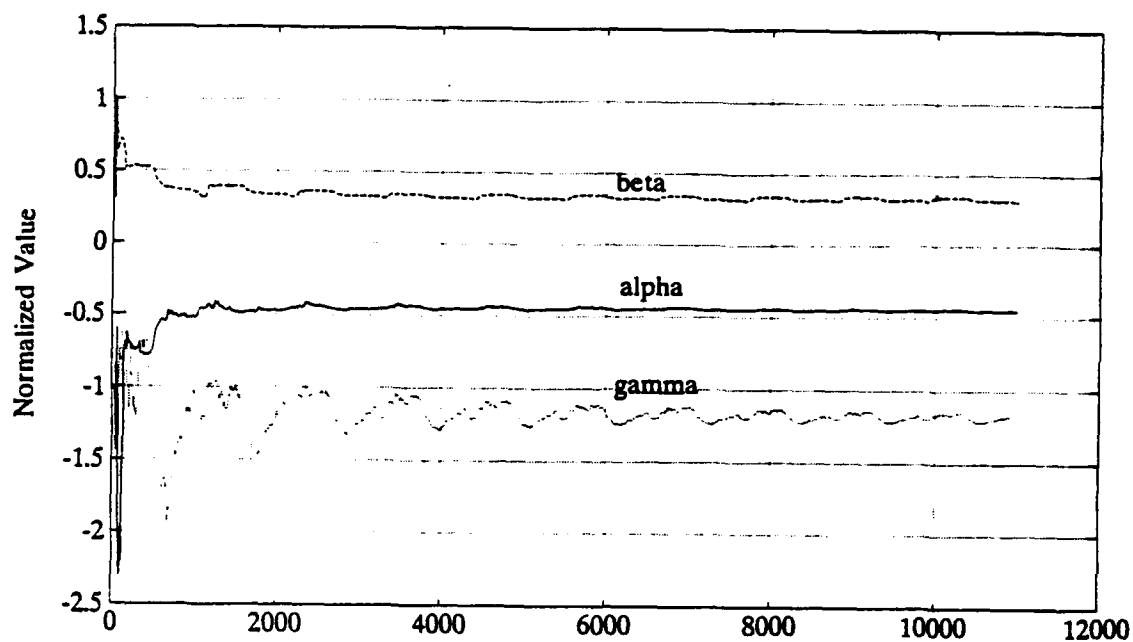
Figure 3.7   Response of α, β and γ to Mixed Weighing
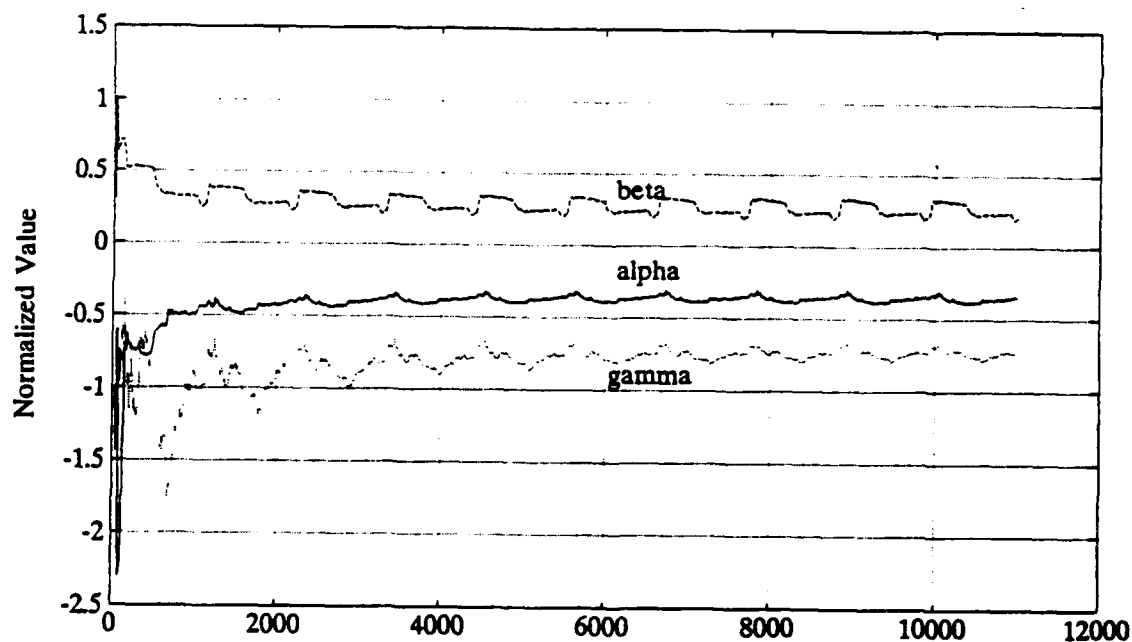
Figure 3.8   Response of α, β and γ to Equal Weighing

40

The identification procedure began with the initial parameter estimates from Warner, the steady state estimation error covariance identified as described earlier and the measurement error covariance of 0.0094. The data was run through the filter 10 times to ensure convergence of the parameter estimates. The values of α, β and γ listed in Table 3.1 are the mean values of the final run of the data through the filter. The initial parameter values from Warner for α, β and γ are summarized in Table 3.1 along with the identified values of α, β and γ from each of the six combinations of the **B** matrix weighing and parameter noise covariance **Q**. The identified values of α, β and γ were each run in the propulsion system Equation 3.1 and the velocity and acceleration error calculated. The standard deviation and variance of both the velocity and acceleration errors are included in Table 3.1 for comparison to the original estimates. From Table 3.1, it is seen that the parameters identified with unequal **B** matrix weighing and a value of parameter noise covariance $= 1 \times 10^{-6}$ provides the parameters which produce the minimal velocity and acceleration errors. The filter run which produced the best estimate of parameters is as shown in Figure 3.9 and the simulation results of the original estimates and the revised estimates are shown in Figure 3.10. This comparison of the analytical model to the measured data clearly shows the improvement of the identification of the analytical model from the initial estimates of Warner based on first principles to that of on-line parameter identification.
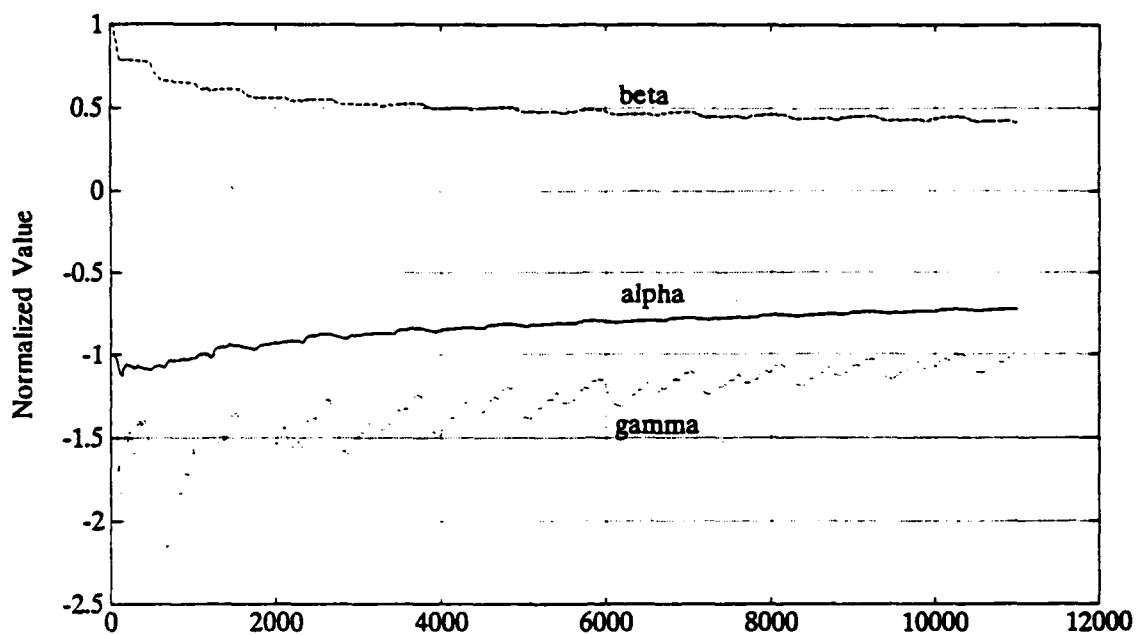
Figure 3.9   Kalman Filter Results of α, β and γ
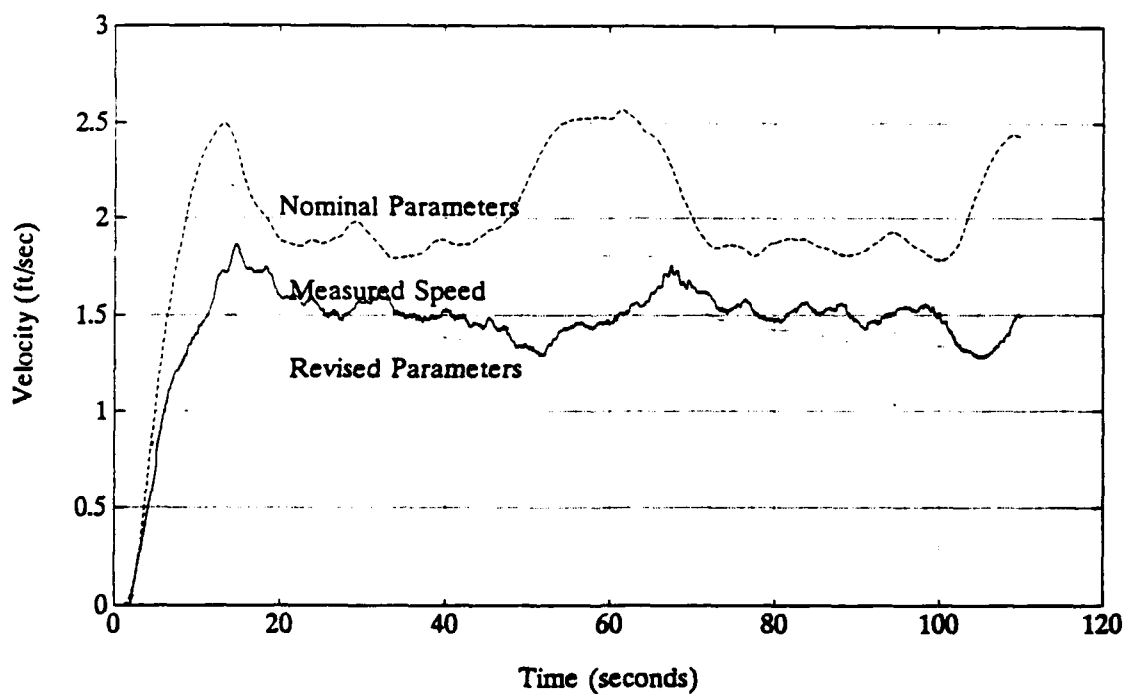
Figure 3.10 Simulation Results of Identified α, β and γ

42

TABLE 3.1   KALMAN PARAMETER FILTER RESULTS FOR SPEED

Q WEIGHING	ORIG. EST.	1×10^{-4} $\neq$	1×10^{-6} $\neq$	1×10^{-8} $\neq$	1×10^{-4} $=$	1×10^{-6} $=$	1×10^{-8} $=$
α (-)	0.0532	0.0195	0.0386	0.0242	0.0160	0.0185	0.0239
β $(\times10^{-7})$	10.988	2.4197	4.5691	3.5288	2.2358	2.2836	3.4495
γ (-)	0.0693	0.0552	0.0734	0.0852	0.0148	0.0505	0.0826
$[\delta_{\dot{u}}]$ STD DEV	0.0969	0.0868	0.0840	0.0847	0.0878	0.0872	0.0848
$[\delta_{\dot{u}}]$ VARIANCE	0.0094	0.0075	0.0071	0.0072	0.0077	0.0076	0.0072
$[\delta_{u}]$ STD DEV	0.2834	0.2720	0.1862	0.2208	0.3617	0.2839	0.2245
$[\delta_{u}]$ VARIANCE	0.0803	0.0740	0.0347	0.0487	0.1308	0.0806	0.0504

F.   PARAMETER IDENTIFICATION: 5 PARAMETER MODEL

Noting that prior to the turn in Figure 3.10, up to time equals 40 seconds, the model speed is underestimated and during the turn time 40 to 75 seconds, the model speed is over estimated. This is a clear indication that this simple system

model is not precise, meaning additional terms are needed in the analytical equation of motion. Specifically, the terms having to do with the effects of a turn which were removed from the longitudinal equation of motion when simplified. These terms need to be reintroduced to provide a more accurate model.

Expanding the system model to include the centrifugal acceleration terms mvr, $X_{rr}r^2$ and $X_{vv}v^2$, the system model becomes

$$\dot{u} = \alpha u|u| + \beta n|n| + \gamma u|u|\delta^2 + \epsilon vr + \kappa r^2 + \lambda v^2 + [\delta_u]$$

The nominal values of ϵ, κ and λ are determined from the parameter estimation of Warner where:

$\epsilon = \dfrac{m}{(m - X_{\dot{u}})} = \dfrac{m}{(m - \frac{1}{2}\rho L^3 \acute{X}_{\dot{u}})}$ is the mass divided by the mass

plus added mass term.

$\kappa = \dfrac{X_{rr}}{(m - X_{u})} = \dfrac{\frac{1}{2}\rho L^4 \acute{X}_{rr}}{(m - \frac{1}{2}\rho L^3 \dot{X}_{u})}$ is the yaw rate body drag

coefficient.

$\lambda = \dfrac{X_{vv}}{(m - X_{u})} + \dfrac{\frac{1}{2}\rho L^2 \acute{X}_{vv}}{(m - \frac{1}{2}\rho L^3 \acute{X}_{u})}$ is the side slip body drag

coefficient.

Note that the value of the sway velocity is not recorded in the NPS AUV II at the present time. An observer developed by Warner (1991) was used to estimate sway velocity (v) for the data processed through the filter.

The data was run through the larger Kalman parameter filter repeatedly 6 times using the final parameter estimate and final estimation error covariance as the initial values for the subsequent run through the filter. The parameter noise covariance of 1×10^{-6} was used because it produced the most favorable results from the 3 parameter model. The parameter values are normalized to 1.0 or -1.0 based on the initial parameter estimate from Warner. The parameter filter produced the results shown in Figure 3.11 for α, β, γ, κ and λ. The mean of each parameter over the final data run through the filter was taken and the normalization removed. These identified values are tabulated with the initial nominal values in Table 3.2. The results of these average coefficients were run on the system model producing the results shown in Figure 3.12. The five parameter analytical model clearly provides a more precise model for the propulsion system but the sway velocity $\mathbf{v}$ is not measured and is not available for the control of the longitudinal speed of the NPS AUV II.

TABLE 3.2   IDENTIFIED PROPULSION SYSTEM PARAMETERS

Parameter	Original Estimate by Warner	Kalman Parameter Identification
α	-0.05319	-0.0276
β	10.9887×10^{-7}	4.7682×10^{-7}
γ	-0.06935	-0.0301
κ	-3.2802	-1.4233
λ	-0.1425	-0.0618
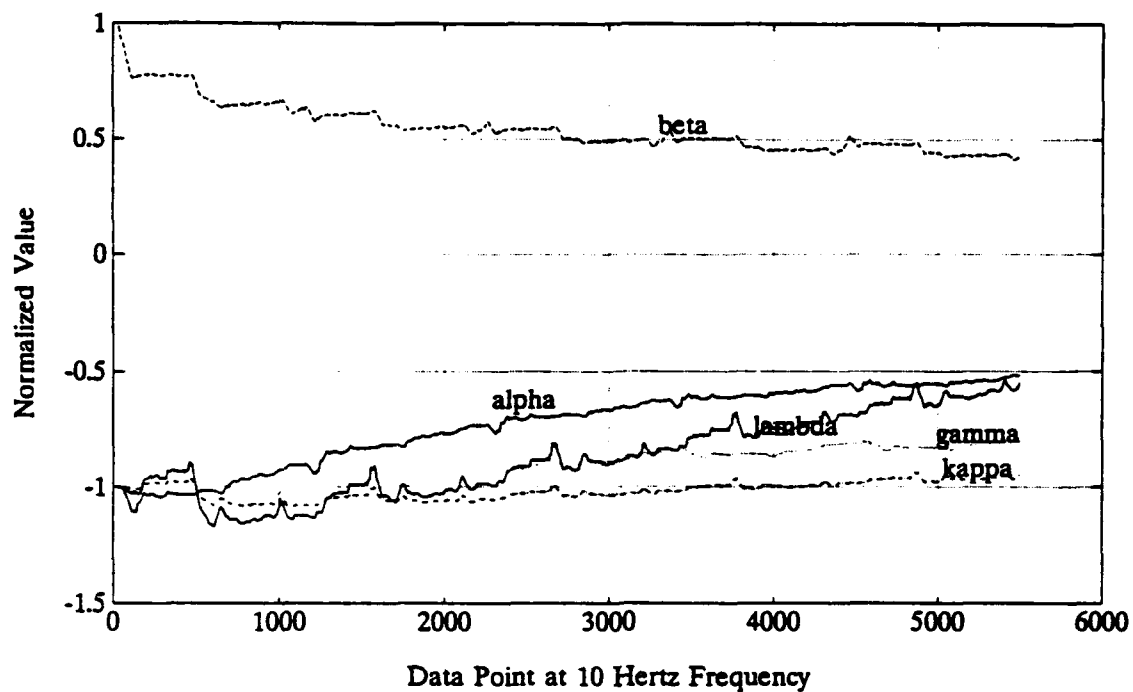
Figure 3.11   Identification Results of α, β, γ, κ **and** λ
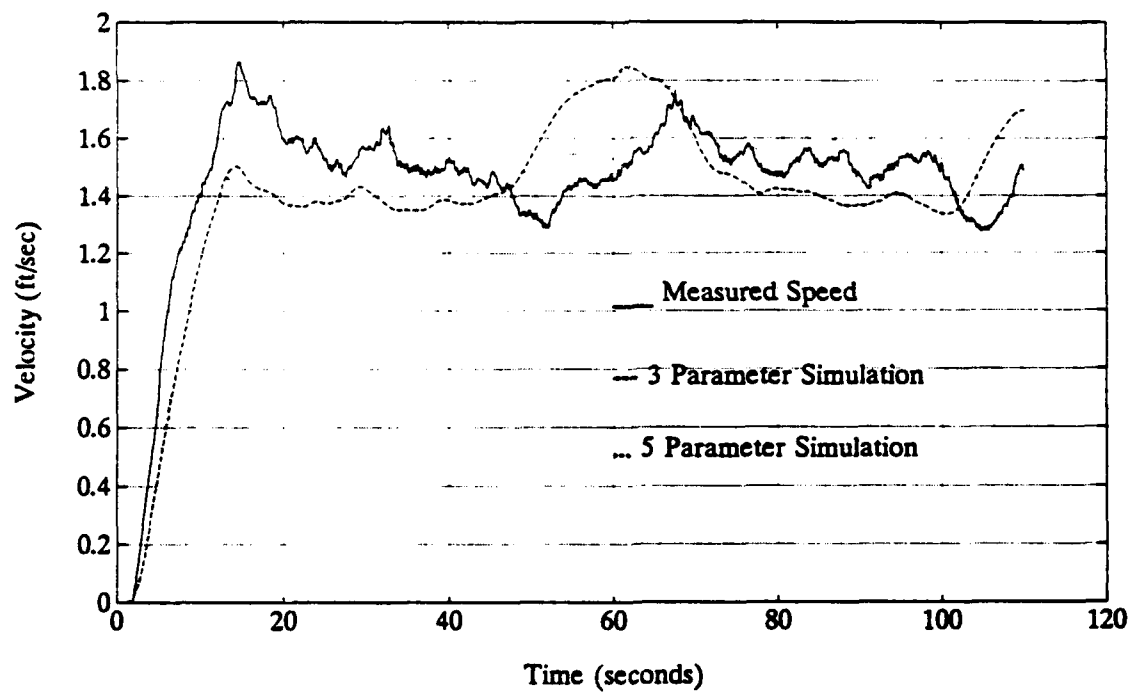
Figure 3.12   Simulation Results of α, β, γ, κ **and** λ

47

G. SLIDING MODE CONTROLLER DESIGN

1. Development of Control Law

In the design of the sliding mode speed controller the simpler 3 parameter analytical model was used because the sway velocity **v** is not available as a measurement to be used as an input to the speed controller. Using the system equation denoted by Equation 3.1 repeated here:

$$\dot{u} = \alpha u|u| + \beta n|n| + \gamma u|u|\delta^2 + [\delta_a] \qquad (3.1)$$

and the sliding surface defined as:

$$\sigma(t) = s^T \tilde{x}(t) \qquad (3.5)$$

$$\dot{\sigma}(t) = s^T \dot{\tilde{x}}(t) = -\eta_0^2 \tanh\left(\frac{s^T \tilde{x}(t)}{\phi}\right)$$

applying a direct application of sliding mode control theory to the non-linear equation of motion, a non-linear sliding mode control law can be developed as follows where:

$$\tilde{x} = u - u_d \qquad \text{and} \qquad \dot{\tilde{x}} = \dot{u} - \dot{u}_d$$

48

Substituting Equation 3.1 into Equation 3.5 and expanding yields:

$$s^{T}(\alpha u|u| + \beta n|n| + \gamma u|u|\delta^2 + [\delta_a] - \dot{u}_d)$$
$$= -\eta_0^2 \tanh\left(\frac{s^{T}(u - u_d)}{\phi}\right)$$

(3.6)

For a first order system $s = s^{T} = 1.0$ rearranging Equation 3.6 and solving for $\beta n|n|$ yields:

$$\beta n|n| = -\alpha u|u| - \gamma u|u|\delta^2 - [\delta_a] + \dot{u}_d$$
$$-\eta_0^2 \tanh\left(\frac{s^{T}(u - u_d)}{\phi}\right)$$

(3.7)

where $[\delta_a]$ is unknown but bounded and is removed from the control law. solving for n and retaining the proper sign provides the following nonlinear control law:

$$n = \pm \sqrt{\left| \begin{array}{c} -\dfrac{\alpha}{\beta}u|u| - \dfrac{\gamma}{\beta}u|u|\delta^2 + \dfrac{1}{\beta}\dot{u}_d) \\[2mm] -\dfrac{\eta_0^2}{\beta}\tanh(s^{T}(u - u_d)) \end{array} \right|}$$

(3.8)

where the $\pm$ in the control law indicates the sign of the argument is retained.

49

2. Determination of the Control Law Gain and Boundary Layer Thickness

For the system to be stable $\sigma = s^T \dot{\tilde{x}}$ must be < 0. Determination of the sliding mode switching term gain η is made by substituting the control law Equation 3.7 without the $[\delta_u]$ term into Equation 3.1, the open loop system equation. Multiplying through by s^T and solving for η gives the minimum value of η to guarantee stability.

$$\eta_0^2 > \frac{|[\delta_u]|}{|1.0|} \qquad (3.9)$$

A bound is placed on $[\delta_u]$ by using the maximum value for a 100% guaranteed stability. A *confidence interval can be* constructed using a stochastic method with the known standard deviation of the $[\delta_u]$ to calculate a value of η which will guarantee stability in a probabilistic sense.

Having determined the minimum value of η, the next step is to determine the desired boundary layer thickness for the switching term. As discussed in Chapter II, the boundary layer allows for a smooth transition from positive to negative sign on the switching term in conjunction with the hyperbolic tangent function. The desired value of ϕ is selected using the

plot shown in Figure 3.13 by entering the plot at the ordinate
of the minimum allowable value of η as determined earlier and
proceeding in the direction of the abscissa to the acceptable
value of speed error allowed. The curve of φ passing through
this point is the value of φ to use to guarantee stability and
an acceptable amount of speed error prior to saturation of the
con.roller.
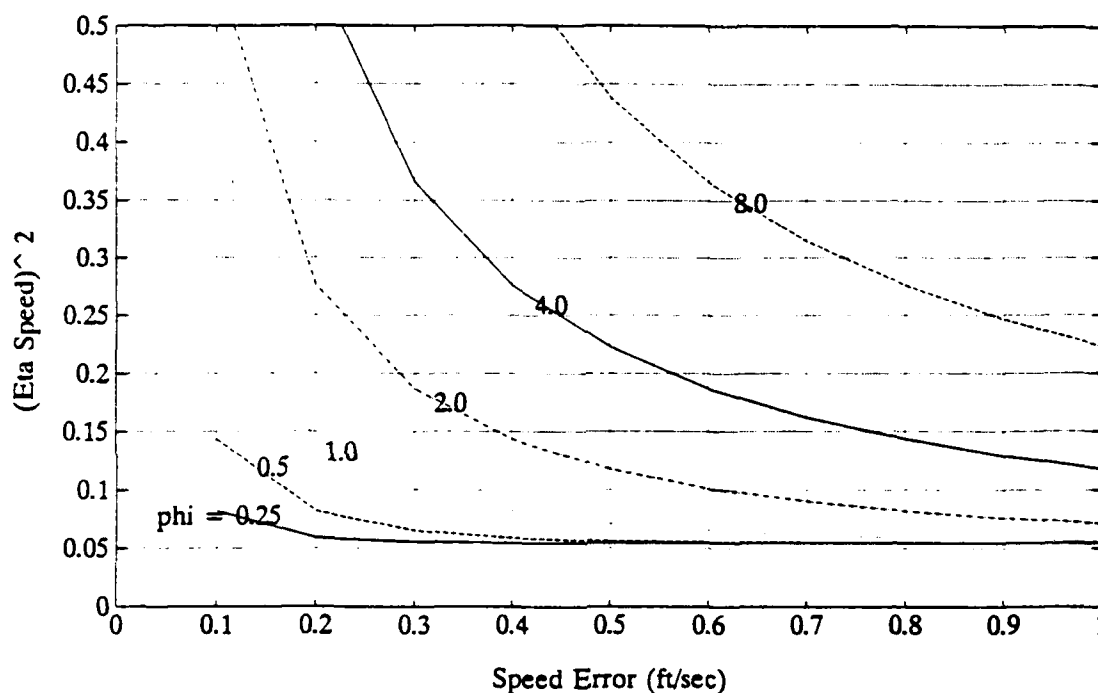
Figure 3.13 Relationship Between η, φ and acceptable speed error

Figure 3.13 was constructed on the basis that if the
vehicle is operating in a steady state condition and an error
between actual speed and commanded speed is encountered, and
this speed error is less than the allowable speed error used
in determining φ, the speed controller will not saturate.
Stated in equivalent terms the value of φ selected will

determine the amount of allowable speed error before the speed controller saturates. A saturated speed controller means that the maximum possible shaft rpm is being commanded and the propulsion system is limited to this maximum.

H. PERFORMANCE OF THE SLIDING MODE CONTROLLER

The sliding mode controller control law was coded into the operating system of the NPS AUV II and tested in the swimming pool. Two values of η were tested. The first test, with a value of $\eta = 2.0$ is shown in Figure 3.14 and the second test, with a value of $\eta = 1.0$ is shown in Figure 3.15. The commanded speed for the test was $u = 1.5$ (ft/sec). The response of the vehicle to the control law was good in that the commanded speed of 1.5 was achieved on the average. The oscillations in speed and propeller rpm from time 0 to time 40 are caused by two effects: 1) the noise on the speed sensor is large and is amplified in the speed error component of the control law by the value of η. 2) The value of η used was too large for the system and increased the levels of propeller speed saturation, and therefore began to send the controller into oscillations. In Figure 3.15, for the lower value of $\eta = 1.0$, the response of the vehicle is less oscillatory. The control law is fairly effective in maintaining constant speed through the turn commencing at time equals 40 to 60 seconds.
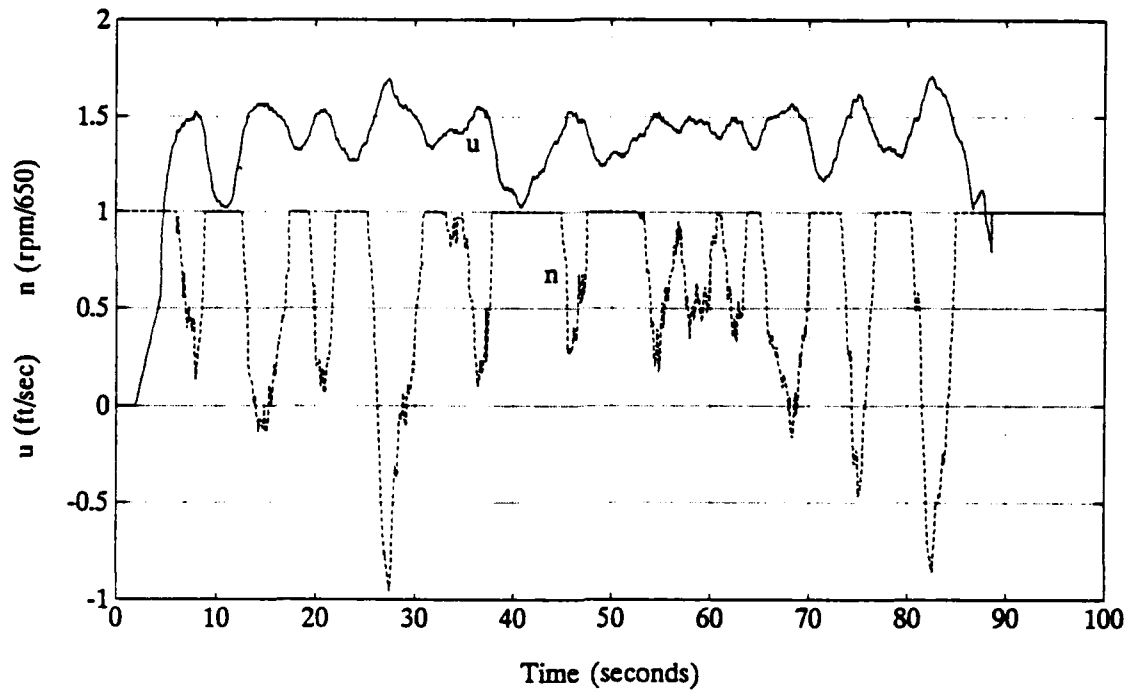
Figure 3.14 Test Of Sliding Mode Speed Controller $\eta = 2.0$
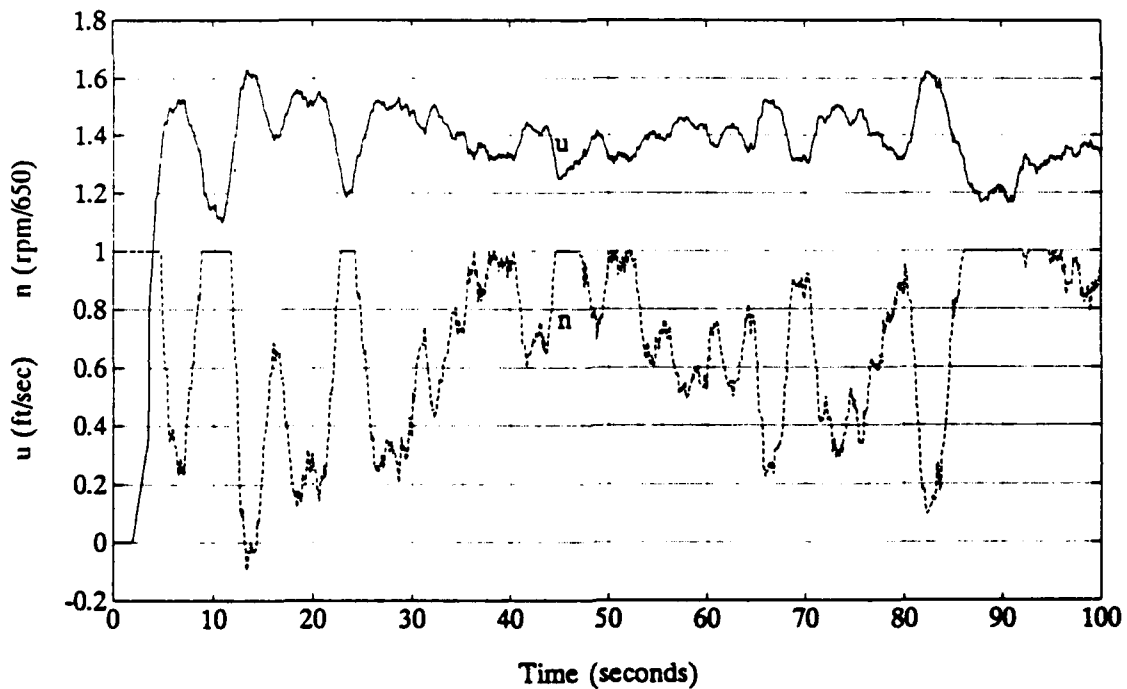
Figure 3.15 Test Of Sliding Mode Speed Controller $\eta = 1.0$

Improvements to the sliding mode speed controller to minimize the commanded rpm oscillations can be accomplished by using a Kalman State Filter to provide a cleaner speed signal to the controller. The Kalman State Filter is developed in the next section. The speed controller gain η can be reduced to a lower value which will still maintain guaranteed stability of the controller.

I. DESIGN OF KALMAN FILTER FOR THE SPEED SENSOR

1. Linearized Kalman State Filter

The first step in the construction of a Kalman state filter is to identify the system equation. For the system equation we simplified Equation 3.1 to include only the α, β and $[\delta_u]$ term, where the $[\delta_u]$ term is the system noise.

$$\dot{u} = \alpha u|u| + \beta n|n| + [\delta_u]$$

Linearizing the system equation about the nominal operating point u_0 and n_0 the system equation takes on the following form.

$$\dot{u} = \alpha u_0 u + \beta n_0 n + [\delta_u]$$

The system equation is now in the proper form for use in a Kalman State Filter with the plant noise covariance equal to the covariance of $[\delta_u]$, The measurement equation is a direct input from the paddle wheel speed sensor with the measurement noise covariance analyzed directly from the rate of change of the speed sensor recorded data file.

The initial state estimate is taken as the first recorded data point of speed from the speed sensor. The initial estimation error covariance is set to zero because the filter starts with the state and the state estimate equal therefore the estimation error is zero. The nature of the Kalman filter will allow the estimation error covariance to converge to a steady state value quickly.

2. Nonlinear Kalman Filter

Construction of a nonlinear Kalman filter requires update of the system equation on each time step in the discrete time system. To accomplish this the value of α_n and β_n are calculated at each time step using the estimated speed u and the input rpm n and then the system equation is discretized and the filter equations reapplied. The same system and measurement noise covariances are used and the initial state estimate is equal to the first recorded data point. The estimation error is zero and therefore the initial estimation error covariance is again set equal to zero. This nonlinear filter is much slower computationally and the results are not as good as the linear filter. The nonlinear filter shows more lag time than the linear filter, therefore the choice was made to use the linearized filter. The results of the linearized and nonlinear filter are shown in Figure 3.16. It is readily apparent that the linear filter does a satisfactory job in providing a clean and accurate speed
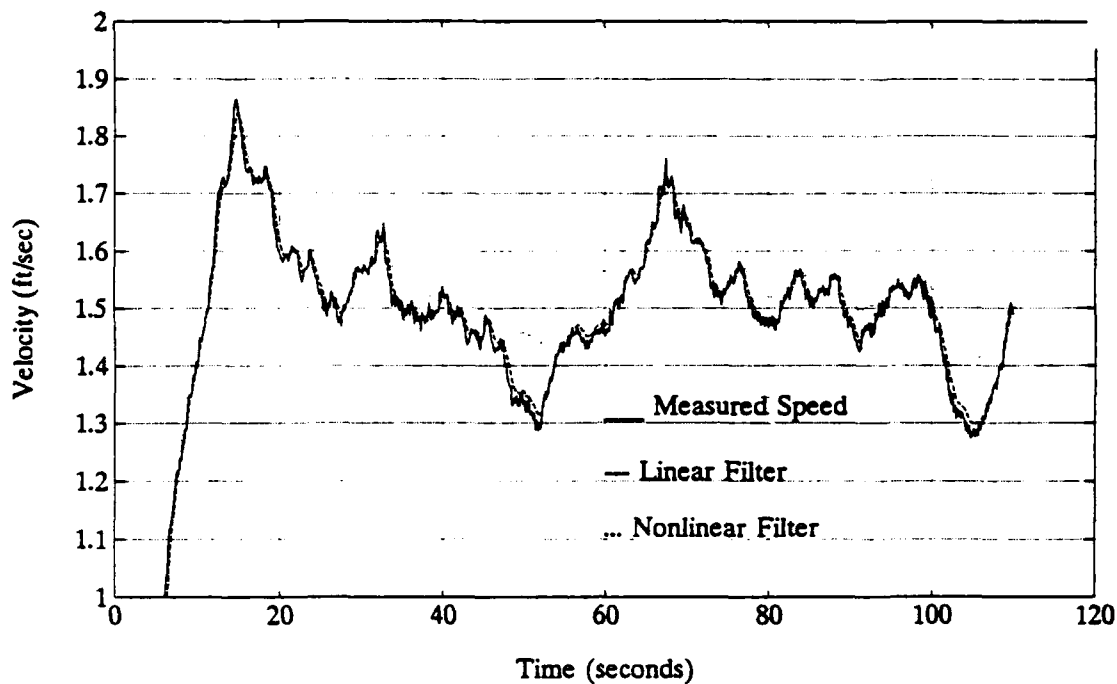
Figure 3.16 Linear and Nonlinear Kalman Filter Results

signal to the sliding mode speed controller.

J. CLOSED LOOP SIMULATION OF SLIDING MODE SPEED CONTROLLER WITH LINEAR KALMAN STATE FILTER

The linear Kalman State Filter was now used to filter the speed signal for the closed loop testing of the sliding mode speed controller with a value of η = 1.0. Realistic noise levels are injected into the measurement of the system model. The combined model output and state noise are fed into the linear Kalman State Filter prior to the state signal being processed by the sliding mode speed controller to close the loop on the simulation. Figure 3.17 shows the block diagram of the closed loop system. Figure 3.18 shows the commanded speed, measured system output speed and the sliding mode speed

56

controller commanded rpm. It is believed that a combination of both a speed sensor state filter and a lowering of the nonlinear switching term gain are appropriate for the proper operation of the sliding mode speed controller.
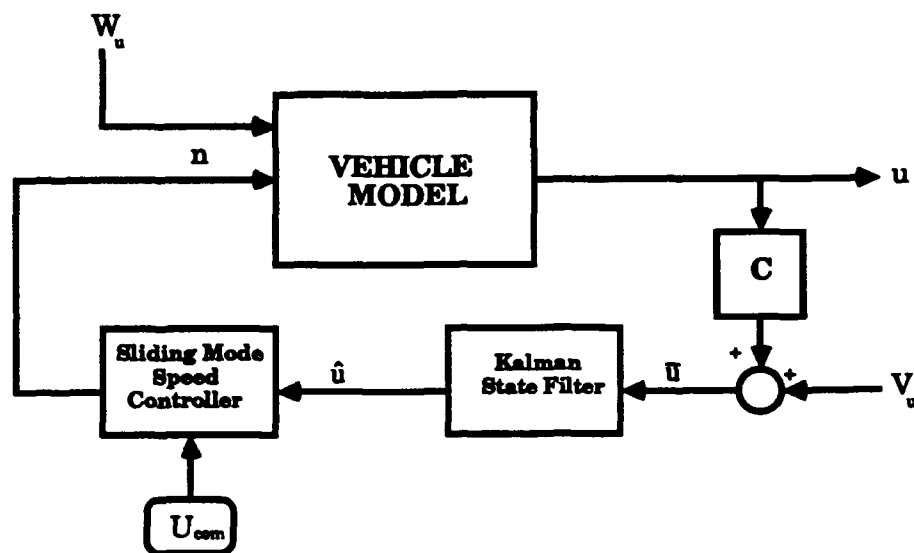
Figure 3.17 **Block Diagram of Closed Loop Testing of Sliding Mode Speed Controller With Inputs From the Kalman State Filter**
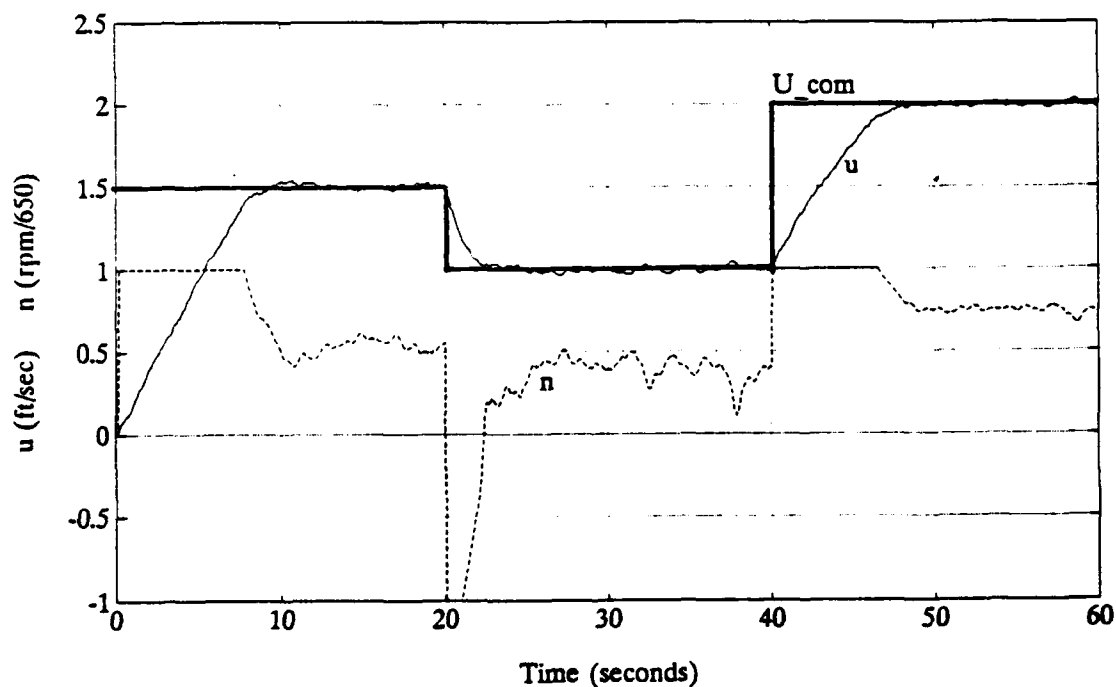
Figure 3.18 **Results Of The Closed Loop Simulation Using a Kalman State Filter and The Sliding Mode Speed Controller**

K. SUMMARY

It is proved in this chapter that the Kalman Parameter Filter is a valuable tool in system identification and is easily used as an on-line real time system parameter identifier. Even for a simple analytical model of the propulsion system, reasonable parameters can be estimated in real time and bounds placed on these estimates. If these estimates are exceeded, a fault monitor alarm can be initiated and further diagnostics preformed. It is beyond the scope of this thesis to pursue the diagnostics of this fault monitor but is within the scope to implement the on-line parameter estimator in the vehicles autopilot.

The sliding mode speed controller was easily adapted to this highly nonlinear system and provided reasonable results for initial testing, however it is believed that even better performance of the sliding mode speed controller will be realized when a state filter is used on the input speed signal to the speed controller.

IV.   STEERING SYSTEM CONTROL

A.   INTRODUCTION

The purpose of this chapter is to identify and verify the steering system parameters from experimental data recorded from trial runs of the NPS AUV II in the Naval Postgraduate School swimming pool. The parameters will then be used to update the full 6 DOF computer model developed by Warner (1991). Secondly, the design and testing of a sliding mode controller for the NPS AUV II, based on the refined steering system model, will be given.

B.   OUTLINE OF STEERING SYSTEM

The steering system for the NPS AUV II consists of four NACA 0015 control surfaces (rudders). Each of the rudders may be independently operated to control the vehicles orientation with respect to roll and yaw. At present, both upper and lower bow rudders act in unison as well as both upper and lower stern rudders. The bow and stern rudders also operate in equal but opposite directions thereby providing an additive couple to the input steering moment. Figure 1.1 shows the location of the rudders on the vehicle. Figure 4.1 shows the functional block diagram of the steering system. The steering controller receives inputs from the steering system Kalman State Filter for signals of r yaw rate and ψ heading angle. These signals

60
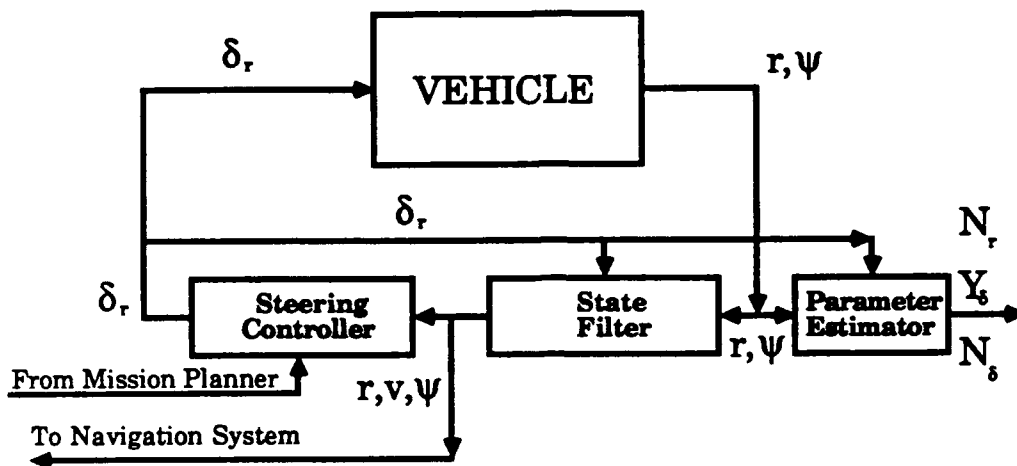
Figure 4.1   Functional Block Diagram of the Steering System

are compared to the commanded yaw rate and heading and used to compute a commanded rudder deflection by a sliding mode control law. The vehicles sensors also send a signal to the Kalman Parameter Estimator to provide an on-line fault monitor for N_r and N_δ. The monitoring of these parameters are a good indication of a system malfunction from internal diagnostics.

The vehicles equations of motion as developed by Boncal (1987) are further simplified with the system parameters scaled by Warner (1991) to a horizontal steering system model. The steering system is modeled by using Equation 2.2, sway equation of motion; Equation 2.5, yaw equation; and the Euler equation relations for $\dot{X}, \dot{Y}$ and ψ. The equations are simplified with the following assumptions:

1. The vehicle is operating in level flight without roll p, $\dot{p}$, q, $\dot{q}$, θ, ϕ and $w = 0$.

2. The body drag forces are negligible.

$$m\dot{v} + mx_G\dot{r} - Y_r\dot{r} - Y_v\dot{v} = -mur + Y_r ur + Y_v uv + u^2(Y_{\delta_{rb}}\delta_{rb} + Y_{\delta_{rs}}\delta_{rs})$$

$$I_z\dot{r} + mx_G\dot{v} - N_r\dot{r} - N_v\dot{v} = -mx_G ur + N_r ur + N_v uv + u^2(N_{\delta_{rb}}\delta_{rb} + N_{\delta_{rs}}\delta_{rs})$$

$$\dot{X} = u\cos\psi - v\sin\psi$$

$$\dot{Y} = u\sin\psi + v\cos\psi$$

$$\dot{\psi} = r$$

Rearranging and noting that the bow and stern rudder operate with equal magnitudes of deflection but opposite direction and that the size and shape of the bow and stern rudder is identical, therefore $Y_{\delta_{rb}} = Y_{\delta_{rs}}$ and $\delta_{rb} = -\delta_{rs}$. From the geometry of the vehicle $N_{\delta_{rb}} = 0.283\,L\,Y_{\delta_{rb}}$ and $N_{\delta_{rs}} = -0.377\,L\,Y_{\delta_{rs}}$. Using the above relations the sway and yaw equations can be written as:

$$(m - Y_v)\dot{v} + (mx_G - Y_r)\dot{r} = Y_v uv + (Y_r - m)ur + Y_\delta u^2 \delta_r \qquad \textbf{(4.1)}$$

$$(mx_G - N_v)\dot{v} + (I_z - N_r)\dot{r} = N_v uv + (N_r - mx_G)ur + N_\delta u^2 \delta_r \qquad \textbf{(4.2)}$$

62

where:

$\delta_r = \delta_{rs} = -\delta_{rb}$ rudder angle deflection in radians

$Y_\delta = Y_{\delta_{rs}} - Y_{\delta_{rb}} = 0.0$ lateral rudder force

$N_\delta = N_{\delta_{rs}} - N_{\delta_{rb}} = -0.377 L Y_{\delta_{rs}} - 0.283 L Y_{\delta_{rb}} = -4.8194 Y_{\delta_{rs}}$

rudder coupling moment

The state space form of the sway, yaw and heading equations are written as follows:

$$\dot{x} = M^{-1}Ax + M^{-1}Bu + W$$

where:

$x = [v \ r \ \psi]^T$ is the state vector

$$M = \begin{bmatrix} (m - Y_v) & (mx_G - Y_r) & 0 \\ (mx_G - N_v) & (I_z - N_r) & 0 \\ 0 & 0 & 1 \end{bmatrix} \text{ is the mass matrix}$$

$$A = \begin{bmatrix} Y_v u & (Y_r - m)u & 0 \\ N_v u & (N_r - mx_G)u & 0 \\ 0 & 1 & 0 \end{bmatrix} \text{ is the dynamics matrix}$$

$$B = \begin{bmatrix} Y_\delta u^2 \\ N_\delta u^2 \\ 0 \end{bmatrix} \text{ is the input matrix}$$

$$W = \begin{bmatrix} w_v \\ w_r \\ w_\psi \end{bmatrix} \text{ is the system noise vector}$$

63

The system noise vector is assumed to be independent random white noise associated with each state. In addition to the system equations, we require the nonlinear Euler relations for $\dot{X}$ and $\dot{Y}$ to provide the vehicles global position.

C. EXPERIMENTAL WORK WITH NPS AUV II

Of the numerous trials run with the NPS AUV II, the two which were most informative in regards to the steering system parameter identification were the 'Zig-Zag' and 'Figure 8' patterns run in the NPS swimming pool. The 'Zig-Zag' pattern allows an oscillatory forcing function to excite the hydrodynamic terms having to do with small vehicle oscillations. Figure 4.2 shows δ_r the input rudder deflection and the vehicle response in terms of r yaw rate and ψ heading angle. Figure 4.3 shows the same input and outputs for the 'Figure 8' trial run. The 'Figure 8' places the vehicle in a hard turn continuously alternating from side to side. It is noted that the Zig-Zag pattern has one hard turn in the middle of the data due to the finite length of the NPS swimming pool. This one turn can be correlated to the series of turns in the 'Figure 8' data set.
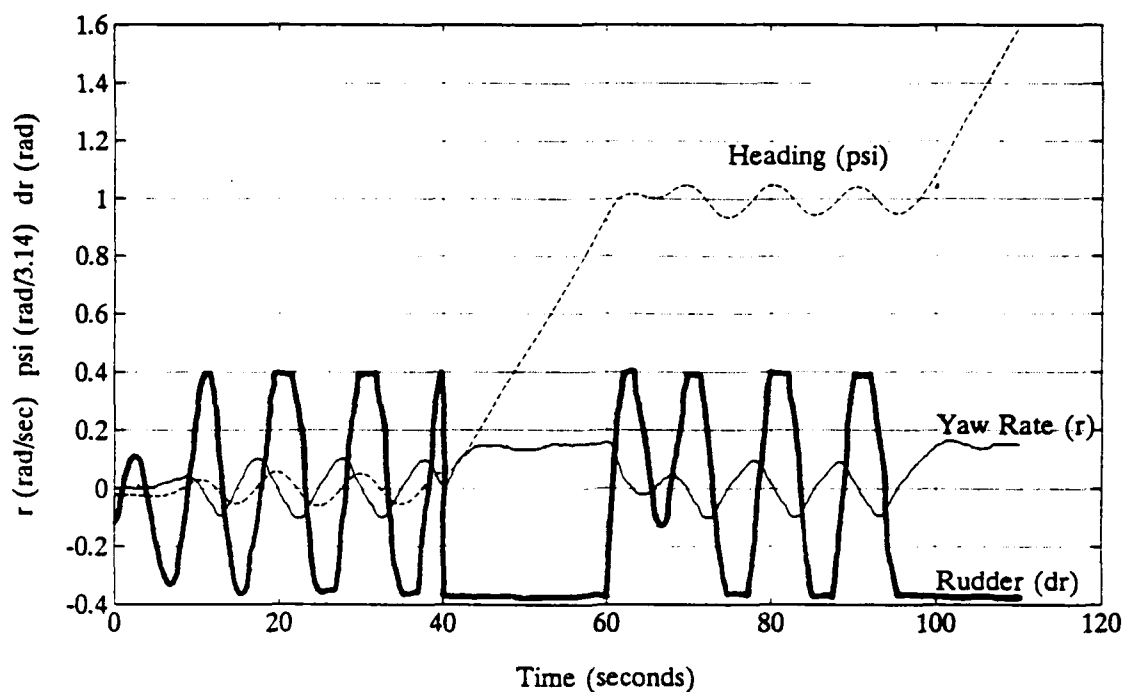
Figure 4.2 δ_r, r and ψ For 'Zig-Zag' Trial

Figure 4.3 δ_r, r and ψ For 'Figure 8' Trial

65
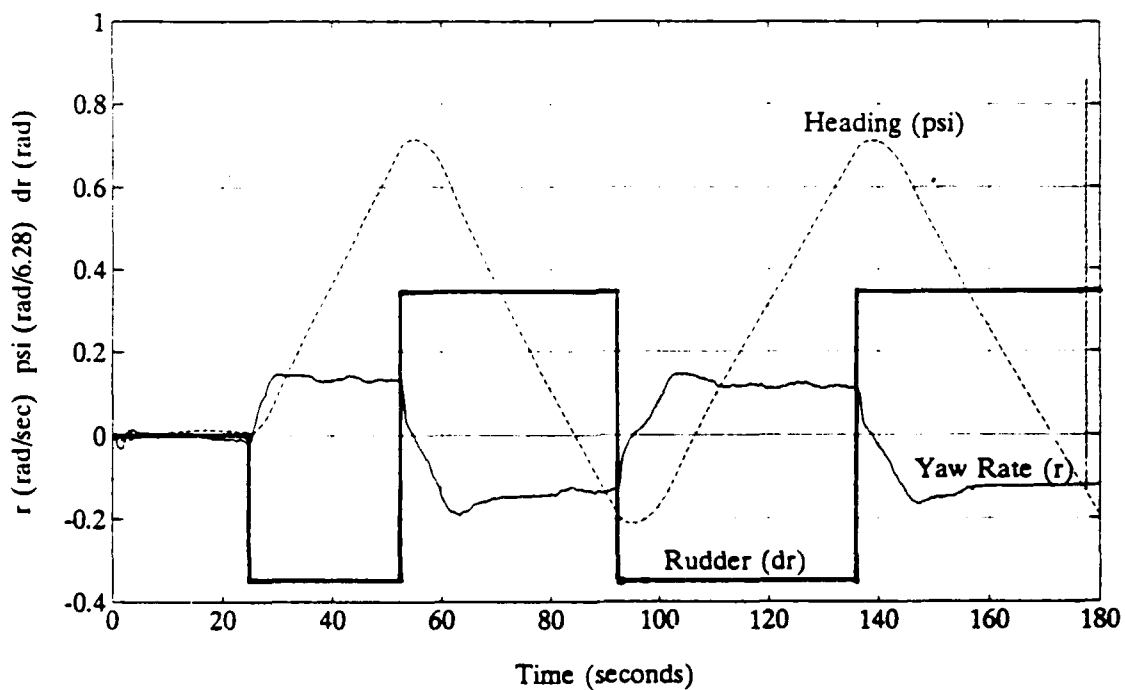
D. PARAMETER IDENTIFICATION

It is desired to develop a simple analytical model for the steering system which can also be used as a fault diagnostics monitor. As discussed earlier, having symmetric bow and stern rudders cancels the effective sway force applied to the vehicle and doubles the yaw moment applied. This canceling effect leaves $Y_\delta = 0$, therefore there is no direct input to Equation 4.1, the sway equation of motion. The only input to the sway equation is from the mass coupling and the yaw rate. In addition, the vehicle is designed to turn quickly from the large input yaw moment. This justifies the use of only the yaw equation of motion for the steering system simplified model because the yaw equation of motion is the only one that is directly forced by the input rudder deflection.

1. First Order Model For Parameter Identification

The sway velocity and acceleration are not measured presently on the NPS AUV II. This makes identification of the sway equation hydrodynamic coefficients impracticable and highly questionable. The following assumption is made to simplify Equation 4.2 to the first order steering model based on yaw rates.

The sway velocity and acceleration are small compared to the yaw rate and yaw acceleration. v and $\dot{v} = 0$.

66

Equation 4.2 simplifies to:

$$(I_z - N_{\dot{r}})\,\dot{r} = (N_r - mx_G)\,ur + N_\delta\,u^2\,\delta_r + \varepsilon_r$$

dividing through by the inertia term:

$$\dot{r} = \frac{(N_r - mx_G)}{(I_z - N_{\dot{r}})}\,ur + \frac{N_\delta}{(I_z - N_{\dot{r}})}\,u^2\,\delta_r + [\varepsilon_r]$$

combining terms to simplify the coefficients to a two parameter equation. The first order equation is now ready for use in the Kalman Parameter Filter as a measurement equation.

$$\dot{r} = (NR)\,ur + (N\delta)\,u^2\,\delta_r + [\varepsilon_r]$$

$$\dot{r} = [\,ur \quad u^2\,\delta_r\,]\begin{Bmatrix} NR \\ N\delta \end{Bmatrix} + [\varepsilon_r] \tag{4.3}$$

where:

$$NR = \frac{(N_r - mx_G)}{(I_z - N_{\dot{r}})} \quad , \quad N\delta = \frac{N_\delta}{(I_z - N_{\dot{r}})} \quad , \quad [\varepsilon_r] = \frac{\varepsilon_r}{(I_z - N_{\dot{r}})}$$

The measurement equation 4.3 contains the two terms **NR** and **Nδ** which can be identified in the same fashion as the propulsion system parameters. The system equation for the parameters has the same form as Equation 3.3, but is written for two parameters. Where **A** is a 2x2 matrix of zeros and **B** is a 2x2 diagonal matrix of weighing values for the noise placed on each of the

67

$$\frac{d}{dt}\begin{Bmatrix} NR \\ N\delta \end{Bmatrix} = \begin{bmatrix} A \end{bmatrix} \begin{Bmatrix} NR \\ N\delta \end{Bmatrix} + \begin{bmatrix} B \end{bmatrix} Q \qquad\qquad (4.4)$$

parameters. For this analysis a weighing of 1.0 for each parameter (equal weighing) is used. Three values of parameter noise Q are tested on the Kalman Parameter Filter.

Equation 4.3 has a term $[\varepsilon_t]$ which is analogous to $[\delta_a]$ from the surge equation. This is the measurement noise and is estimated the same way by playing the Equation 4.3 model with nominal values and subtracting the measured yaw acceleration. If the acceleration error is assumed to be white Gaussian a standard deviation and variance can be computed. Figure 4.4
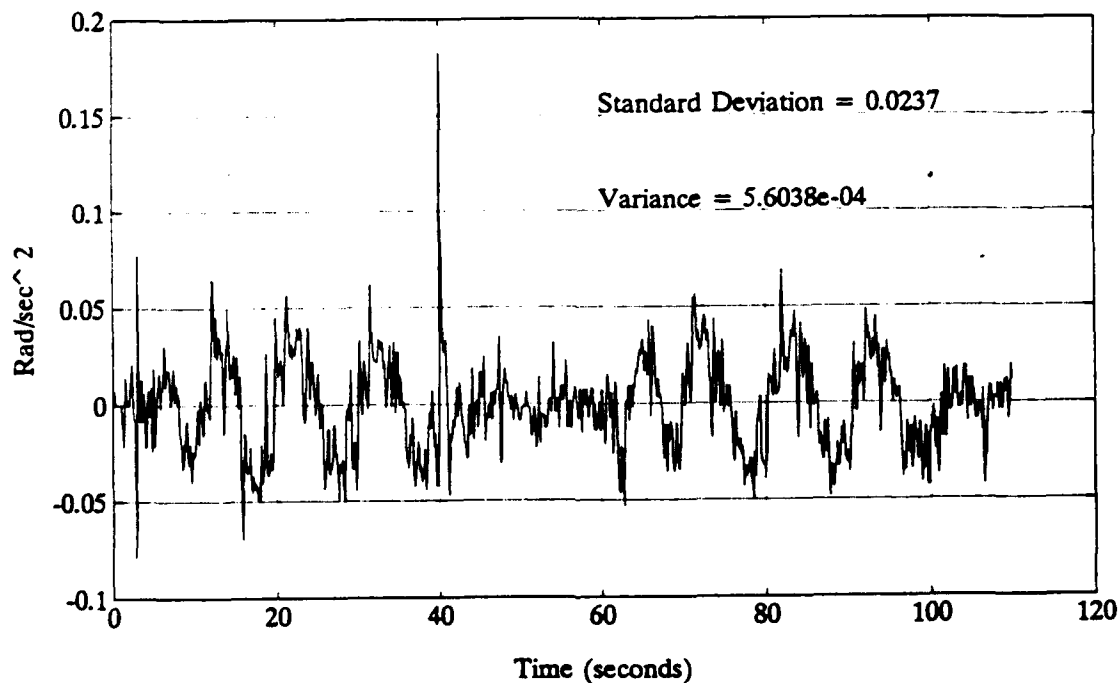
Figure 4.4 Plot of Yaw Acceleration Error

shows the yaw acceleration error between the calculated yaw acceleration and the measured yaw acceleration. The standard

deviation and variance of this error is also indicated in the figure and summarized in Table 4.2 under nominal model.

The N_r coefficient was estimated by Warner and is considered here to be accurate. The objective of this section is to identify the **NR** and **Nδ** coefficients. Nominal values of N_r and N_δ were identified by Warner and are used to calculate the initial parameter estimates of **NR** and **Nδ**. These nominal values are summarized in Table 4.2.

The estimation error covariance of the parameters is not known but is identified by replaying the Kalman Parameter Filter on the experimental data repeatedly as in Chapter III until the Parameter Filter converges to a steady state value of estimation error covariance. The steady state values of estimation error covariance are summarized in Table 4.1 for the three values of **Q** tested on the Parameter Filter.

TABLE 4.1   STEADY STATE ESTIMATION ERROR COVARIANCE

Q	10^{-4}	10^{-6}	10^{-8}
$P_{k_{NR}}$	680.0×10^{-5}	36.93×10^{-5}	3.657×10^{-5}
$P_{k_{N\delta}}$	1190.0×10^{-5}	41.64×10^{-5}	3.418×10^{-5}

Figure 4.5 shows the results of three data passes, for the three values of **Q** tested through the Kalman Parameter Filter, for the estimation of **NR** . The value of **Q** equal to 10^{-6} was

chosen as the best response on a qualitative measure because it is not so fast as to include all the system noise on the parameter being estimated, but is fast enough to identify the variation in NR and Nδ in the turn.
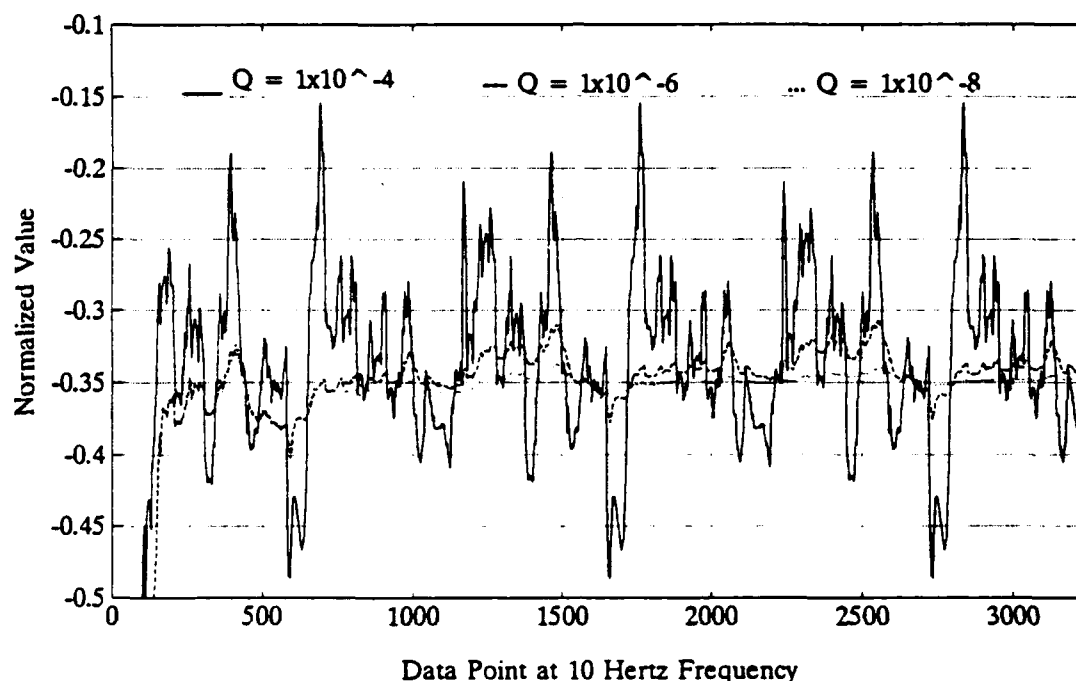
Figure 4.5   Estimation Of NR For Various Values Of Q

The values of **NR** and **Nδ** given in Table 4.2 are the mean value of the final filter run. The final filter run is the run in which the final value of the parameter estimates and the estimation error covariances are the same as the initial values of the filter run. This ensures the filter has converged to as near as possible the steady state values of the actual parameters.

The estimated values of the parameters are now replayed in the simulation of Equation 4.3. The resulting yaw rate error $[\varepsilon_r]$ and yaw acceleration error $[\varepsilon_{\dot{r}}]$ is computed by taking the

70

difference between the measured and modeled values over the data record. The standard deviation and the variance of the yaw rate error and the yaw acceleration error over the data record are tabulated in Table 4.2 for each value of **Q**. The results in the table indicate that for **Q** = 1x10^{-6}, the identified values of **NR** = -0.1709 and **Nδ** = -0.0568 give reduced rate and acceleration errors between the first order model and the experimental data when compared to the nominal model. The filter run with **Q** = 1x10^{-8} required 8 data runs for the estimation error covariance to converge to a steady state value. This filter run gave a better estimate but is too slow at converging, requiring over 15 minutes of real time data to converge to a steady state value. This excessive amount of identification time is too great for an on-line fault monitor and the faster filter with **Q** = 1x10^{-6} was chosen as the fault monitor to use. The simulation results of Equation 4.3 are shown in Figure 4.6 for the nominal values predicted by Warner and the refined values from the first order model. Figure 4.7 shows the yaw acceleration error following parameter identification. The improvement over Figure 4.4 is easily seen as the obvious oscillations have been removed from the acceleration error and the acceleration error now resembles white noise much more closely.
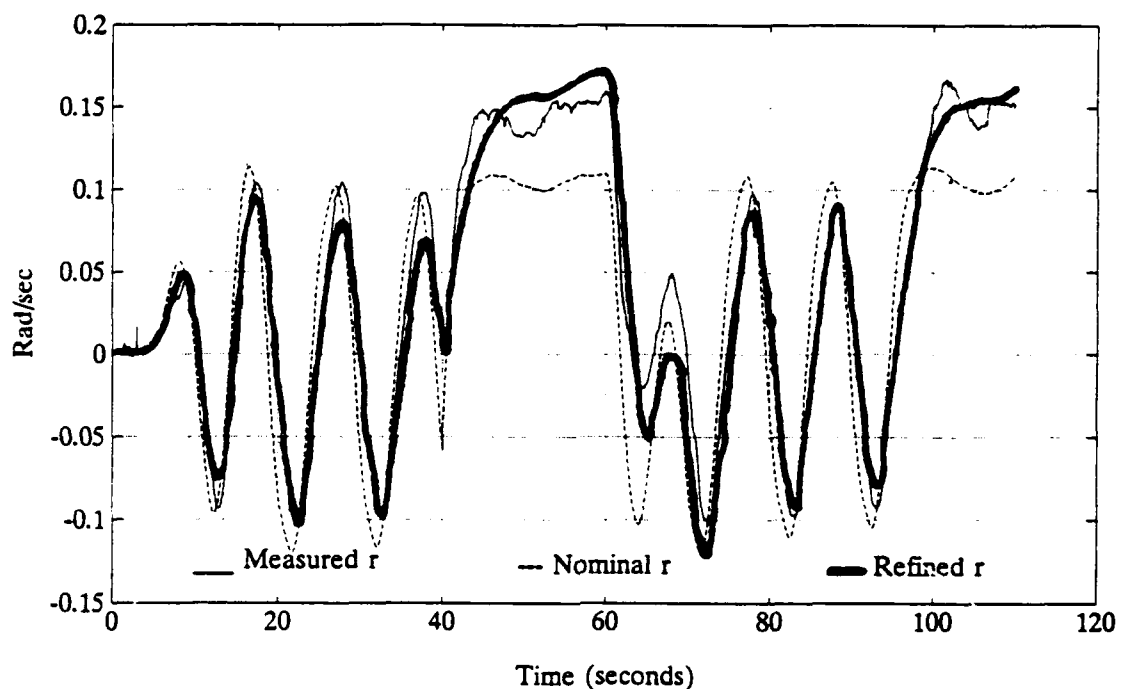
Figure 4.6   Simulation Of Yaw Rate From Nominal Values And
Refined Values Following Identification
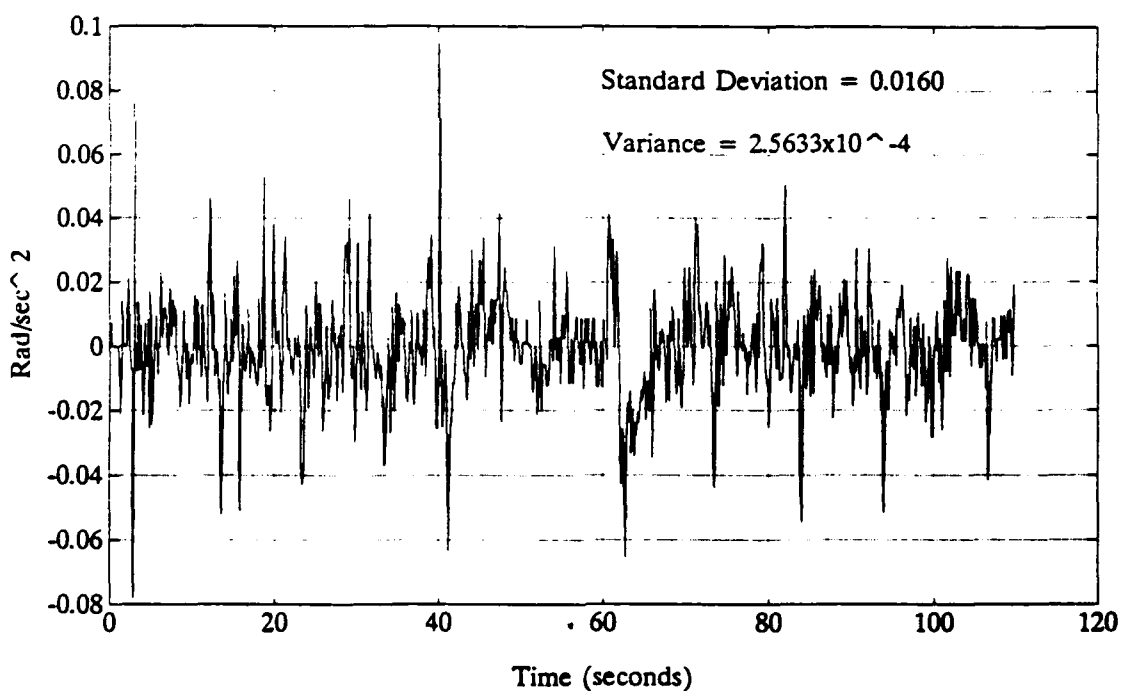
Figure 4.7   Yaw Acceleration Error Following Identification

72

TABLE 4.2   KALMAN PARAMETER FILTER RESULTS FOR STEERING SYSTEM

Q	Nominal Model	10^{-4}	10^{-6}	10^{-8}
NR	-0.5201	-0.1684	-0.1709	-0.1750
Nδ	-0.1073	-0.0562	-0.0568	-0.0573
[ε_r] STD DEV	0.0359	0.0173	0.0172	0.0167
[ε_r] VARIANCE	13.0×10^{-4}	3.00×10^{-4}	2.95×10^{-4}	2.80×10^{-4}
[ε_r] STD DEV	0.0237	0.0161	0.0160	0.0159
[ε_r] VARIANCE	5.60×10^{-4}	2.58×10^{-4}	2.56×10^{-4}	2.54×10^{-4}

2. Identification of Y_δ from N_δ

The input moment due to a rudder deflection is related to the location of the vehicles rudders. Therefore, the lateral force applied to the vehicle by each rudder may be identified. The input moment due to rudder deflection is equal to the lift force developed by the rudder times the distance between the rudders.

$$N_\delta = Y_{\delta_{rs}} x_s - Y_{\delta_{rb}} x_b$$

Where:

$Y_{\delta_{rs}} = Y_{\delta_{rb}}$ due to identical rudders

$x_b = 0.283\,L$ is the distance from the center of the vehicle to the bow rudder

$x_s = -0.377\,L$ is the distance from the center of the vehicle to the stern rudder

Using the above relations, the lateral rudder coefficient $Y_{\delta rs}$ and $Y_{\delta rb}$ can be directly determined when the N_δ coefficient is determined.

$$N_\delta = Y_{\delta_{rs}}(x_s - x_b) = -4.8194\,Y_{\delta_{rs}}$$

$$N_\delta = N\delta(I_z - N_r) \qquad Y_{\delta_{rs}} = Y_{\delta_{rb}} = \frac{-N_\delta}{4.8194}$$

The hydrodynamic coefficients needed for the 6 DOF computer model are the non-dimensional hydrodynamic coefficients defined as follows:

$$\acute{N}_r = \frac{N_r}{\frac{1}{2}\rho L^4} \qquad \acute{Y}_{\delta_{rs}} = \frac{Y_{\delta_{rs}}}{\frac{1}{2}\rho L^2} \qquad \acute{Y}_{\delta_{rb}} = \frac{Y_{\delta_{rb}}}{\frac{1}{2}\rho L^2}$$

$$\acute{N}_{\delta_{rs}} = -0.377\,L\,\acute{Y}_{\delta_{rs}} \qquad\qquad \acute{N}_{\delta_{rb}} = 0.283\,L\,\acute{Y}_{\delta_{rb}}$$

The identification yields the values in Table 4.3 for the non-dimensional hydrodynamic coefficients.

TABLE 4.3   NON-DIMENSIONAL   HYDRODYNAMIC   COEFFICIENTS FROM FIRST ORDER MODEL

$\acute{N}_r$	$\acute{Y}_{\delta_{rs}}$	$\acute{Y}_{\delta_{rs}}$	$\acute{N}_{\delta_{rs}}$	$\acute{N}_{\delta_{rs}}$
-0.00332	0.01241	0.01241	-0.03417	0.02565

3.   Second Order Model For Parameter Identification

The identification results of the simplified first order model were encouraging and a more complicated model including the sway equation is attempted. The desired outcome of the second order model identification is to identify an additional hydrodynamic coefficient Y_v. Construction of the second order model uses the sway and yaw equation in the form of Equations 4.1 and 4.2 written as follows:

$$a_{11}v + a_{12}r = Y_{\delta}u^2\delta_r \qquad 1)$$

$$a_{21}v + a_{22}r = N_{\delta}u^2\delta_r \qquad 2)$$

where:

$$a_{11} = (m - Y_v)s - Y_v u$$

$$a_{12} = (mx_G - Y_r)s - (Y_r - m)u$$

$$a_{21} = (mx_G - N_v)s - N_v u$$

$$a_{22} = (I_z - N_r)s - (N_r - mx_G)u$$

solving equation 1) for **v** sway velocity and substituting into 2) Yields:

$$(a_{22} a_{11} - a_{21} a_{12}) r = (a_{11} N_\delta - a_{21} Y_\delta) u^2 \delta_r$$

expanding and rearranging gives:

$$[As^2 + Bus + Cu^2] r = [Eu^3 + Fu^2 s] \delta_r$$

$$A\ddot{r} + Bu\dot{r} + Cu^2 r = Eu^3 \delta_r + Fu^2 \delta_r$$

where:

$A = (m - Y_v)(I_z - N_r) - (mx_G - N_v)(mx_G - Y_r)$

$B = (mx_G - N_v)(Y_r - m) + (mx_G - Y_r) N_v - (m - Y_v)(N_r - mx_G) - (I_z - N_r) Y_v$

$C = Y_v (N_r - mx_G) - N_v (Y_r - m)$

$E = N_v Y_\delta - Y_v N_\delta$

$F = (m - Y_v) N_\delta - (mx_G - N_v) Y_\delta$

The above equation can be used as a measurement equation for the Kalman Parameter Filter. The hydrodynamic coefficients are mixed in the 5 coefficients of the measurement equation. The **A** coefficient has terms dealing with mass, inertia, added mass and added inertia only. These coefficients are assumed to be accurate from the analysis of Warner (1991). This leaves four independent equations to solve for the six desired damping and input parameters.

76

The following assumptions are used to reduce the number of coefficients to solve for:

1. $Y_\delta = 0$ $Y_{\delta rs} = Y_{\delta rb}$ due to symmetry of bow and stern rudders.

2. N_v and Y_r are small due to vehicle symmetry and are neglected.

The above assumptions have reduced the number of coefficients to solve for from six to three with four independent equations. We now have one redundant equation which can be used as a check of the coefficients. The resulting parameters to be identified by the Kalman Parameter Filter are now:

$$A = (m - Y_v)(I_z - N_r) - (mx_G - N_v)(mx_G - Y_r)$$

$$B = -(mx_G - N_v)m - (m - Y_v)(N_r - mx_G) - (I_z - N_r)Y_v$$

$$C = Y_v(N_r - mx_G)$$

$$E = -Y_v N_\delta$$

$$F = (m - Y_v)N_\delta$$

Using a central difference approximation, the measurement equation is now defined as:

$$\left[\frac{1}{\Delta t^2}(r_{k+1} - 2r_k + r_{k-1}) , \frac{u}{2\Delta t}(r_{k+1} - r_{k-1}) , u^2 r_k , -u^3 \delta_k , -\frac{u^2}{2\Delta t}(\delta_{k+1} - \delta_{k-1})\right]\begin{Bmatrix} A \\ B \\ C \\ E \\ F \end{Bmatrix}$$

Having the measurement equation defined, the parameter system equation is defined the same as the first order model

77

Equation 4.4 with the exception that the dynamics matrix is a 5x5 matrix of zeros and the B matrix is a diagonal 5x5 weighing matrix. Again the parameter noise is not known but the value of $Q = 1 \times 10^{-6}$ was the best for the first order model and was chosen as the value to use for this model. The system error covariance is identified by running a simulation of the measurement equation based on nominal hydrodynamic coefficients and taking the variance of the measurement equation error over the data record as shown in Figure 4.8. The measurement equation error is the difference between the measured yaw acceleration and the modeled yaw acceleration taken at each time step in the data record. The initial parameter estimates used are the initial estimates of Warner. The initial estimation error covariance is set equal to 1.0 for all parameters and the filter is run to achieve steady state values of the estimation error covariance.

The filter was run on entire length of the data set which included the hard turn at the end of the pool with the rudder saturated at 0.4 radians. This pass through the filter produced large jumps in the predicted parameters when the rudder was commanded hard over. This jump in the predicted parameters caused the redundant set of equations to have complex solutions. As a result of the redundant equation giving complex roots, the data set was shortened to the first 40 seconds of data just up to where the rudder was commanded hard over. This shorter data set was run through the parameter
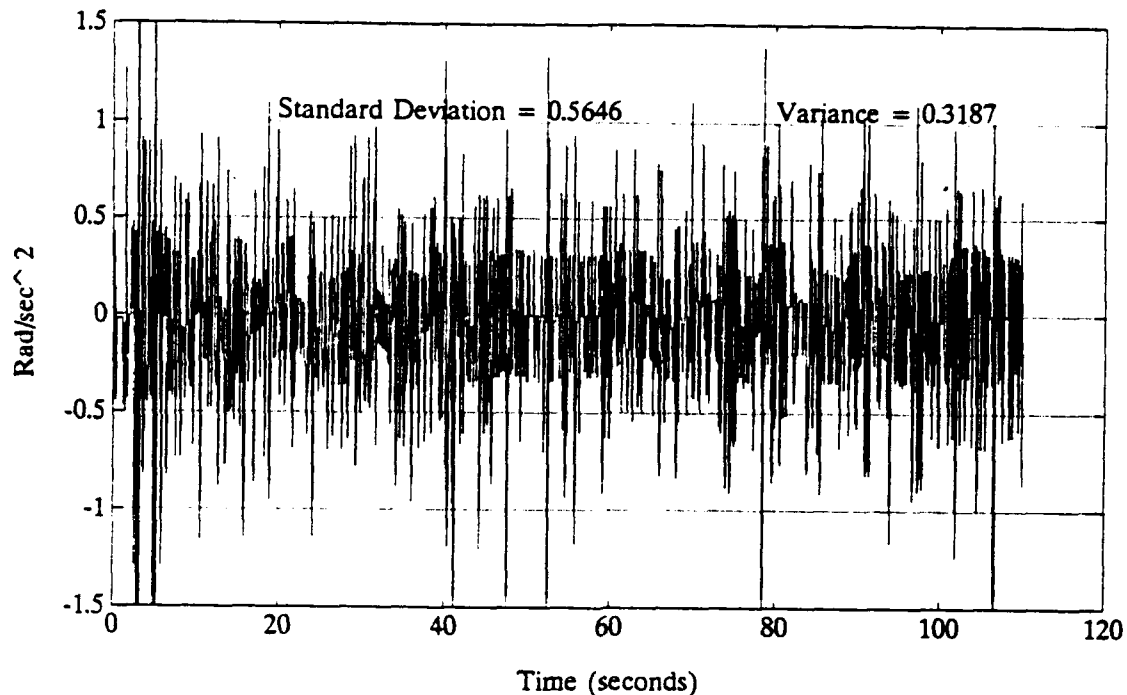
Figure 4.8 Plot Of Yaw Acceleration Error For Second Order Model

filter repeatedly, reinitializing the filter to the final values of the estimated parameters and the estimation error covariance from the previous data pass. The results of this identification of parameters is shown in Figure 4.9.

The figure shows that the A parameter is held constant as this parameter was assumed to be known. The B, E and F parameters appear to be settling to a steady state value but the C parameter is continuing to drift and after the sixth pass through the filter the redundant equation provided complex solutions. Hydrodynamic coefficients are real valued quantities and must not be complex. The parameter filter did provide estimates of the hydrodynamic coefficients prior to appearing questionable in which the redundant solutions

79
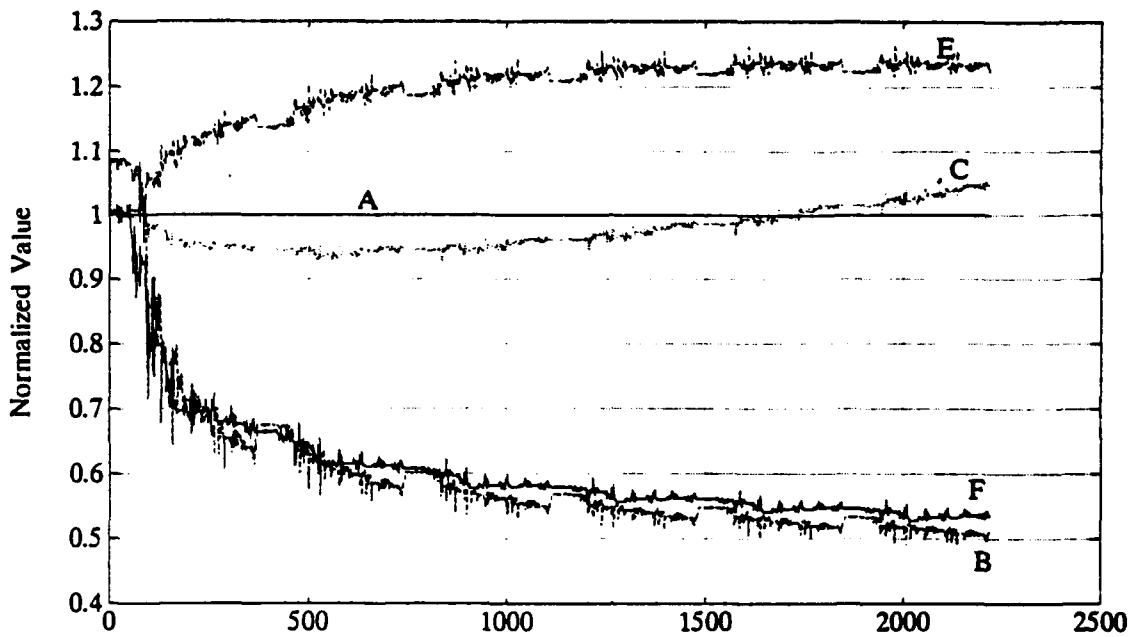
Figure 4.9   Results Of Second Order Parameter Identification

matched. The results of the second order model are well matched to the results of the first order model prior to obtaining complex results, as compared in Table 4.4 below. The results of the second order model are both encouraging and discouraging: encouraging in the fact that the results are so close to those of the simple first order model and discouraging that the parameter filter did not converge to distinct values. The pursuit of a second order model is not continued in this thesis but is recommended for further study.

TABLE 4.4   COMPARISON OF NON-DIMENSIONAL HYDRODYNAMIC COEFFICIENTS FROM FIRST AND SECOND ORDER MODELS

	$\acute{N}_r$	$\acute{Y}_{\delta_r}$	$\acute{Y}_v$
First Order Model	-0.00332	0.01241	N/A
Second Order Model	-0.00460	0.01260	-0.08920

4. Parameter Verification By Sensitivity Analysis

The four coefficients of most importance in the steering system dynamics are Y_v, Y_δ, N_r and N_δ. Of the four coefficients Y_δ and N_δ have a kinematic relationship to each other. The purpose of this section is to study the sensitivity of each of the three independent coefficients on the analytical model of the steering system. The steering system model described earlier of the two state equations (sway and yaw) and the three kinematic relations predicts the vehicles heading, yaw rate and global position in the NPS swimming pool. The analytical model is run holding all coefficients constant and varying one at a time from -60% to +60% in 20% increments from the nominal value as refined from the Kalman Parameter Filter. The results on yaw rate are shown on Figures

81

4.10 to 4.12, and results on predicted sway velocity are shown in Figures 4.13 to 4.15. Vehicle heading is a direct integration of the yaw rate and therefore if the yaw rate can be predicted accurately, the vehicle heading will also be predicted accurately. It is seen from Figures 4.12 and 4.15 that a variation in Y_v has only a small effect on the change in yaw rate but has a dramatic effect on sway velocity. Table 4.9 summarizes the effects on the yaw rate and yaw acceleration errors from varying the Y_v coefficient and indicates that as Y_v increases, the errors decrease. The sway velocity of the NPS AUV II is not measured directly on the vehicle so a direct comparison of measured to modeled sway velocity is not possible. We have forward and left side sonar data, Figures 4.16 and 4.17, which can be used to plot the pool wall when combined with the vehicles dead reckoned position and heading, thereby verifying the predicted position of the vehicle. Using the measured vehicle speed and the measured vehicle heading, only the vehicles sway velocity is needed to accurately define the vehicles dead reckoned position. In this way the correct Y_v can be identified by the amount of sway velocity needed to provide the correct vehicle path in the pool.

From the figures for variations in Y_δ and N_r, it is seen that a change in these coefficients affects both analytical results of yaw rate and sway velocity considerably. It is necessary to settle in on the correct Y_δ and N_r prior to

82

adjusting the Y_v to correct the sway velocity. Table 4.7 shows the yaw rate and yaw acceleration errors for N_r and indicates N_r generates a minimum error when increased by approximately 27%. Table 4.8 shows the yaw rate and yaw acceleration error for Y_δ and indicates that a decrease of 14% is needed to minimize the yaw rate and yaw acceleration errors. Since an increase in N_r has the same effect as a decrease in Y_δ, some smaller percentage in each of these coefficients will produce the minimum yaw rate and yaw acceleration error. From a trial and error approach the combination of an increase of 18% in N_r a and a decrease of 5% in Y_δ produces the minimum errors.

With the Y_δ and the N_r coefficients refined, variations of the Y_v coefficient are investigated to provide the most accurate prediction of the vehicle path based on measured vehicle data of speed and heading, and the simulated sway velocity from the analytical model. The Y_v coefficient is correctly identified when the forward and left side sonar data effectively trace the correct boundary of the swimming pool. An increase of 20% in Y_v is seen to give the best vehicle track in the pool. Figure 4.18 shows the vehicle paths from the dead reckoning navigation system with and without sway velocity included and the forward looking sonar trace as it identifies the pool boundary. It is pointed out that for the trace without the sway velocity the track is tighter and shows the length of the pool is greater than actual. By including the properly calibrated sway velocity in the dead reckoning

navigation system the length of the pool is indicated correctly.

Figure 4.19 shows the same vehicle tracks for with and without sway velocity and shows the trace of the left side sonar as it traces out the side of the pool. It is pointed out that the sonar trace without the sway velocity correction shows the pool narrower than it actually is. The sonar trace with the sway velocity correction indicates the true width of the pool.

The final identified steering parameters are summarized as follows in Table 4.5 and the rate and acceleration errors are summarized in Table 4.6.

TABLE 4.5   FINAL   NON-DIMENSIONAL   STEERING   SYSTEM HYDRODYNAMIC COEFFICIENTS

$\acute{Y}_v$	$\acute{Y}_{\delta_{r\bullet}}$	$\acute{Y}_{\delta_{r\bullet}}$
-0.1070	0.0118	0.01118

$\acute{N}_r$	$\acute{N}_{\delta_{r\bullet}}$	$\acute{N}_{\delta_{r\bullet}}$
-0.0039	-0.0325	0.0244

TABLE 4.6   FINAL YAW RATE AND YAW ACCELERATION ERRORS

STD DEV $[\varepsilon_r]$	VARIANCE $[\varepsilon_r]$	STD DEV $[\varepsilon_r]$	VARIANCE $[\varepsilon_r]$
0.0160	2.56×10^{-4}	0.0159	2.52×10^{-4}
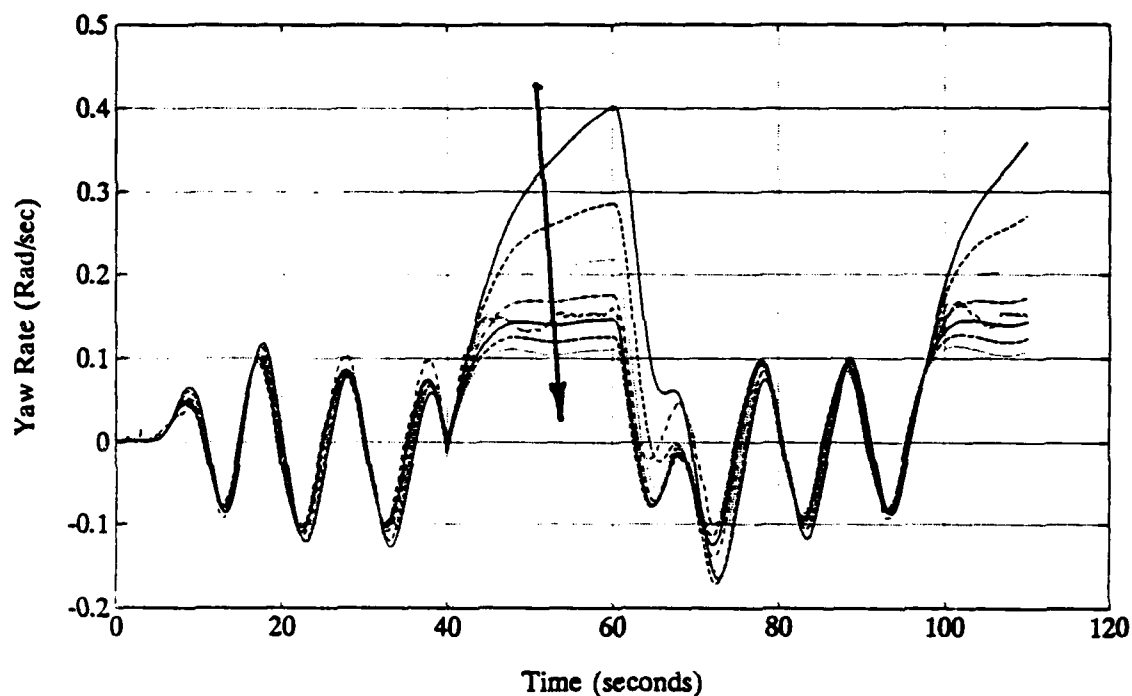
Figure 4.10 Parameter Sensitivity of N_r on Yaw Rate
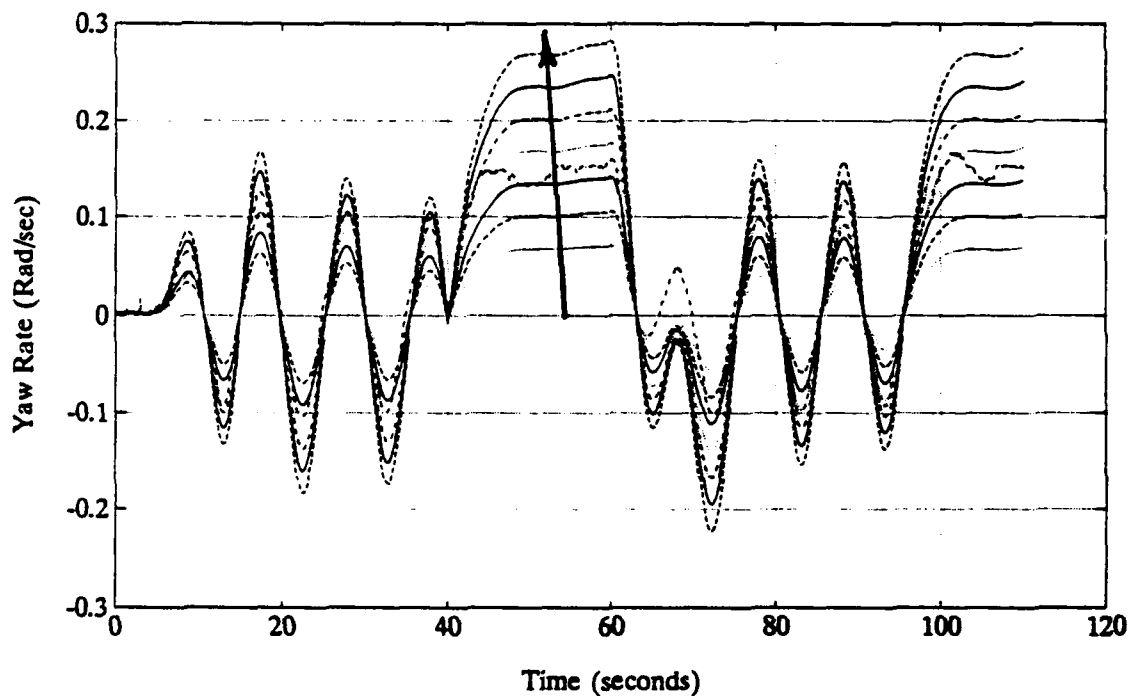
Figure 4.11 Parameter Sensitivity of Y_δ on Yaw Rate

85
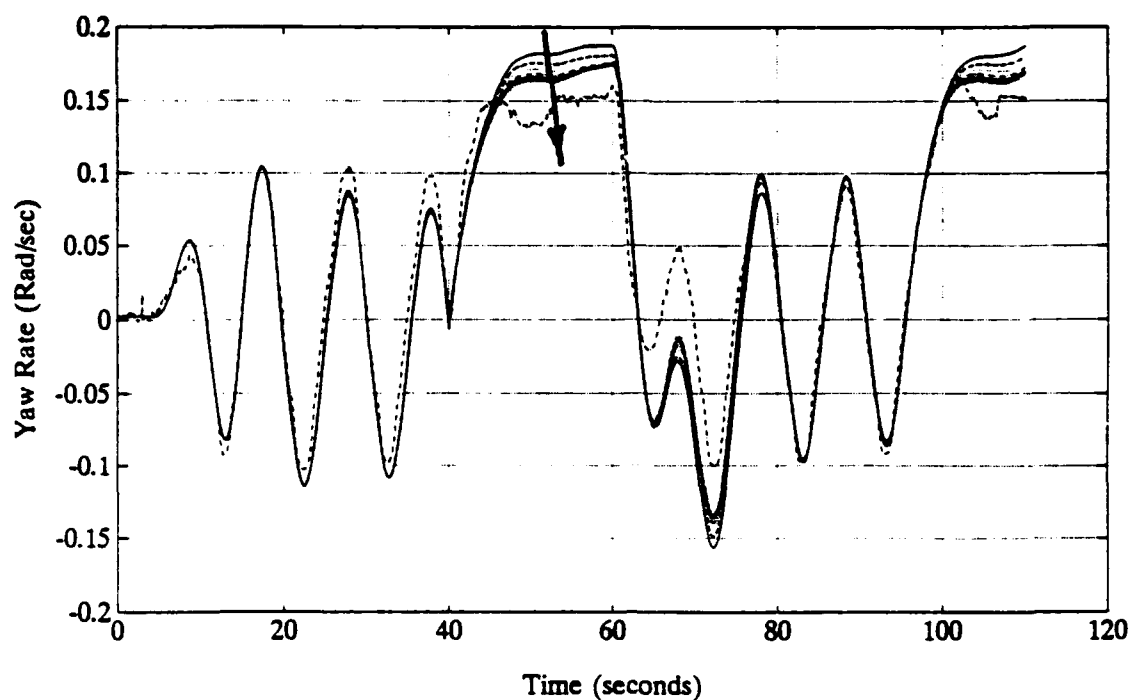
Figure 4.12 Parameter Sensitivity of Y_v on Yaw Rate
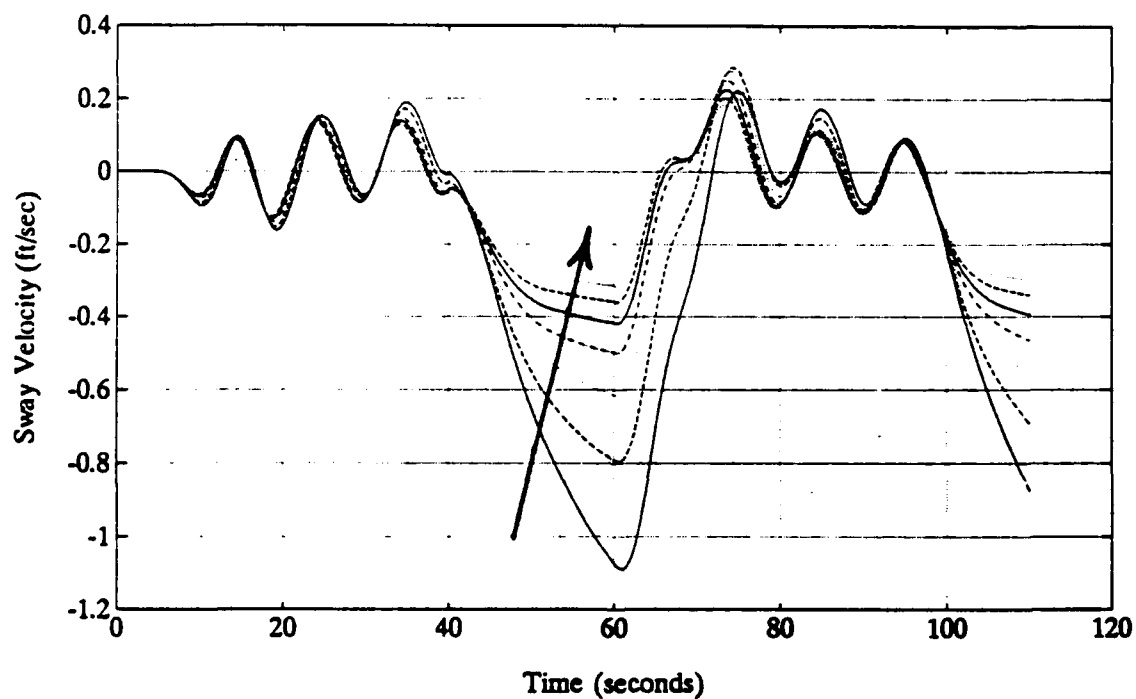
Figure 4.13 Parameter Sensitivity of N_r on Sway Velocity

86
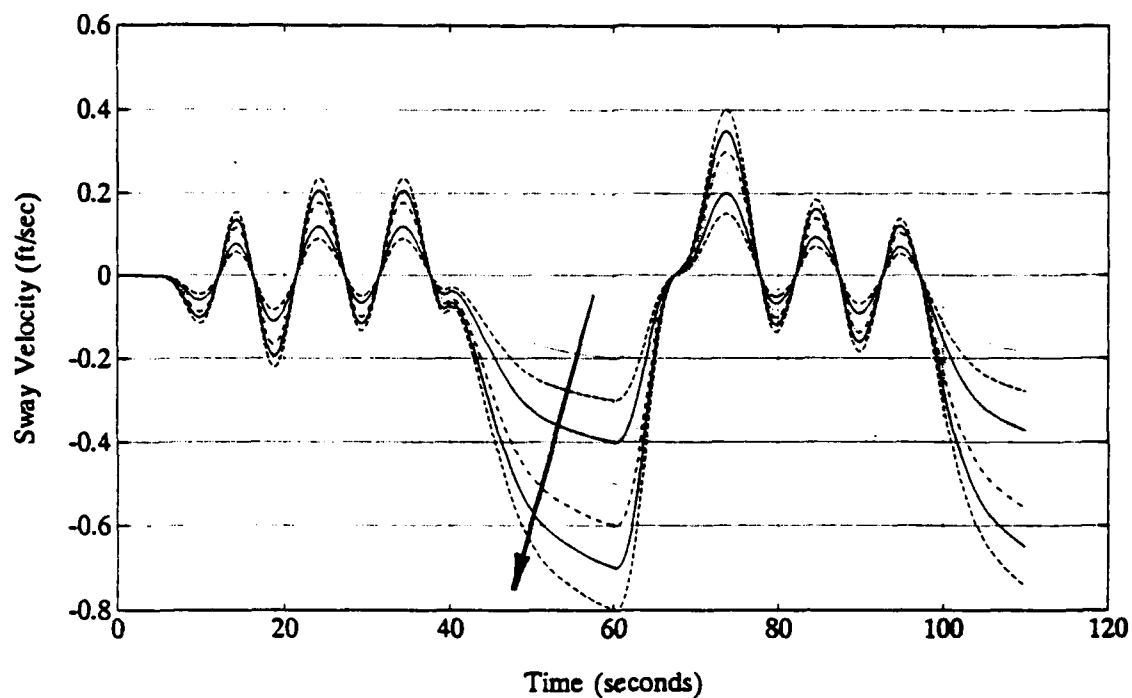
Figure 4.14 Parameter Sensitivity of Y_δ on Sway Velocity
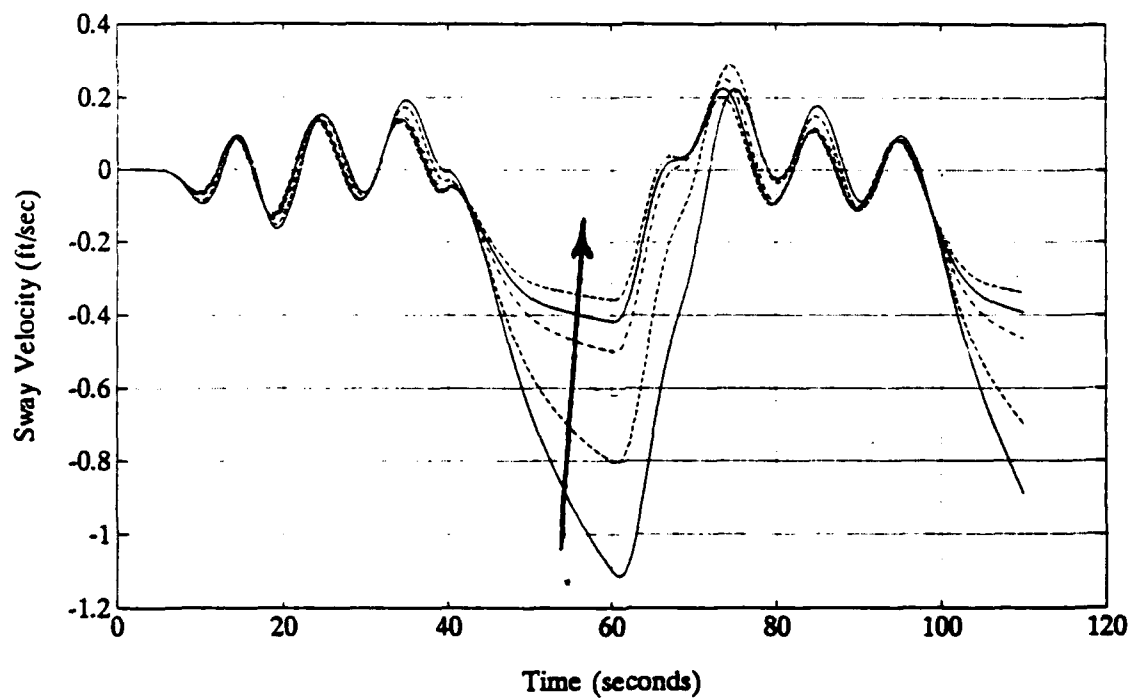
Figure 4.15 Parameter Sensitivity of Y_v on Sway Velocity

87
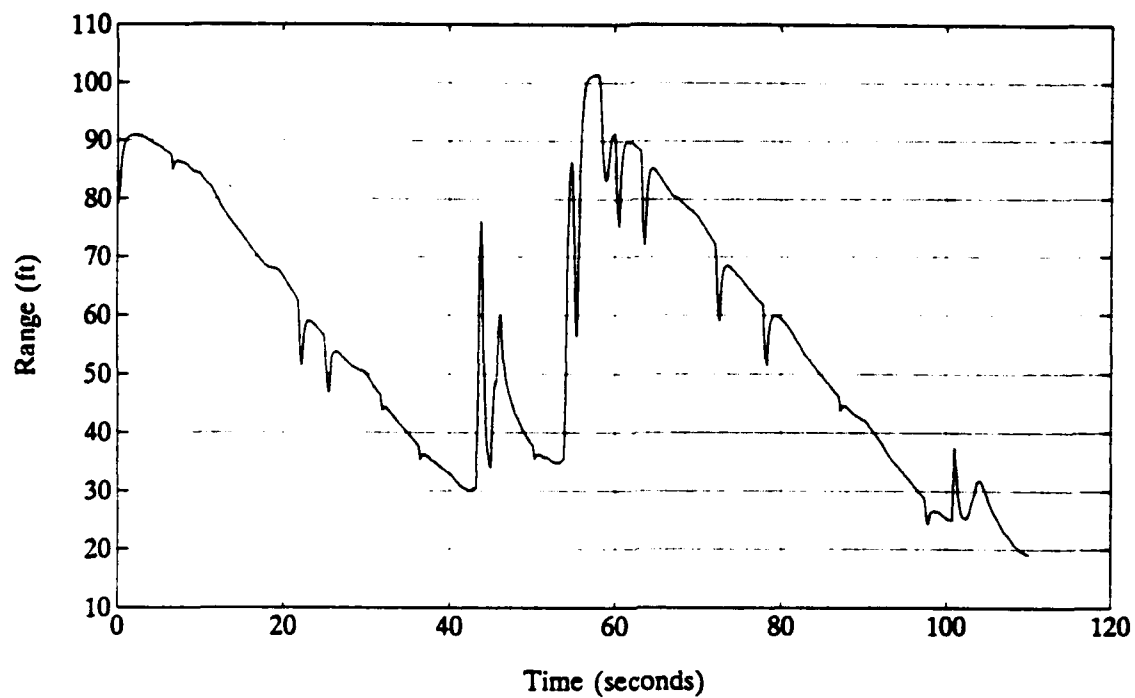
Figure 4.16 Forward Sonar Trace During 'Zig Zag' Trial
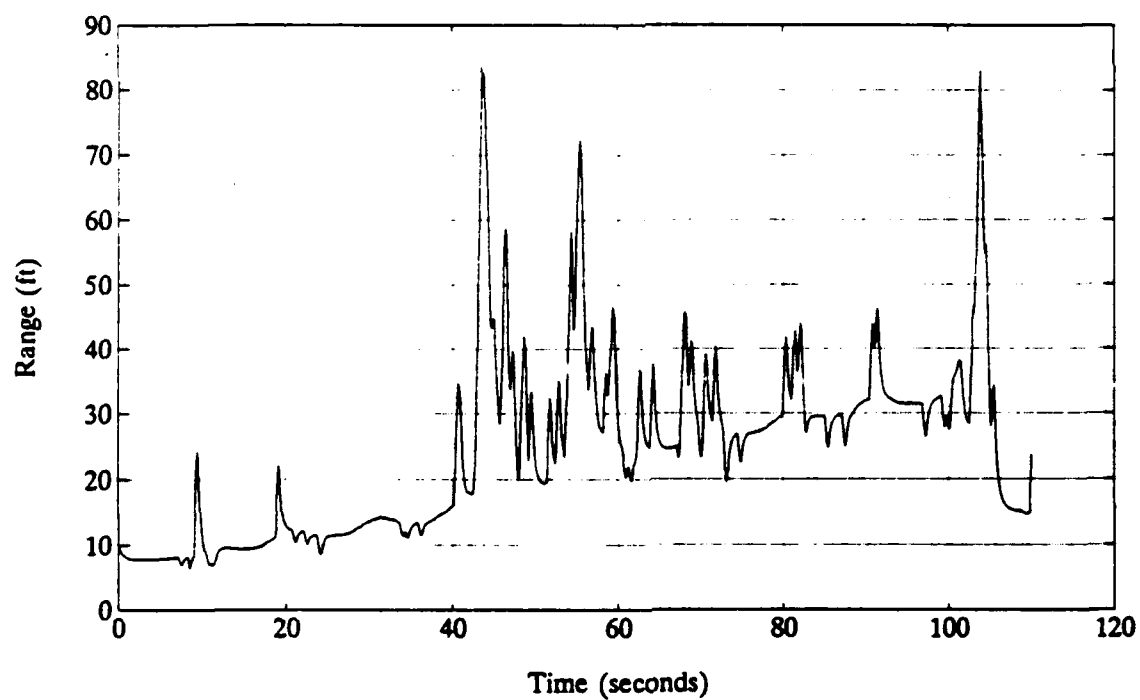
Figure 4.17 Left Side Sonar Trace During 'Zig Zag' Trial

88
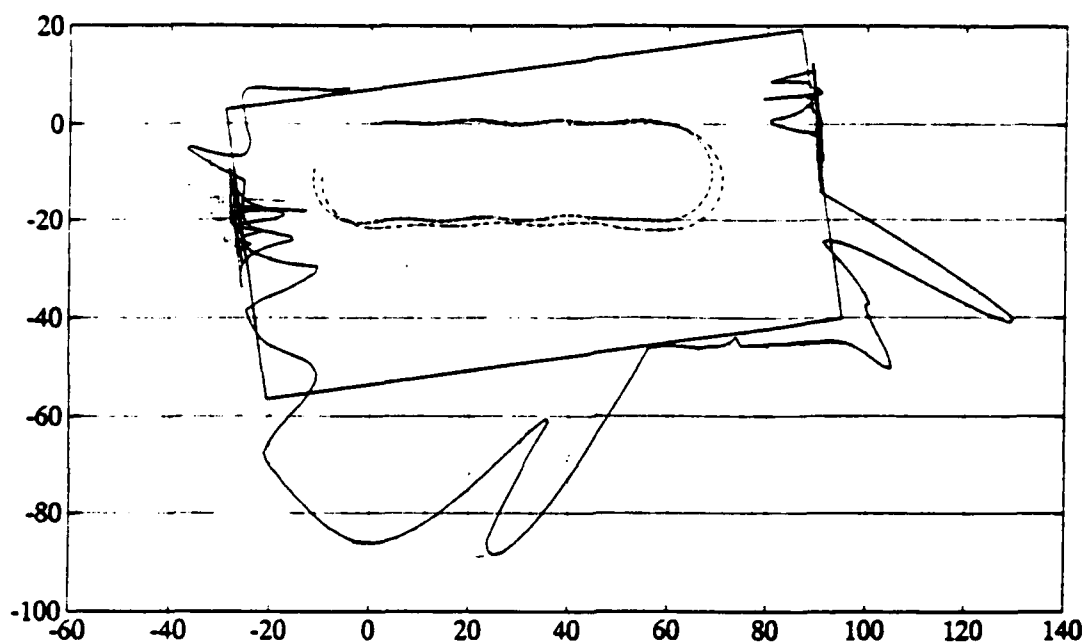
Figure 4.18 Vehicle Track From Navigation System With And Without Sway Velocity Correction Showing Corresponding Forward Sonar Traces
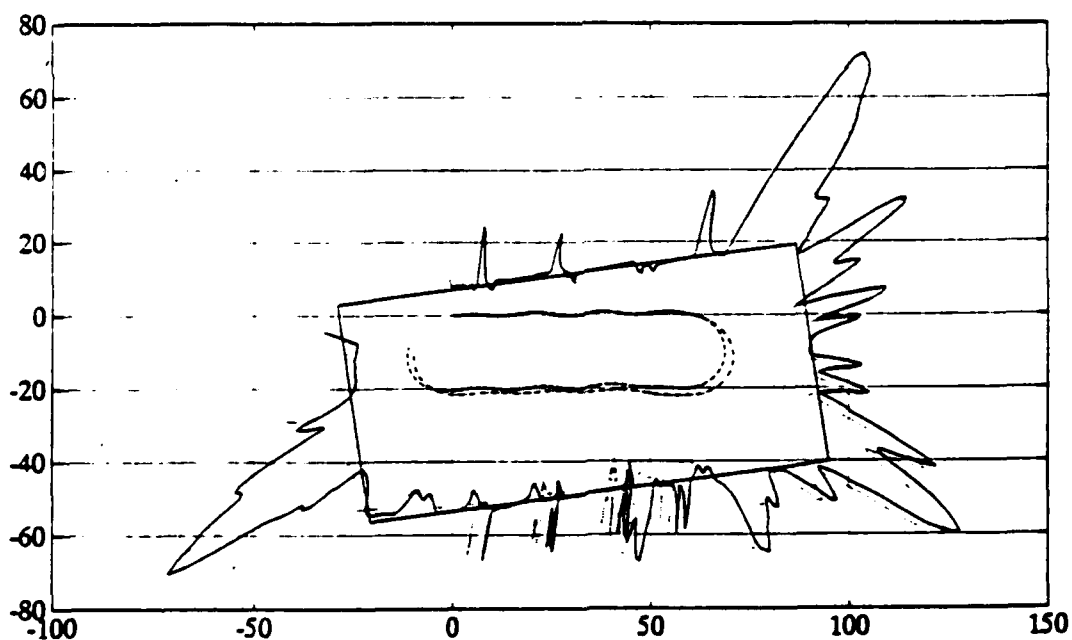
Figure 4.19 Vehicle Track From Navigation System With And Without Sway Velocity Correction Showing Corresponding Left Side Sonar Trace

89

TABLE 4.7   PARAMETER SENSITIVITY OF N_r

PERCENT CHANGE	STD DEV $[\varepsilon_r]$	VARIANCE $[\varepsilon_r]$	STD DEV $[\varepsilon_r]$	VARIANCE $[\varepsilon_r]$
-60%	0.0910	83.0×10^{-4}	0.0236	5.57×10^{-4}
-40%	0.0574	33.0×10^{-4}	0.0202	4.09×10^{-4}
-20%	0.0360	13.0×10^{-4}	0.0180	3.23×10^{-4}
Nominal	0.0227	5.15×10^{-4}	0.0166	2.74×10^{-4}
+20%	0.0168	2.83×10^{-4}	0.0159	2.52×10^{-4}
+40%	0.0176	3.09×10^{-4}	0.0157	2.48×10^{-4}
+60%	0.0215	4.61×10^{-4}	0.0160	2.57×10^{-4}

TABLE 4.8   PARAMETER SENSITIVITY OF Y_δ

PERCENT CHANGE	STD DEV $[\varepsilon_r]$	VARIANCE $[\varepsilon_r]$	STD DEV $[\varepsilon_r]$	VARIANCE $[\varepsilon_r]$
-60%	0.0450	20.0×10^{-4}	0.0248	6.15×10^{-4}
-40%	0.0290	8.39×10^{-4}	0.0202	4.08×10^{-4}
-20%	0.0183	3.35×10^{-4}	0.0171	2.94×10^{-4}
Nominal	0.0227	5.15×10^{-4}	0.0166	2.74×10^{-4}
+20%	0.0371	14.0×10^{-4}	0.0187	3.49×10^{-4}
+40%	0.0541	29.0×10^{-4}	0.0227	5.18×10^{-4}
+60%	0.0718	52.0×10^{-4}	0.0279	7.80×10^{-4}

TABLE 4.9   PARAMETER SENSITIVITY OF Y_v

PERCENT CHANGE	STD DEV $[\epsilon_r]$	VARIANCE $[\epsilon_r]$	STD DEV $[\epsilon_r]$	VARIANCE $[\epsilon_r]$
-60%	0.0290	8.43×10^{-4}	0.0170	2.88×10^{-4}
-40%	0.0262	6.88×10^{-4}	0.0168	2.83×10^{-4}
-20%	0.0242	5.84×10^{-4}	0.0167	2.78×10^{-4}
Nominal	0.0227	5.15×10^{-4}	0.0166	2.74×10^{-4}
+20%	0.0216	4.67×10^{-4}	0.0165	2.71×10^{-4}
+40%	0.0208	4.33×10^{-4}	0.0164	2.68×10^{-4}
+60%	0.0202	4.07×10^{-4}	0.0163	2.66×10^{-4}

E. SLIDING MODE CONTROLLER DESIGN

The design of the sliding mode steering controller follows directly from the development of sliding mode theory in Chapter II. The applicable equations to describe the steering system are the sway, yaw and Euler relation for ψ. The use of the sway equation requires the sway velocity to be measured as an input to the steering controller. It is noted here that the Kalman State Filter provides an optimal estimate of sway (v) velocity based on system parameters which could be used as an input to the steering controller. Lienard (1990) showed that a steering controller would function satisfactory without the input of sway velocity using only inputs of yaw rate (r) and heading angle (ψ). In order to keep the steering system controller as simple as possible the reduced order controller proven by Lienard is developed here for the NPS AUV II.

To begin the design of the steering controller the SIMO subsystem equations must be identified to fit the form of Equation 2.1. The steering system equations of yaw and Euler relation for heading are written in state space form as:

$$\begin{Bmatrix} \dot{r} \\ \dot{\psi} \end{Bmatrix} = \begin{bmatrix} \dfrac{(N_r - mx_G)}{(I_z - N_{\dot{r}})}u_0 & 0 \\ 1 & 0 \end{bmatrix} \begin{Bmatrix} r \\ \psi \end{Bmatrix} + \begin{bmatrix} \dfrac{N_\delta}{(I_z - N_{\dot{r}})}u_0^2 \\ 0 \end{bmatrix} \delta_r$$

The equations are linearized about the nominal operating point of $u_0 = 1.5$ (ft/sec) and the state error vector is defined as:

$$\tilde{x} = \begin{Bmatrix} \tilde{r} \\ \psi \end{Bmatrix} = \begin{Bmatrix} r - r_{com} \\ \psi - \psi_{com} \end{Bmatrix}$$

with $u(t) = \delta_r$ we can make a direct substitution into equation 2.5, the sliding mode control law.

The three terms which remain to be determined are the nonlinear switching term gain η, the boundary layer thickness ϕ and the **s** for the sliding surface definition. Following the method outlined in Chapter II, the **s** is defined as the right eigenvector of $(A - Bk)^T$, the transpose of the desired closed loop system dynamics, which corresponds to the zero eigenvalue. At this point in the process, it is necessary to choose the desired poles of the closed loop system dynamics, again noting that one of the poles must be placed at the origin to allow the decomposition of the sliding mode control law. The open loop poles of the refined system are [0   -0.2564]. Therefore, we already have a pole at the origin due to the direct integration of ψ from r. The remaining pole is on the negative real axis and it is desired to move this pole to -1.0, thereby increasing the response of the sliding surface dynamics. By placing this pole at -1.0 the performance of the sliding mode controller can be compared directly to the previously designed proportional derivative (PD) controller which has been tested on the NPS AUV II. Using the linearized system equation, desired poles of [0   -1.0]

94

and standard pole placement techniques, the eigenvectors of the closed loop system dynamics transposed is:

$$\begin{bmatrix} 1.0 & 0.7071 \\ 0.0 & 0.7071 \end{bmatrix}$$

with **s** defined as the right eigenvector corresponding to the zero eigenvalue $s = \begin{bmatrix} 0.7071 \\ 0.7071 \end{bmatrix}$ and $s^T = [0.7071 \quad 0.7071]$.

The remaining terms to define in the control law are the nonlinear switching term gain η and the boundary layer thickness ϕ. As shown in Chapter II, the nonlinear switching term gain must be greater than the bounded value of the unknown modeling errors. The system identification procedure used earlier in this chapter produced a plot of Yaw acceleration error, Figure 4.7. This yaw acceleration error can be bounded by taking the absolute maximum value of the error and ensuring that η is larger than this value thereby guaranteeing stability. Alternatively, a stochastic method can be used to provide a confidence bound on the value of η required to have the yaw acceleration error contained within the bounds of η.

Once the minimum value of the nonlinear switching term gain is determined, a value of ϕ, the boundary layer thickness is estimated based on the desired amount of allowable state error on the system. It is noted here that with all controllers, the tighter the desired control, the higher the

controller gains must be which result in larger actuator movements for the same stated error. It is desirable to design a controller which will give a trade off on excessive actuator response to system accuracy. The boundary layer term will accomplish this task by adjusting the slope of the hyperbolic tangent function through the origin and thereby controlling the amount of state error allowed prior to saturation of the control actuator.

By assuming the state error to be zero, the sliding mode control law will command zero actuator response. Taking the sliding mode control law and reducing it to only the nonlinear switching term yields:

$$u(t) = - [s^T B]^{-1} \eta_0^2 \tanh\left(\frac{s^T(\tilde{X})}{\phi}\right)$$

Knowing the maximum amount of actuator response or movement u_{max} and solving the above equation for η gives a relation for the value of η which will cause the control actuator to saturate for a given value of state error.

$$\eta_0^2 = \frac{u_{max}}{[s^T B]^{-1} \tanh\left(\frac{s^T(\tilde{X})}{\phi}\right)}$$

This is stated equivalently as the amount of state error that will cause the controller actuator to saturate for a given value of η. By holding ϕ fixed and varying the amount of state error, a plot of η versus state error can be generated for a
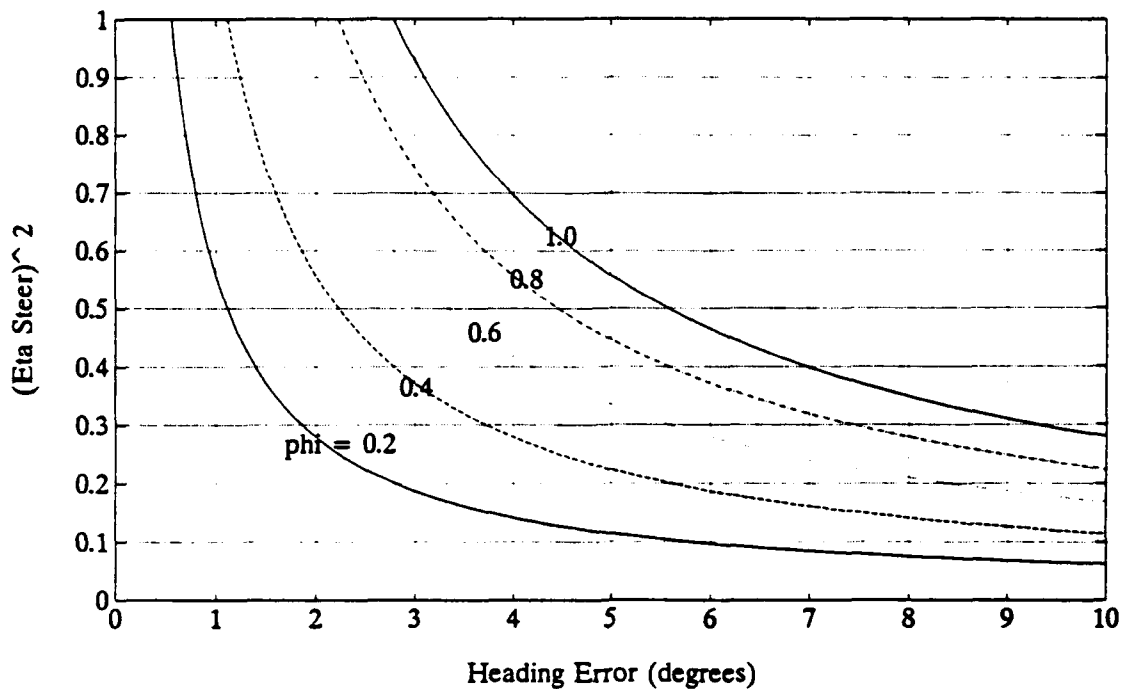
Figure 4.20 Plot Of η vs State Error For Various Values Of ϕ

fixed value of ϕ. A family of these curves is generated in Figure 4.20 where u_{max} = 0.4 radians, the limit of rudder deflection. The desired boundary layer thickness is chosen as follows: enter the plot at the required value of η and the allowable amount of state error. The intersection of these two points will give the value of ϕ, which in combination with the nonlinear switching term gain η will cause the control actuator to saturate when this amount of state error is reached.

Following this design procedure creates a sliding mode control which is guaranteed to be stable and has the capability of controlling the amount of allowable steady state error.

97

F. PERFORMANCE OF THE SLIDING MODE CONTROLLER

The testing of the sliding mode controller was performed in the Naval Postgraduate School swimming pool. During testing the controller appeared to be as precise as the PD controller with the exception that the rudders were noted to have high frequency deflections commanded to them when the vehicle was in straight line motion. This high frequency chatter was not seen in the PD controller. Detailed analysis of the results of the sliding mode controller in a turn are shown in Figure 4.21. The figure shows the yaw rate of the PD controller compared to the resulting yaw rate of the sliding mode controller for three different values of nonlinear switching term gains. The turn commanded required the rudder to swing hard over for each of the controllers. It is noted that the turn is nearly the same with respect to yaw rate for any particular controller. Figure 4.22 shows the heading angle of the vehicle through the turn also indicating that the vehicle turns the same with any controller as expected when turning with the rudders saturated. Coming out of the turn is where the advantage of a sliding mode controller is seen. By decoupling the control law to provide the nonlinear switching term with its own gain, allows the sliding mode controller to use a higher gain to restore the system to the sliding surface and when on the surface the argument of the nonlinear switching term is zero and does not contribute to the control law. Once on the sliding surface the desired dynamics of the
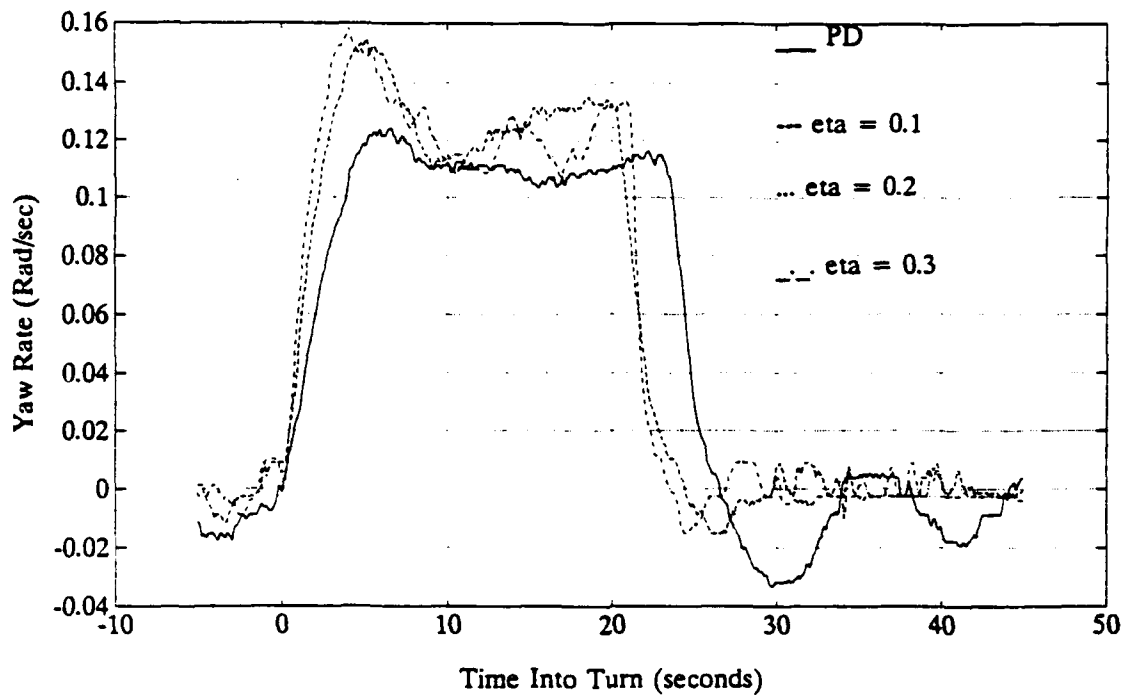
Figure 4.21 Comparison of Sliding Mode and PD Controller Yaw Rate Entering a Turn
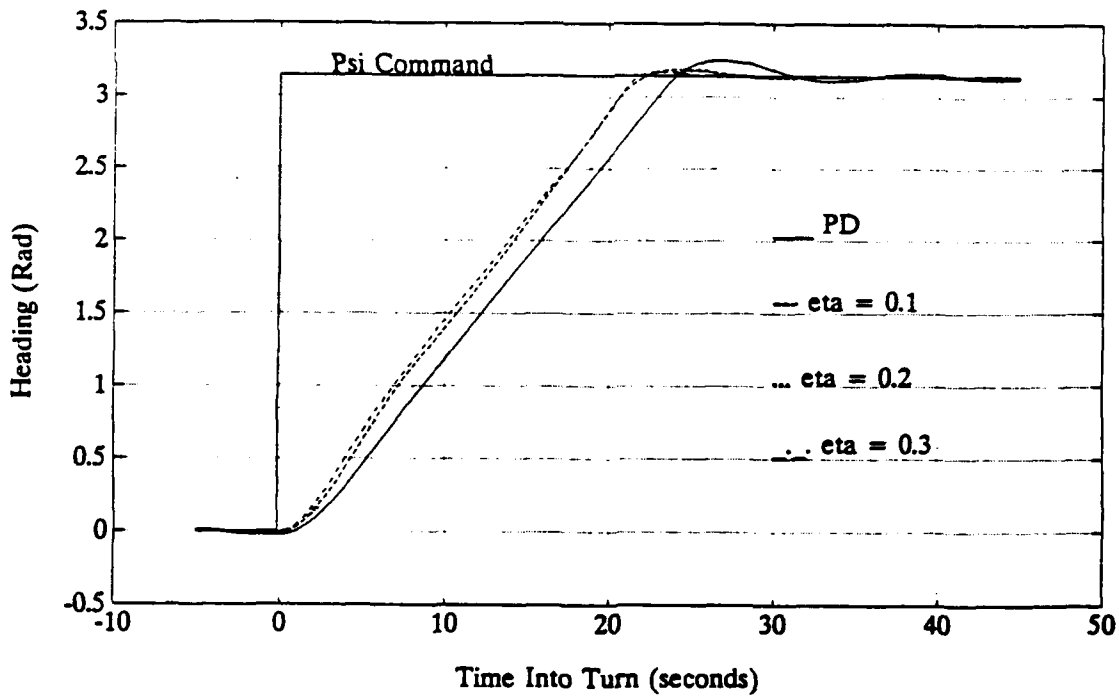
Figure 4.22 Comparison of Heading Entering a Turn For a Sliding Mode and PD Controller

99

closed loop system take the dominant role in the control law and continue to drive the state error to zero. This is the advantage of a sliding mode control law. When the system is operating on the sliding surface, the desired closed loop dynamics dominate the control law, but when the system is forced off the sliding surface by either an external disturbance or a commanded disturbance, the nonlinear switching term with its large gain place extra control on the system to first drive it to the sliding surface and then let the sliding surface dynamics take over to continue to drive the state error to zero. The proof of this quality in a sliding mode controller is shown in Figure 4.23, looking at the vehicle heading coming out of the turn when the nonlinear switching term is returning the system to the sliding surface. It is clearly seen that as the gain η is increased from 0.1 to 0.3 the system is driven more rapidly to the sliding surface and therefore provides a tighter controller for the steering system. The PD controller with approximately the same closed loop system dynamics shows much more over shoot and then numerous oscillations before achieving a steady course. Figure 4.24 shows the rudder deflections for the PD and sliding mode controllers corresponding to vehicle headings of Figure 4.23. It is important to note that the $\eta = 0.2$ has nearly the same amount of maximum rudder deflection as the PD controller but responds more quickly than the PD controller. The final proof to the advantage of a sliding mode controller to the PD
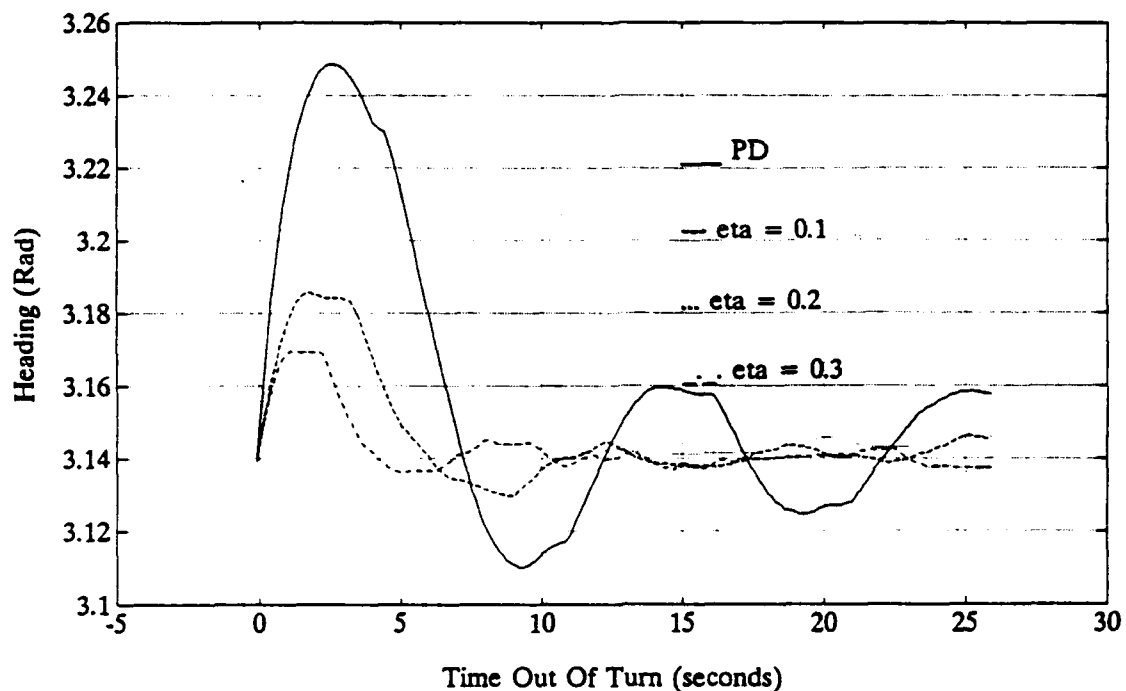
Figure 4.23 Comparison of Sliding Mode and PD Controller Heading Exiting a Turn
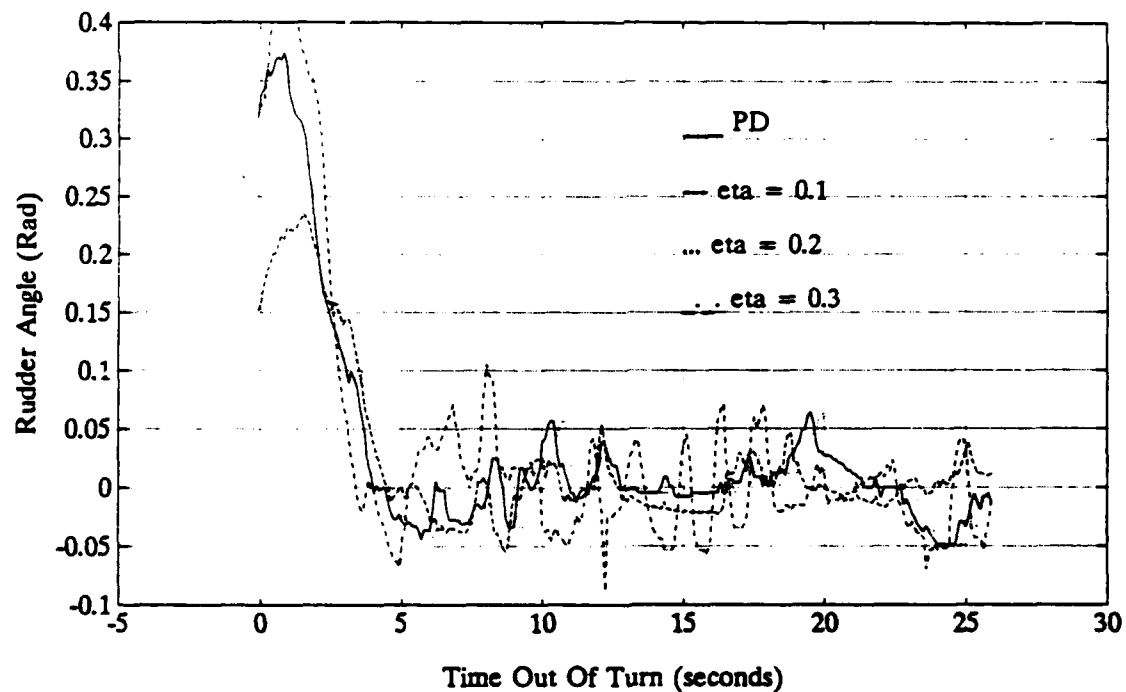
Figure 4.24 Comparison of Sliding Mode and PD Controller Rudder Deflection Exiting a Turn

controller is the direct comparison of the $\eta = 0.2$ to the PD controller where it is seen that the commanded rudder deflections coming out of the turn are similar but the heading overshoot and the time required to achieve a steady course are much reduced due to the effect on the control law by the nonlinear switching term.

Even though the sliding mode controller appears superior to the PD controller with the same closed loop dynamics, the high frequency oscillations noted during testing of the vehicle in straight line motion are caused by the nonlinear switching term. This is due to the high gain η that can be used to drive small errors when the system is off the sliding surface to return it to the sliding surface. The reality of imperfect sensors and noise on the signals from the sensors is amplified by the nonlinear switching term gain and places the same high frequency sensor noise on the control surface. The result of this high frequency noise is clearly evident as a disadvantage of a sliding mode controller. Figure 4.23 shows that the heading of the vehicle is controlled with greater precision, Figure 4.24 shows that excessive noise is placed on the control surface when in steady flight. This excessive chatter is detrimental to actuator life.

G. DESIGN OF KALMAN STATE FILTER FOR THE STEERING SYSTEM

From the above discussion the potential of a Kalman State Filter to reduce the sensor noise of the yaw rate gyro and the heading gyro is indicated. An additional advantage of the Kalman State Filter is that it is an optimal estimator and will also estimate sway velocity. While sway velocity is not needed as an input to the steering system controller, it is necessary as an improvement to the dead reckoning navigation system.

The design of the Kalman State Filter for the Steering system follows the procedure outlined in Chapter II for a general Kalman filter. The system equations needed for the steering system Kalman State Filter are the sway, yaw and Euler relation for heading. These three equations are written in state space form as follows:

$$\dot{x} = M^{-1}Ax + M^{-1}Bu + [\varepsilon_x]$$

where: $x = \begin{bmatrix} v \\ r \\ \psi \end{bmatrix}$ is the state vector, $[\varepsilon_x]$ = the modeling error vector in the state equations or equivalently stated as the system noise vector and $u = \delta_r$ the commanded rudder deflection.

$$M = \begin{bmatrix} (m - Y_v) & (mx_G - Y_r) & 0 \\ (mx_G - N_v) & (I_z - N_r) & 0 \\ 0 & 0 & 1 \end{bmatrix} \quad \text{is the mass matrix}$$

$$A = \begin{bmatrix} Y_v u_0 & (Y_r - m) u_0 & 0 \\ N_v u_0 & (N_r - mx_G) u_0 & 0 \\ 0 & 1 & 0 \end{bmatrix} \quad \text{is the steering system dynamics}$$

$$B = \begin{bmatrix} Y_\delta u_c^2 \\ N_\delta u_0^2 \\ 0 \end{bmatrix} \quad \text{is the system input matrix}$$

The measurements available are **r** yaw rate and ψ heading angle. This provides the following measurement equation:

$$Y = \begin{bmatrix} 0 & 1 & 0 \\ 0 & 0 & 1 \end{bmatrix} \begin{Bmatrix} r \\ \psi \end{Bmatrix} + \begin{Bmatrix} v_r \\ v_\psi \end{Bmatrix}$$

The plant noise covariance can be taken as the variance of the parameter identification error of Figure 4.7 and the measurement noise covariance can be taken as the square of the standard deviations of the individual measurements. Appendix A gives the standard deviation and the variance of each of the NPS AUV II's measured states. Appendix A was created based on the actual noise experienced by each of the vehicles sensors. The initial state estimate is set equal to the initial data point in the data record. This allows the initial estimation error covariance to be set equal to zero.

The filter results are shown in Figure 4.25 and 4.26. Figure 4.25 shows an improvement in the yaw rate signal while Figure 4.26 shows little if any improvement in the heading signal. The heading gyro by its own design gives a very clean signal and does not require filtering. In addition to the yaw rate and heading filtered signals an optimal estimation based on the system parameters is given for v, the sway velocity, in Figure 4.26.
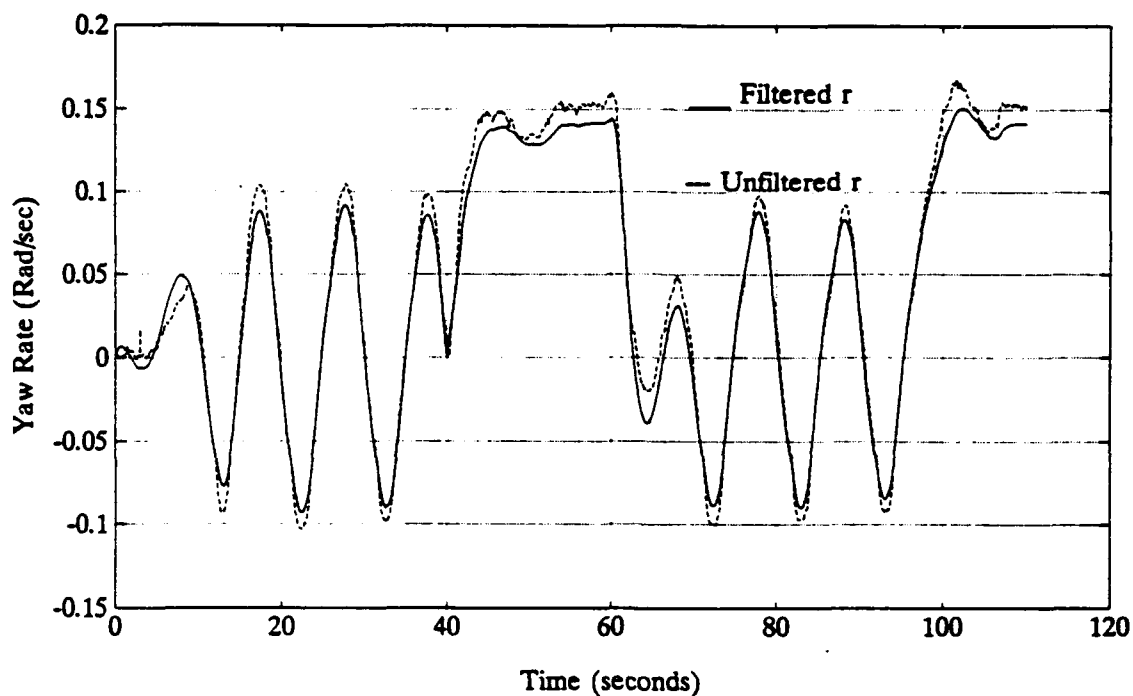
Figure 4.25 Kalman State Filter Results Yaw Rate
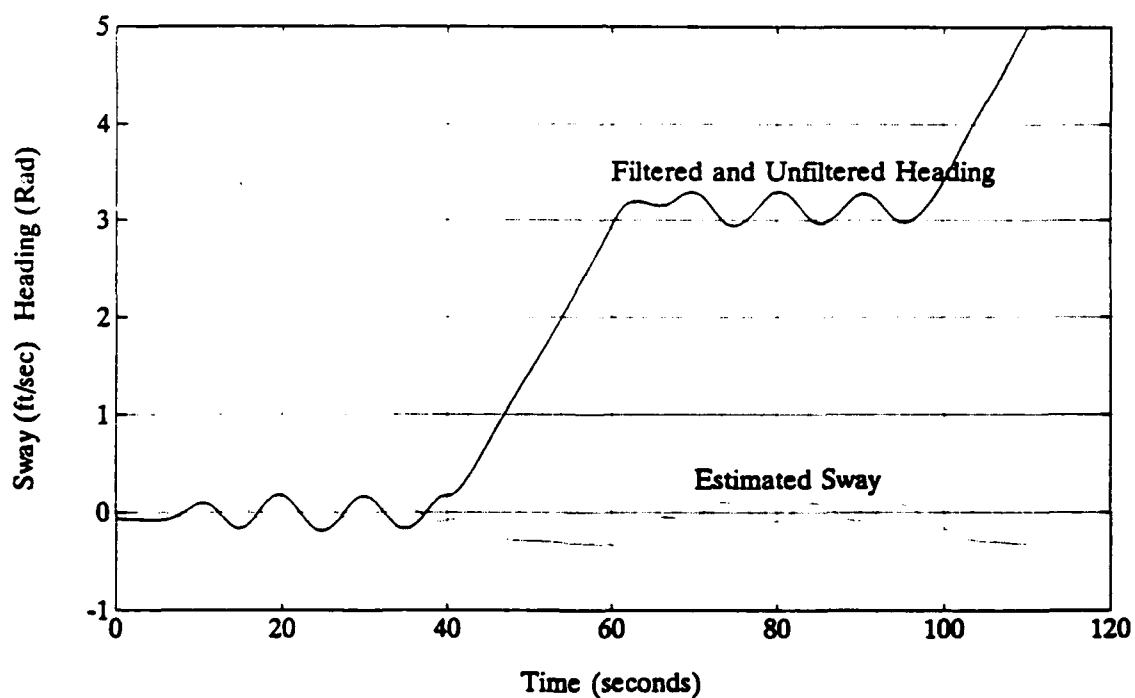
Figure 4.26 Kalman State Filter Results for Heading and Estimation of Sway Velocity

H. CLOSED LOOP SIMULATION OF SLIDING MODE STEERING CONTROLLER WITH FILTERED INPUTS

Figure 4.27 shows the block diagram of the closed loop simulation model incorporating the vehicle model, the injection of signal noise on the measured states of the vehicle model, the Kalman State Filter to provide clean
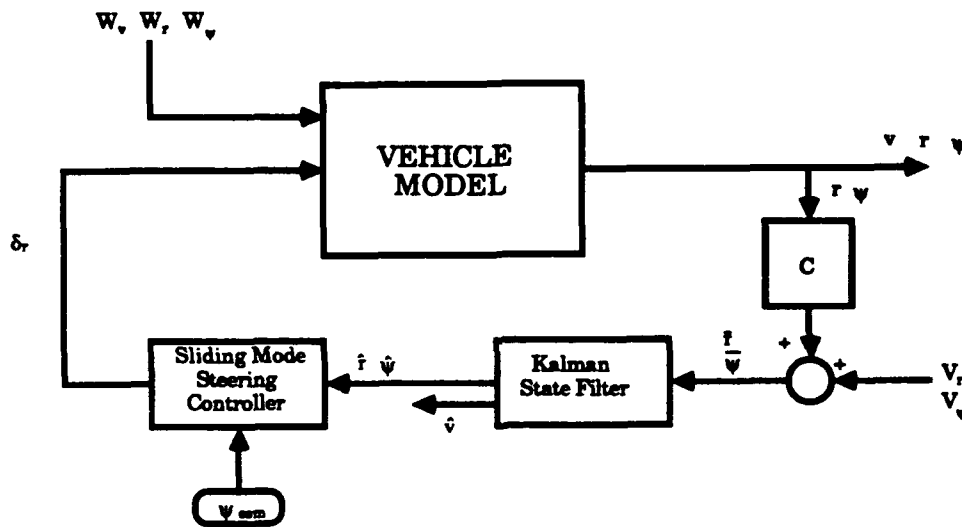
Figure 4.27 Block Diagram of Closed Loop Simulation with Kalman State Filter

signals to the sliding mode steering controller. Figure 4.28 shows the commanded heading and the vehicles noisy heading, indicating the control system is stable when the Kalman State Filter is used in the control system and tracks the commanded heading. In addition to the simulated heading, the heading of the experimental results for the sliding mode controller with

$\eta = 0.2$ are given. The simulation of the closed loop system used a sliding mode controller with the same η as the experimental trial for comparison. The results are very close indicating the accuracy of the analytical model. Figure 4.29 shows the vehicle's noisy yaw rate, the filtered yaw rate and the experimental yaw rate. The experimental yaw rate does not show the same magnitude in the turn as the simulated yaw rate and is attributed to the forward rudder stalling when its angle of attack is greater than 0.4 radians. This stall causes a reduction in lift force by the plane surface and increased drag which is not included in the analytical model of the NPS AUV II. Figure 4.30 shows the rudder command from the simulation for the sliding mode control law using both filtered and unfiltered signals compared to the experimental rudder command. The rudder commands are very similar for the experimental and unfiltered signals showing that the measurement noise is adequately modeled as a white noise. The filtered rudder command controlled the simulation indicating adequate control with the Kalman State Filter in the control loop.
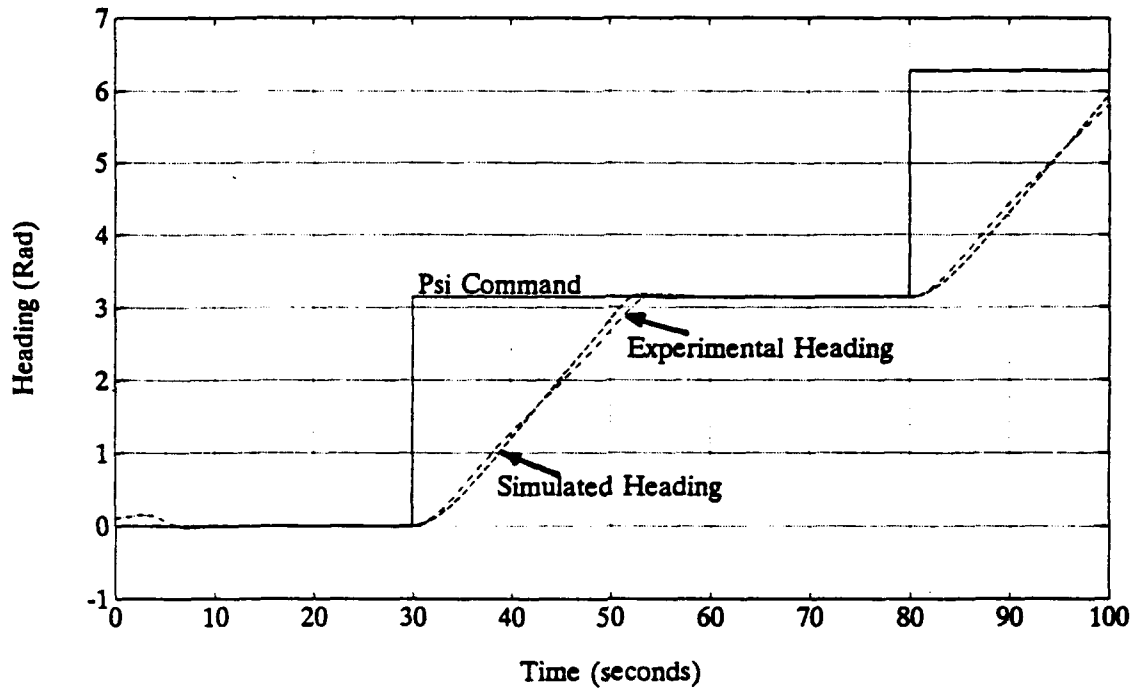
Figure 4.28 Heading Results of Closed Loop Simulation Compared to Experimental Data
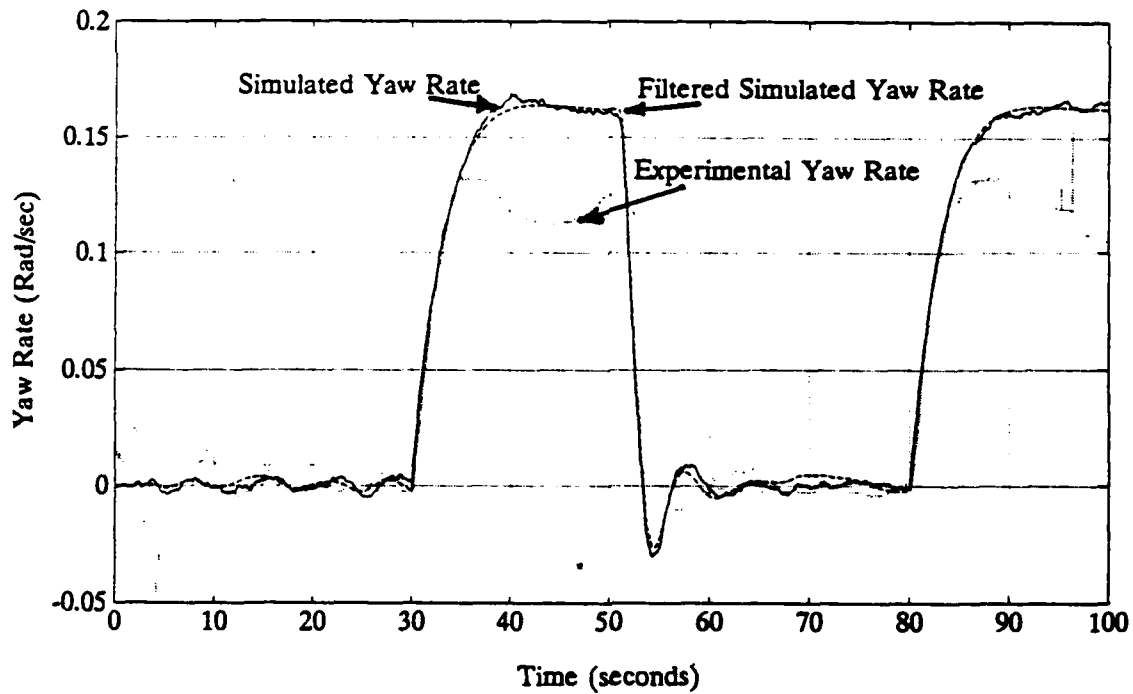
Figure 4.29 Yaw Rate Results of Closed Loop Simulation Compared to Experimental Data
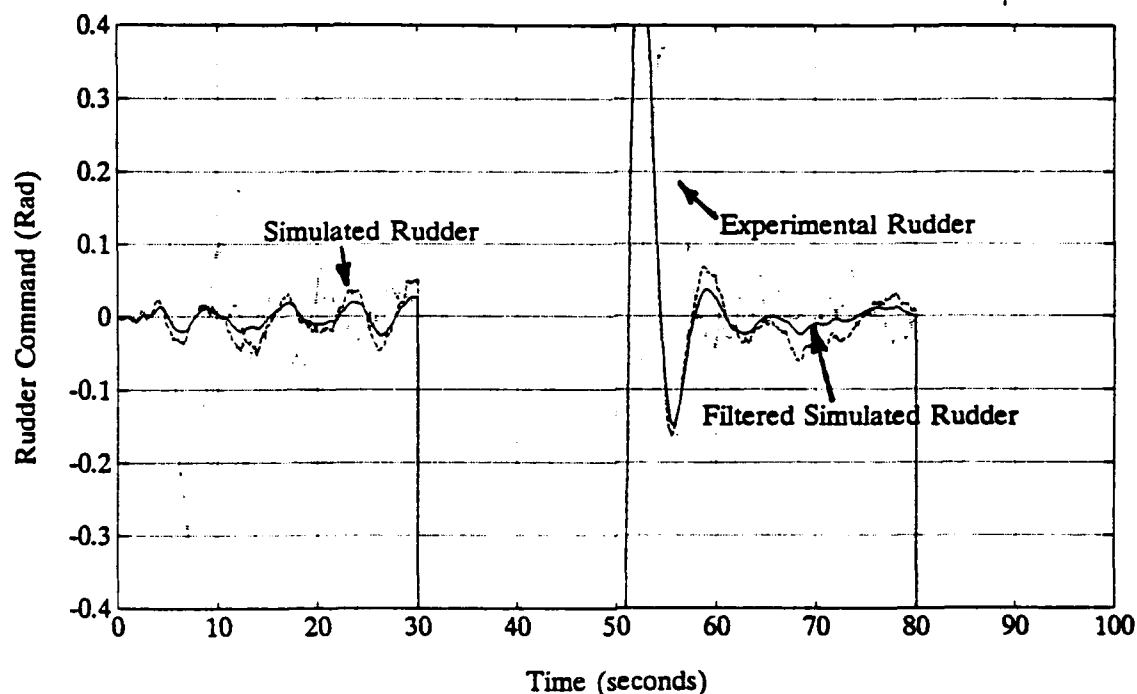
Figure 4.30 Rudder Command Results of Closed Loop Simulation Compared to Experimental Data

I.   IMPROVED NAVIGATION SYSTEM

The optimal estimation of sway velocity, filtered vehicle speed and heading is fed into the dead reckoning navigation system. The play back of vehicle position with the optimal estimation of sway velocity included in the navigation system is shown in Figure 4.31. The plotting of the sonar record shows the vehicle navigation system is accurate as confirmed by the outline of the pool drawn by the sonar traces.
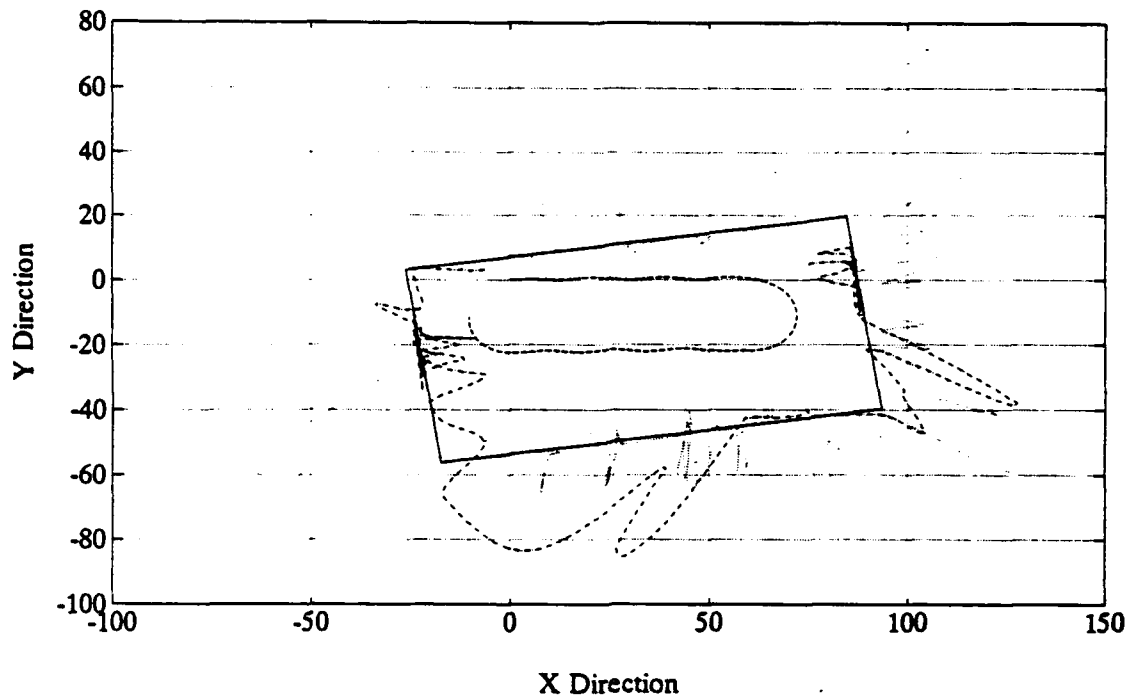
Figure 4.31 Vehicle Position In Swimming Pool Verified By Sonar Ranges

J. SUMMARY

This chapter has shown how a simplified analytical model could be used as a Kalman Parameter Filter to identify system parameters and predict possible system faults based on the identified parameter exceeding the specified bounds.

The application of a sliding mode controller to the steering system was proven to be a more robust controller than a typical PD controller. It is also shown that a sliding mode controller is more susceptible to high frequency chatter originating from the vehicles sensors.

The application of the Kalman State Filter has shown that the advantages of a sliding mode controller can be retained

111

when the sensor signals are filtered to remove the high frequency noise. The Kalman State Filter also supplies an optimal estimation of the sway velocity needed for the improved accuracy of the dead reckoning navigation system.

V. DIVING SYSTEM CONTROL

A. INTRODUCTION

The purpose of this chapter is to identify and verify the diving system parameters from experimental data. The procedure followed here is identical to that followed in Chapters III and IV. The presentation here will give the specific parameters identified and describe the source of the input parameters without a detailed description of the theory developed in Chapters II, III and IV. Following identification of the system parameters, a sliding mode diving controller is developed for the NPS AUV II.

B. OUTLINE OF THE DIVING SYSTEM

The diving system for the NPS AUV II consists of four NACA 0015 control surfaces (planes). Each of the planes may be independently operated to control the vehicles orientation with respect to roll and pitch. At present, both left and right bow planes act in unison as well as both left and right stern planes. The bow and stern planes also operate in equal but opposite directions thereby providing an additive couple to the input diving moment. Figure 1.1 shows the location of the planes on the vehicle. Figure 5.1 shows the functional block diagram of the diving system. The diving controller receives inputs from the diving system Kalman State Filter for

signals of q pitch rate, θ pitch angle and z depth. These signals are compared to the commanded pitch rate, pitch angle and depth and used to compute a commanded plane deflection by a sliding mode control law. The vehicle's sensors also send these signals to the Kalman Parameter Estimator to provide an on-line fault monitor for M_q and M_δ. The monitoring of these parameters are a good indication of a system malfunction from internal diagnostics.
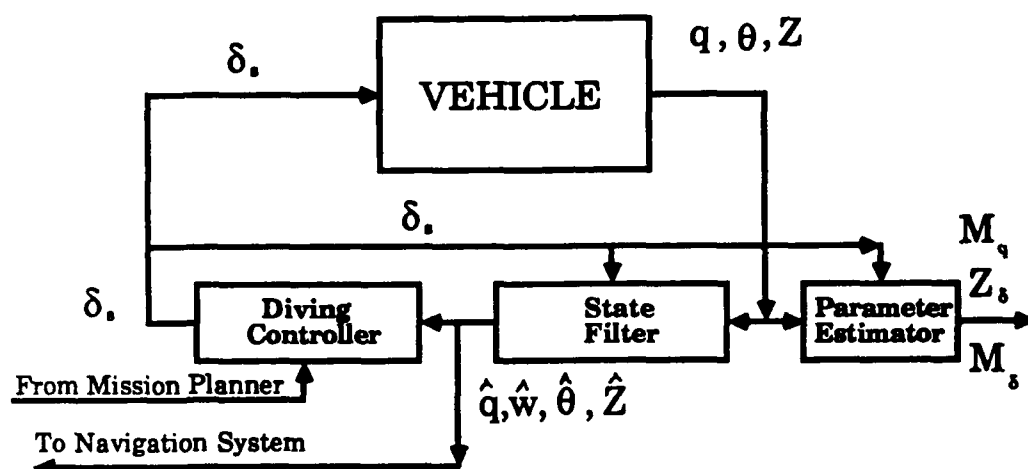
Figure 5.1   Functional Block Diagram of the Diving System

The vehicles equations of motion as developed by Boncal (1987) are further simplified with the system parameters scaled by Warner (1991) to a vertical diving system model. The diving system is modeled by using Equation 2.3, heave equation of motion; Equation 2.6, pitch equation; and the Euler equation relations for $\dot{X}$, $\dot{Z}$ and θ.

114

The equations are simplified with the following assumptions:

1. The vehicle is operating in straight line motion without roll, therefore p, $\dot{p}$, r, $\dot{r}$, ψ, ϕ and $v = 0$.

2. The body drag forces are negligible.

$$m\dot{w} - mx_G\dot{q} - Z_q\dot{q} - Z_{\dot{w}}\dot{w} = muq + Z_quq + Z_wuw + u^2(Z_{\delta_b}\delta_b + Z_{\delta_s}\delta_s)$$

$$I_y\dot{q} - mx_G\dot{w} - M_{\dot{q}}\dot{q} - M_{\dot{w}}\dot{w} = -mx_Guq + M_quq + M_wuw - z_GW\sin\theta + u^2(M_{\delta_b}\delta_b + M_{\delta_s}\delta_s)$$

$$\dot{X} = u\cos\theta + w\sin\theta$$

$$\dot{Z} = -u\sin\theta + w\cos\theta$$

$$\dot{\theta} = q$$

Rearranging and noting that the bow and stern planes operate with equal magnitudes of deflection but opposite direction and that the size and shape of the bow and stern planes are identical, therefore $Z_{\delta_b} = Z_{\delta_s}$ and $\delta_b = -\delta_s$. From the geometry of the vehicle $M_{\delta_b} = 0.283\,L\,Z_{\delta_b}$ and $M_{\delta_s} = -0.377\,L\,Z_{\delta_s}$. Using the above relations the heave and pitch equations can be written as:

$$(m - Z_{\dot{w}})\dot{w} + (-mx_G - Z_{\dot{q}})\dot{q} = Z_wuw + (Z_q + m)uq + Z_\delta u^2\delta_s \qquad \textbf{(5.1)}$$

$$(-mx_G - M_{\dot{w}})\dot{w} + (I_z - M_{\dot{q}})\dot{q} = M_wuw + (M_q - mx_G)uq \\ - z_GW\sin\theta + M_\delta u^2\delta_s \qquad \textbf{(5.2)}$$

where:

$\delta_s = -\delta_b$ plane angle deflection in radians

$Z_\delta = Z_{\delta_s} - Z_{\delta_b} = 0.0$ vertical plane force

$M_\delta = M_{\delta_s} - M_{\delta_b} = -0.377 L Z_{\delta_s} - 0.283 L Z_{\delta_b} = -4.8194 Z_{\delta_s}$

plane coupling moment

The state space form of system equations is written as follows:

$$\dot{x} = M^{-1}Ax + M^{-1}Bu + W$$

where:

$x = [w \ q \ \theta]^T$ is the state vector

$$M = \begin{bmatrix} (m - Z_w) & (-mx_G - Z_q) & 0 \\ (-mx_G - M_w) & (I_z - M_q) & 0 \\ 0 & 0 & 1 \end{bmatrix} \text{ is the mass matrix}$$

$$A = \begin{bmatrix} Z_w u & (Z_q + m)u & 0 \\ M_w u & (M_q - mx_G)u & -z_G W \\ 0 & 1 & 0 \end{bmatrix} \text{ is the dynamics matrix}$$

$$B = \begin{bmatrix} Z_\delta u^2 \\ M_\delta u^2 \\ 0 \end{bmatrix} \text{ is the input matrix}$$

$$W = \begin{bmatrix} w_w \\ w_q \\ w_\theta \end{bmatrix} \text{ is the system noise vector}$$

The input noise vector is the independent random white noise signals associated with the measurement noise of each state. In addition, the system equations require the nonlinear Euler relations for $\dot{X}$ and $\dot{Z}$ to provide the vehicles global position.

C. EXPERIMENTAL WORK WITH NPS AUV II

The experimental data set in which the most information on the diving system parameters were obtained, is from the 'Porpoise' data file. This experimental run was performed by superimposing a sinusoidal dive plane command on the existing dive plane command generated from the PD diving controller. The desired effect of this trial was to excite the vertical plane equations of motion and thereby obtain a data file of the response of the vehicle to the forced input. Figure 5.2 shows the input plane deflection δ_s and the depth response of the vehicle. Figure 5.3 shows the q pitch rate and θ pitch angle response to the same input plane deflection δ_s.

D. PARAMETER IDENTIFICATION

The desired simple analytical model for the diving system is now developed. Having symmetric planes cancels the effective heave force applied to the vehicle and doubles the pitch moment applied. This canceling effect leaves $Z_\delta = 0$. Therefore, there is no direct input to Equation 5.1, the heave equation of motion, analogous to the sway equation of Chapter

117
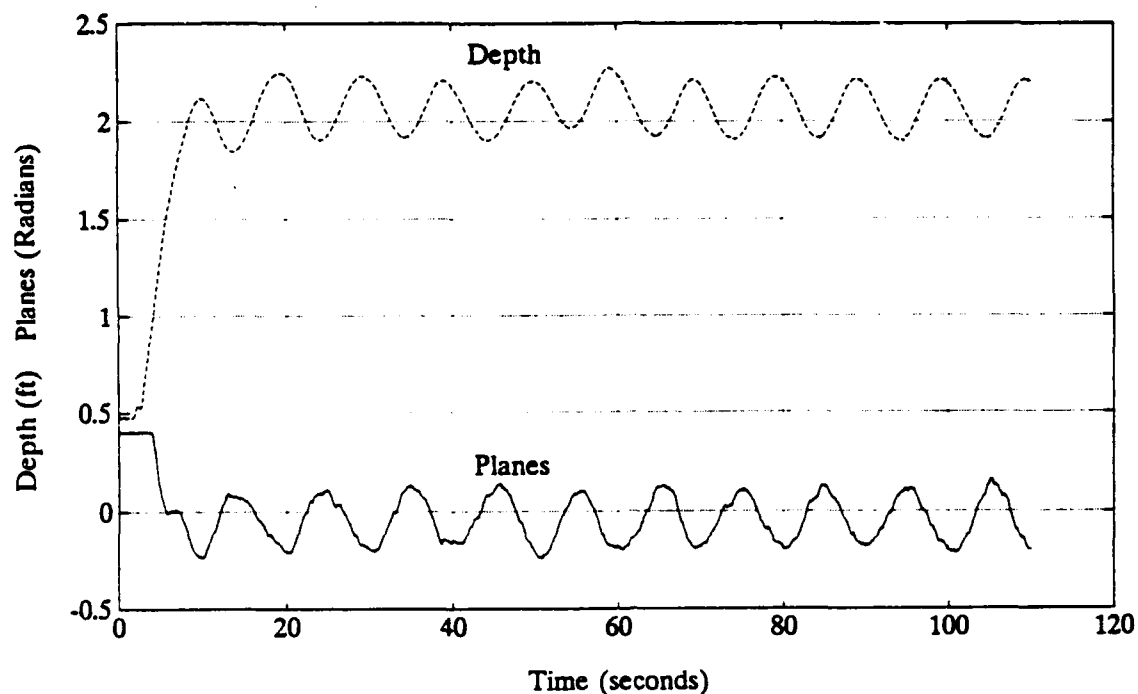
Figure 5.2 δ_s **Input and Z Depth Response for 'Porpoise' Trial**
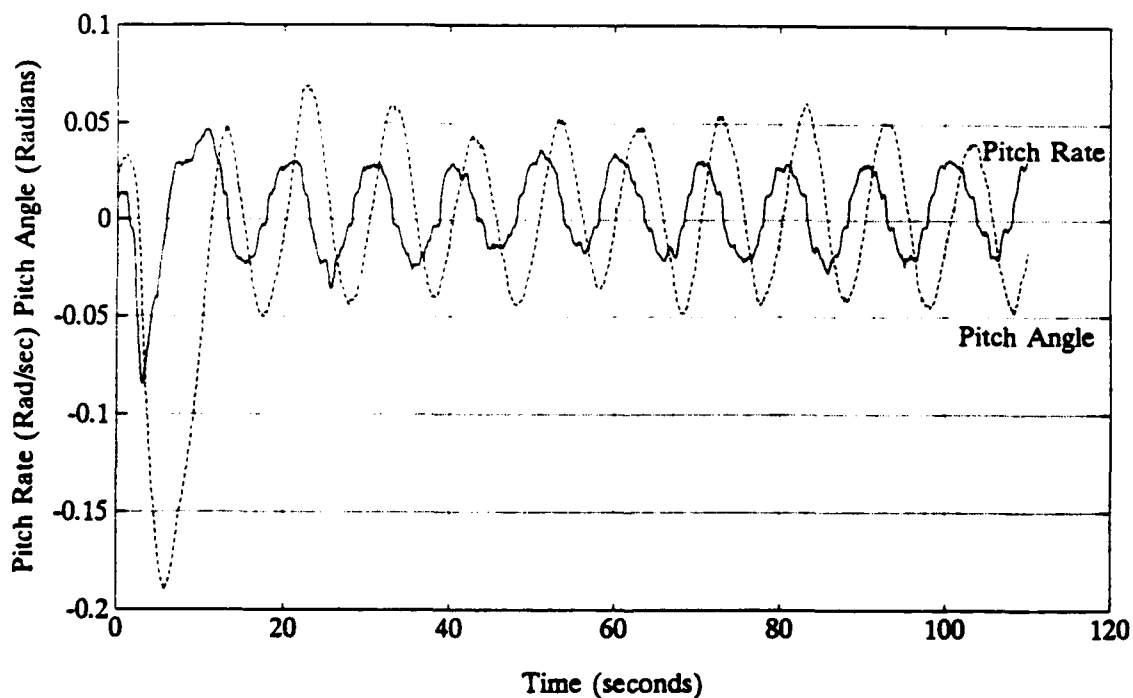
Figure 5.3 **q and** θ **Response For** δ_s **Input To 'Porpoise' Trial**

118

IV. The only input to the heave equation is from the mass coupling and the pitch rate. This justifies the use of only the pitch equation of motion for the diving system simplified model.

1. First Order Model For Parameter Identification

The heave velocity and acceleration are not measured presently on the NPS AUV II. The following assumptions are made to simplify Equation 5.2 to the first order diving model.

1.   The heave velocity and acceleration are small compared to the pitch rate and pitch acceleration, therefore w and $\dot{w} = 0$.

2.   The vertical righting arm z_G is known from inclining experiments in a testing tank.

Equation 5.2 simplifies to:

$$(I_y - M_{\dot{q}})\,\dot{q} = (M_q - mx_G)\,uq - z_G W\sin\theta + M_\delta u^2\delta_s + \varepsilon_q$$

dividing through by the Inertia term:

$$\dot{q} = \frac{(M_q - mx_G)}{(I_y - M_{\dot{q}})}uq - \frac{z_G W\sin\theta}{(I_y - M_{\dot{q}})} + \frac{M_\delta}{(I_y - M_{\dot{q}})}u^2\delta_s + [\varepsilon_r]$$

combining terms to simplify the coefficients to a two parameter equation. The first order equation is now ready for use in the Kalman Parameter Filter as a measurement equation.

119

$$\dot{q} = (MQ) \, u \, q + (M\delta) \, u^2 \, \delta_s - M\Theta \sin\theta + [\varepsilon_q]$$

$$\dot{q} = [\, u\,q \quad u^2\,\delta_s \,] \begin{Bmatrix} MQ \\ M\delta \end{Bmatrix} - M\Theta \sin\theta + [\varepsilon_q]$$

(5.3)

where,

$$MQ = \frac{(M_q - mx_G)}{(I_y - M_{\dot{q}})} \qquad M\delta = \frac{M_\delta}{(I_y - M_{\dot{q}})}$$

$$M\Theta = \frac{z_G W}{(I_y - M_{\dot{q}})} \qquad [\varepsilon_q] = \frac{\varepsilon_q}{(I_y - M_{\dot{q}})}$$

The measurement Equation 5.3 contains the two terms **MQ** and **Mδ** which can be identified in the same fashion as the steering system parameters. The **MΘ** term in Equation 5.3 is known from static inclining tests of the vehicle and the pitch angle θ is measured on board the vehicle. The **MΘ sin(θ)** term is treated as a known in the measurement equation and **MΘ** is not allowed to vary.

The system equation for the parameters is the same as for the steering system.

$$\frac{d}{dt} \begin{Bmatrix} MQ \\ M\delta \end{Bmatrix} = \begin{bmatrix} A \end{bmatrix} \begin{Bmatrix} MQ \\ M\delta \end{Bmatrix} + \begin{bmatrix} B \end{bmatrix} Q$$

where **A** is a 2x2 matrix of zeros and **B** is a 2x2 diagonal weighing matrix. Three values of parameter noise **Q** are also tested on the diving Kalman Parameter Filter.

120

Equation 5.3 has a term $[\varepsilon_q]$ which is analogous to $[\delta_a]$ from the surge equation. This is the measurement noise and is estimated by playing the Equation 5.3 model with nominal values and subtracting the measured pitch acceleration. Figure 5.4 shows the pitch acceleration error between the calculated
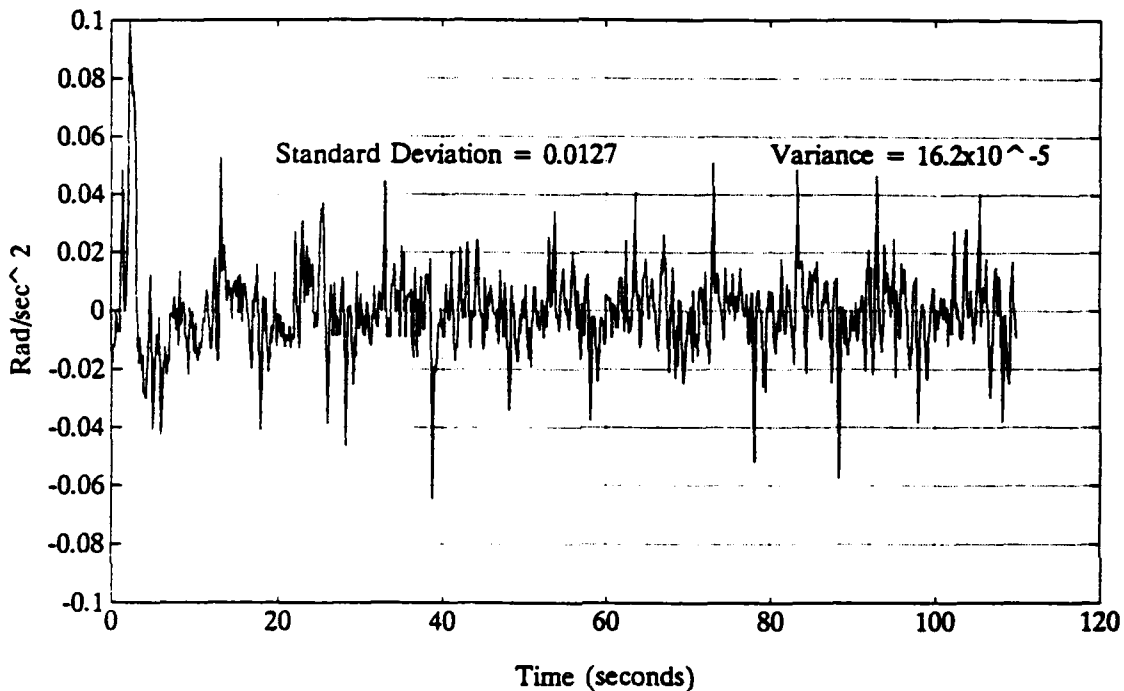
Figure 5.4   Plot of Pitch Acceleration Error

pitch acceleration and the measured pitch acceleration. The standard deviation and variance of this error is also indicated in the figure and summarized in Table 5.2 under nominal model.

The M_q coefficient was estimated by Warner and is considered here to be accurate. The objective of this section is to identify the MQ and Mδ coefficients. Nominal values of M_q and M_δ were identified by Warner and are used to calculate

the initial parameter estimates of **MQ** and **Mδ**. These nominal values are summarized in Table 5.2.

The estimation error covariance of the parameters is not known but is identified by replaying the Kalman Parameter Filter on the experimental data until the Parameter Filter converges to a steady state value of estimation error covariance. The data was run through the filter numerous times until the estimation error covariance and the estimated parameter converged. Convergence is defined here as when the final filter values are the same as the initial filter values. The variation in estimation error covariance and estimated parameter over the data file are now identical on any subsequent pass. The steady state values of estimation error covariance are summarized in Table 5.1 for the three values of Q tested on the Parameter Filter.

TABLE 5.1   STEADY STATE ESTIMATION ERROR COVARIANCE

Q	10^{-4}	10^{-6}	10^{-8}
$P_{K_{mq}}$	98.0×10^{-5}	9.00×10^{-5}	1.50×10^{-5}
$P_{K_{m\delta}}$	179.0×10^{-5}	16.0×10^{-5}	6.00×10^{-5}

Figure 5.5 shows three passes of the data through the filter for the estimation of **MQ** for each of the three values of Q tested. At the start of each data pass there is a large transient in the parameter estimation due to the initial dive

122
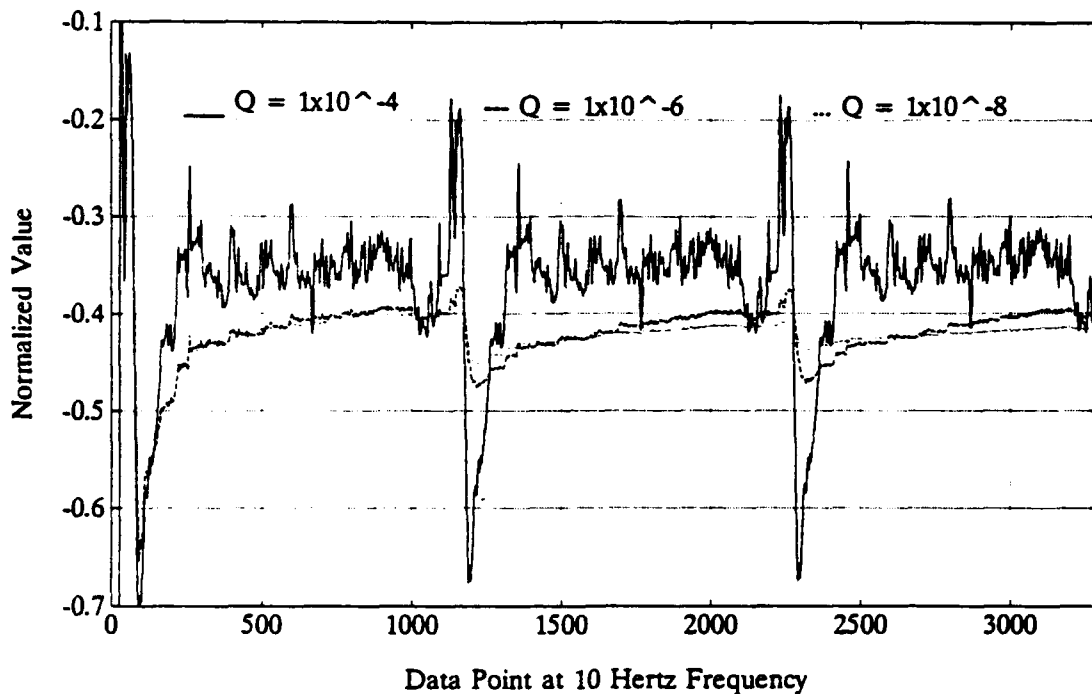
Figure 5.5   Estimation Of MQ For Various Values Of Q

transient. The initial dive transient is caused when the dive command is executed, the diving moment generated by the planes attempts to lift the after portion of the vehicle out of the water while the forward portion is pitching down into the water. The lifting of the after portion out of the water places an external force on the vehicle which is not included in our simplified diving model. This is what causes the M_q parameter to increase in magnitude on the initial dive transient. The magnitude increases to account for the increase in pitch damping caused by the external force of the water surface acting on the vehicle.

The dive transient has a duration of about 20 seconds or 200 data points at the beginning of the data file. Following the initial dive transient, the parameter estimator settles to

123

a steady state value during the remainder of the submerged porpoise maneuver. The value of M_q and M_δ identified by the parameter filter and listed in Table 5.2 are the mean value of the final filter pass, excluding the dive transient. These values of identified parameters are believed to be accurate for a fully submerged vehicle.

The value of Q equal to 10^{-6} was again chosen as the best response on a qualitative measure because it is not so fast as to include all the system noise on the parameter being estimated, but is fast enough to identify the variation in MQ and Mδ.

The estimated values of the parameters are now replayed in the simulation of Equation 5.3. The resulting pitch rate error and pitch acceleration error are computed over the data record following the diving transient. The standard deviation and the variance of the pitch rate error $[\varepsilon_q]$ and the pitch acceleration error $[\varepsilon_q]$ are tabulated in Table 5.2 for each value of Q. The results in the table indicate that for Q = 1×10^{-6} the identified values of MQ = -0.2423 and Mδ = -0.0304 give reduced rate and acceleration errors between the first order model and the experimental data when compared to the nominal model. The simulation of Equation 5.3 is shown in Figure 5.6 for the nominal values predicted by Warner and the refined values from the first order model. Figure 5.7 shows the pitch acceleration error following parameter identification.
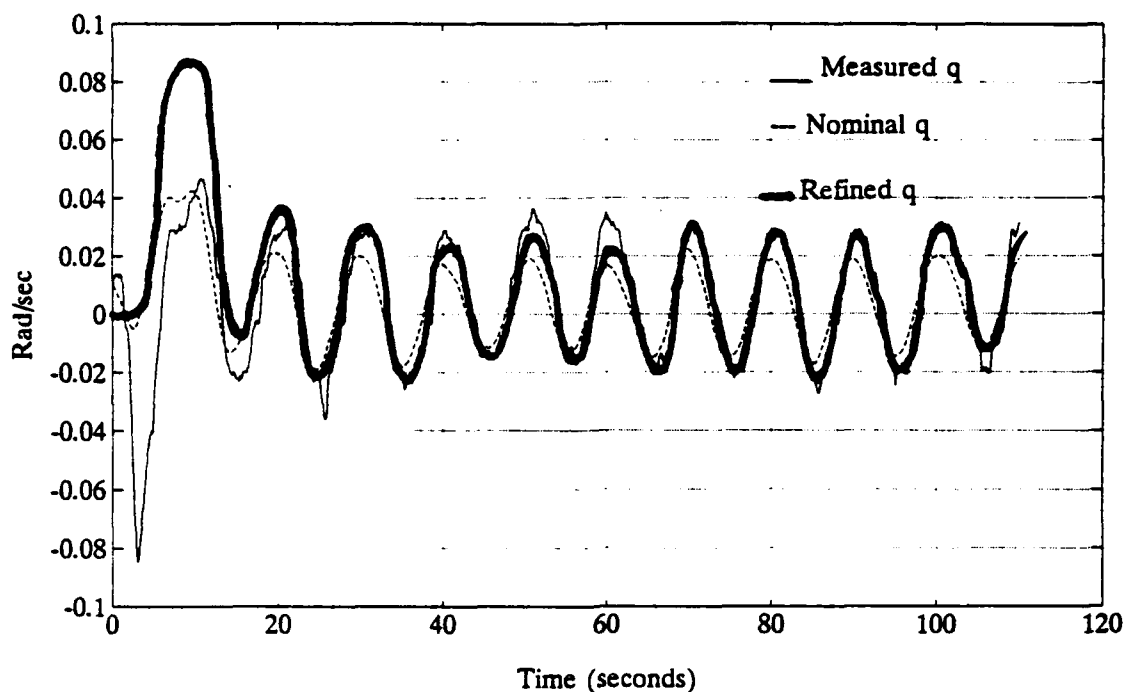
Figure 5.6   Simulation   Results   Of   Nominal   And   Refined   Hydrodynamic Coefficients

Standard Deviation = 0.0116   Variance = 13.5×10^{-5}
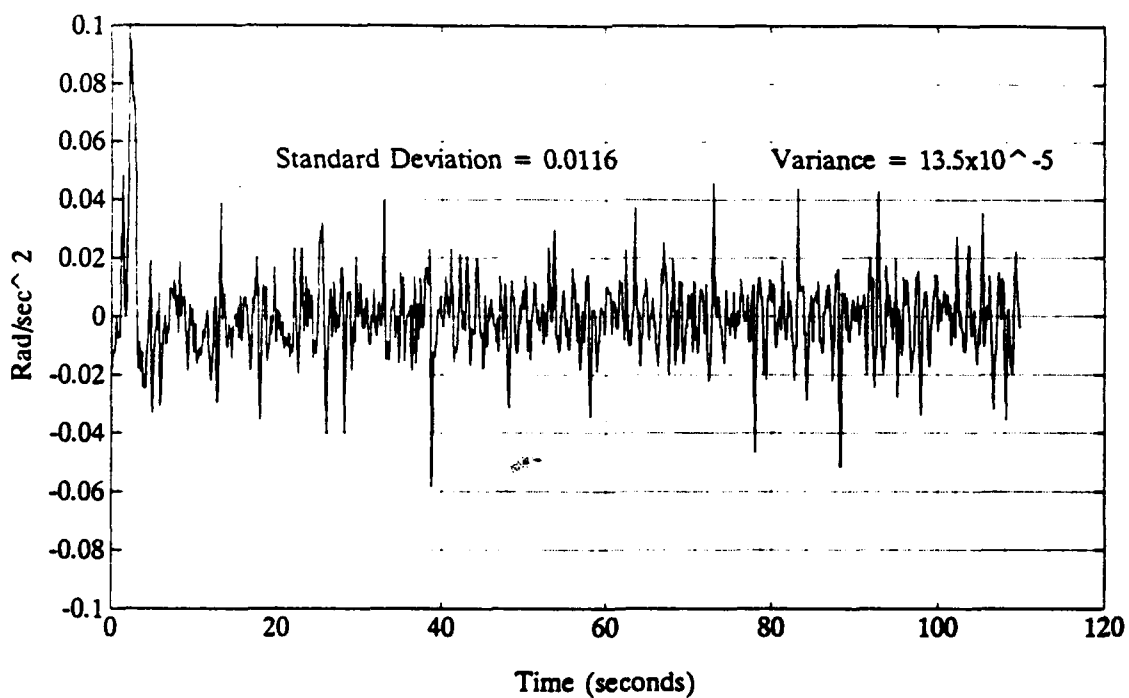
Figure 5.7   Pitch Acceleration Error Following Identification

125

TABLE 5.2   KALMAN PARAMETER FILTER RESULTS FOR DIVING SYSTEM

Q	Nominal Model	10^{-4}	10^{-6}	10^{-8}
MQ	-0.5865	-0.2142	-0.2423	-0.2404
Mδ	-0.0348	-0.0295	-0.0304	-0.0298
[ϵ_q] STD DEV	0.0091	0.0042	0.0041	0.0041
[ϵ_q] VARIANCE	8.27×10^{-5}	1.75×10^{-5}	1.68×10^{-5}	1.70×10^{-5}
[ϵ_q] STD DEV	0.0127	0.0117	0.0116	0.0116
[ϵ_q] VARIANCE	16.2×10^{-5}	13.9×10^{-5}	13.5×10^{-5}	13.6×10^{-5}

2.   Identification of Z_δ from M_δ

The input moment due to a plane deflection is related to the location of the vehicles planes. The diving relations are identical to the steering relations. Therefore, the vertical force applied to the vehicle by each plane may be identified. The input moment due to plane deflection is equal to the lift force developed by the plane times the distance between the planes.

126

$$M_\delta = Z_{\delta_s} x_s - Z_{\delta_b} x_b$$

where:

$Z_{\delta_s} = Z_{\delta_b}$ due to identical planes

$x_b = 0.283\,L$ is the distance from the center of the vehicle

to the bow planes

$x_s = -0.377\,L$ is the distance from the center of the vehicle

to the stern planes, therefore:

$$M_\delta = Z_{\delta_s}(x_s - x_b) = -4.8194\,Z_{\delta_s}$$

Using the above relations, the vertical plane coefficient Z_{δ_s}

and Z_{δ_b} can be directly determined when the M_δ coefficient is

determined.

$$M_\delta = M\delta(I_y - M_q) \qquad Z_{\delta_s} = Z_{\delta_b} = \frac{-M_\delta}{4.8194}$$

The hydrodynamic coefficients needed for the 6 DOF computer
model are the non-dimensional hydrodynamic coefficients
defined as follows:

$$\acute{M}_q = \frac{M_q}{\frac{1}{2}\rho L^4} \qquad \acute{Z}_{\delta_s} = \frac{Z_{\delta_s}}{\frac{1}{2}\rho L^2} \qquad \acute{Z}_{\delta_b} = \frac{Z_{\delta_b}}{\frac{1}{2}\rho L^2}$$

$$\acute{M}_{\delta_s} = -0.377 L \acute{Z}_{\delta_s} \qquad \acute{M}_{\delta_b} = 0.283 L \acute{Z}_{\delta_b}$$

The identification yields the values in Table 5.3 for the non-dimensional diving hydrodynamic coefficients.

TABLE 5.3 NON-DIMENSIONAL HYDRODYNAMIC COEFFICIENTS FROM FIRST ORDER MODEL

$\acute{M}_q$	$\acute{Z}_{\delta_s}$	$\acute{Z}_{\delta_b}$	$\acute{M}_{\delta_s}$	$\acute{M}_{\delta_b}$
-0.0147	0.0205	0.0205	-0.0564	0.0424

3. Parameter Verification By Sensitivity Analysis

Similar to the steering system , the four coefficients of most importance in the diving system dynamics are Z_w, Z_δ, M_q and M_δ. Of the four coefficients, Z_δ and M_δ have a kinematic relationship to each other. the purpose of this section is to study the sensitivity of each of the three independent coefficients on the analytical model of the diving system. The analytical model is run holding all coefficients constant and varying one at a time from -60% to +60% in 20% increments from the nominal value as refined from the Kalman Parameter Filter. The results on pitch rate are shown in Figures 5.8 to 5.10, and results on predicted heave velocity are shown in Figures 5.11 to 5.13. Pitch angle is a direct integration of the pitch

rate and therefore if the pitch rate can be predicted accurately, the pitch angle will also be predicted accurately. It is seen from Figures 5.10 and 5.13 that a variation in Z_w has no effective change on pitch rate and has only a small effect on heave velocity. Table 5.8 summarizes the effects on the pitch rate and pitch acceleration errors from varying the Z_w coefficient. This indicates minimal effects on pitch rate and pitch acceleration errors as Z_w is varied. The heave velocity of the NPS AUV II is not measured directly on the vehicle so a direct comparison of measured to modeled heave velocity is not possible. Vehicle depth is recorded directly from a depth cell. The depth record can be differentiated to produce a record of depth rate. The depth rate is equivalent to $\dot{z}$, of the Euler relation. Using a small angle approximation for the pitch angle, the Euler relation can be written as:

$$\dot{z} = w - u\theta$$

of which only w is not measured. The correct Z_w can be identified by the amount of heave velocity needed to minimize the error in the Euler relation for depth rate.

From the figures for variations in Z_δ and M_q, it is seen that a change in these coefficients affects both analytical results of pitch rate and heave velocity considerably. It is necessary to settle in on the correct Z_δ and M_q prior to adjusting the Z_w coefficient to correct the heave velocity. Table 5.6 indicates M_q generates a minimum error when

increased by approximately 8%. Table 5.7 shows the pitch rate and pitch acceleration error for Z_δ and indicates that an increase of 5% is needed to minimize the pitch rate and pitch acceleration errors. From a trial and error approach, the combination of an increase of 4% in M_q and an increase of 3% in Z_δ produces the minimum errors.

With the M_q and Z_δ coefficients refined, variations of the Z_w coefficient are investigated to minimize the error in the depth rate equation. A factor of 10 increase in Z_w is seen to give the minimum error. Figure 5.14 shows a plot of the measured depth rate $\dot{Z}$, and the calculated depth rate from the estimated heave velocity minus the $u*\sin(\theta)$ term. This match of the estimated depth rate to the measured depth rate gives the best estimate of the Z_w coefficient. It is also noted here that the major contribution to the depth rate is from the $u*\sin(\theta)$ term and little if any directly from the heave velocity. The implication of this is that the NPS AUV II has very little side slip in the vertical plane.

The final identified diving parameters are summarized as follows in Table 5.4 and the rate and acceleration errors are summarized in Table 5.5.

TABLE 5.4 FINAL NON-DIMENSIONAL DIVING SYSTEM HYDRODYNAMIC COEFFICIENTS

$\acute{Z}_w$	$\acute{Z}_{\delta_s}$	$\acute{Z}_{\delta_b}$
-0.7844	-0.0211	-0.0211

$\acute{M}_q$	$\acute{M}_{\delta_s}$	$\acute{M}_{\delta_b}$
-0.0153	-0.0581	0.0436

TABLE 5.5 FINAL PITCH RATE AND PITCH ACCELERATION ERRORS

STD DEV $[\varepsilon_q]$	VARIANCE $[\varepsilon_q]$	STD DEV $[\varepsilon_q]$	VARIANCE $[\varepsilon_q]$
0.0111	1.24×10^{-4}	0.0149	2.23×10^{-4}

131
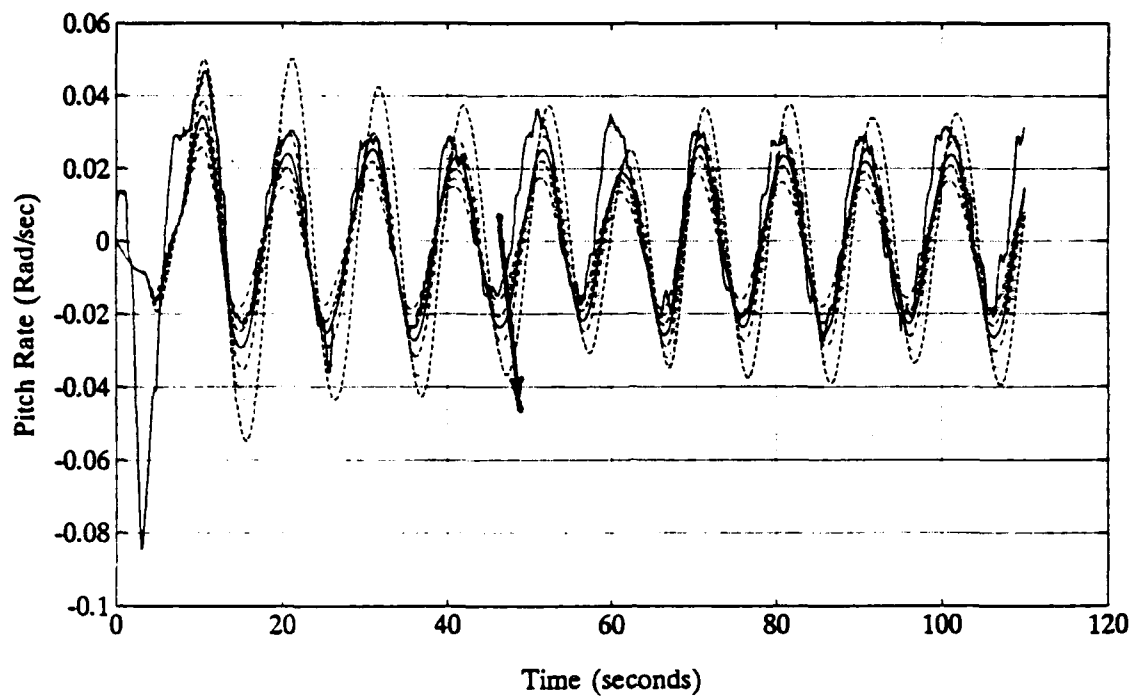
Figure 5.8   Parameter Sensitivity of M_q on Pitch Rate
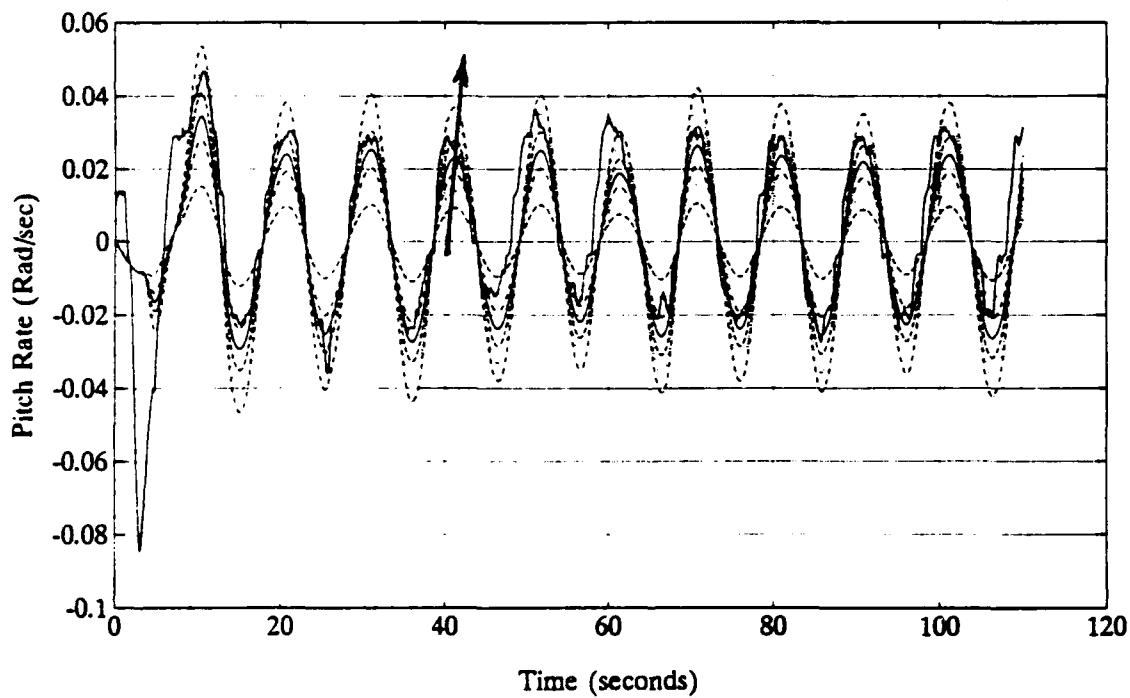
Figure 5.9   Parameter Sensitivity of Z_δ on Pitch Rate

132
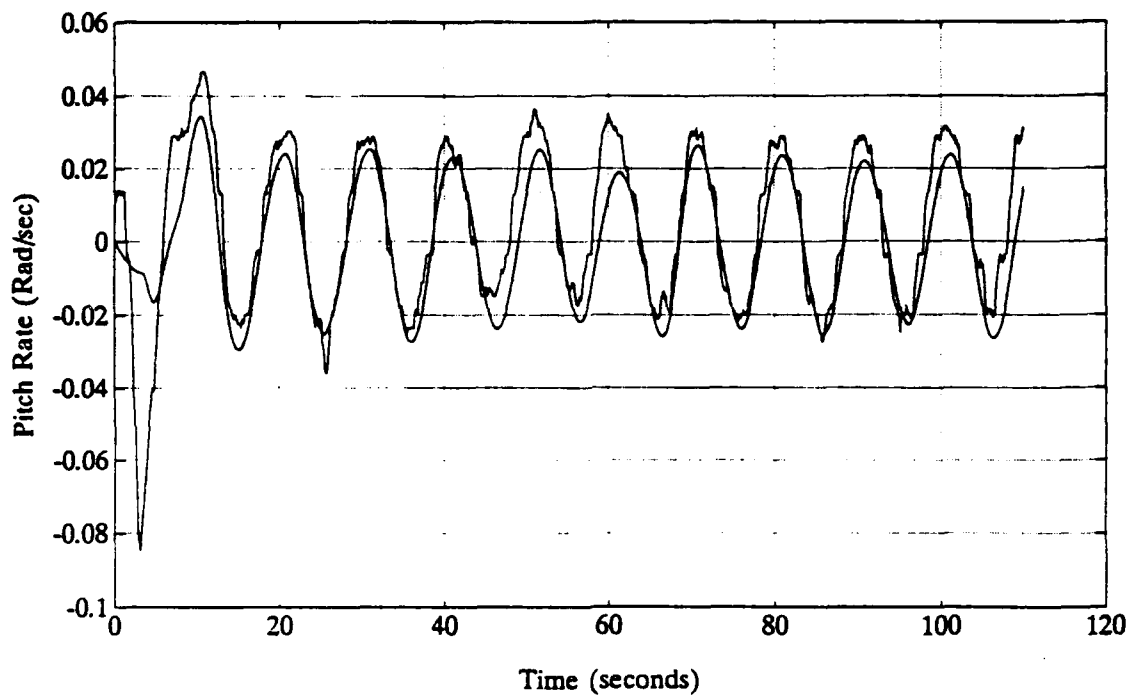
Figure 5.10 Parameter Sensitivity of Z_w on Pitch Rate
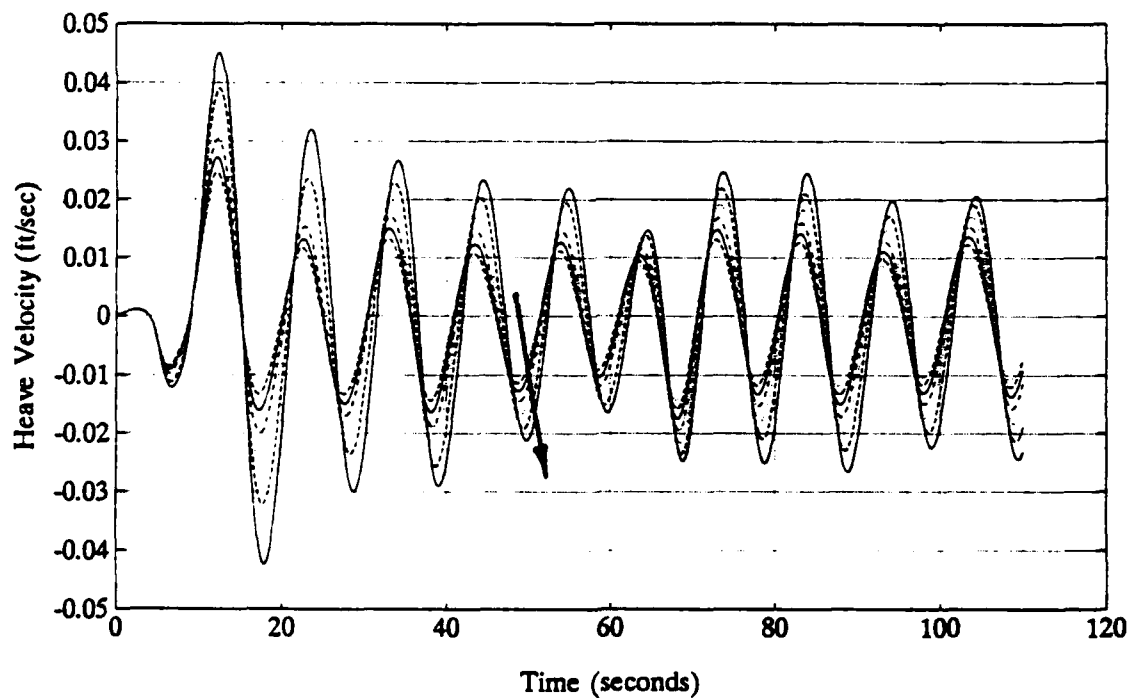
Figure 5.11 Parameter Sensitivity of M_q on Heave Velocity

133
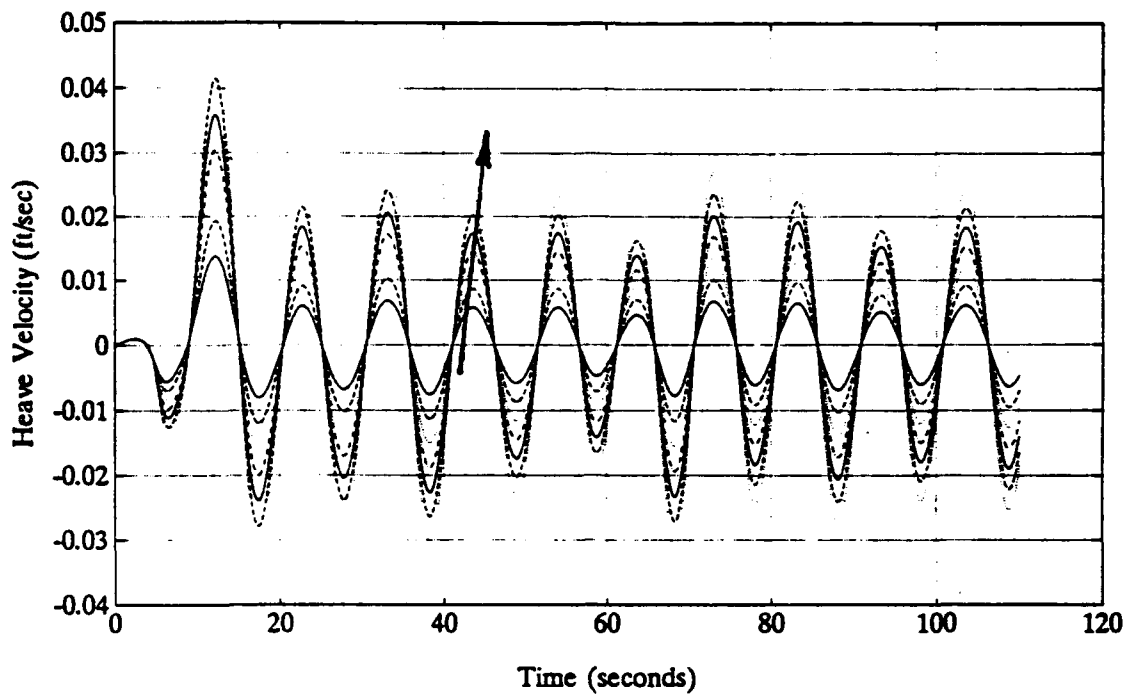
Figure 5.12 Parameter Sensitivity of Z_δ on Heave Velocity
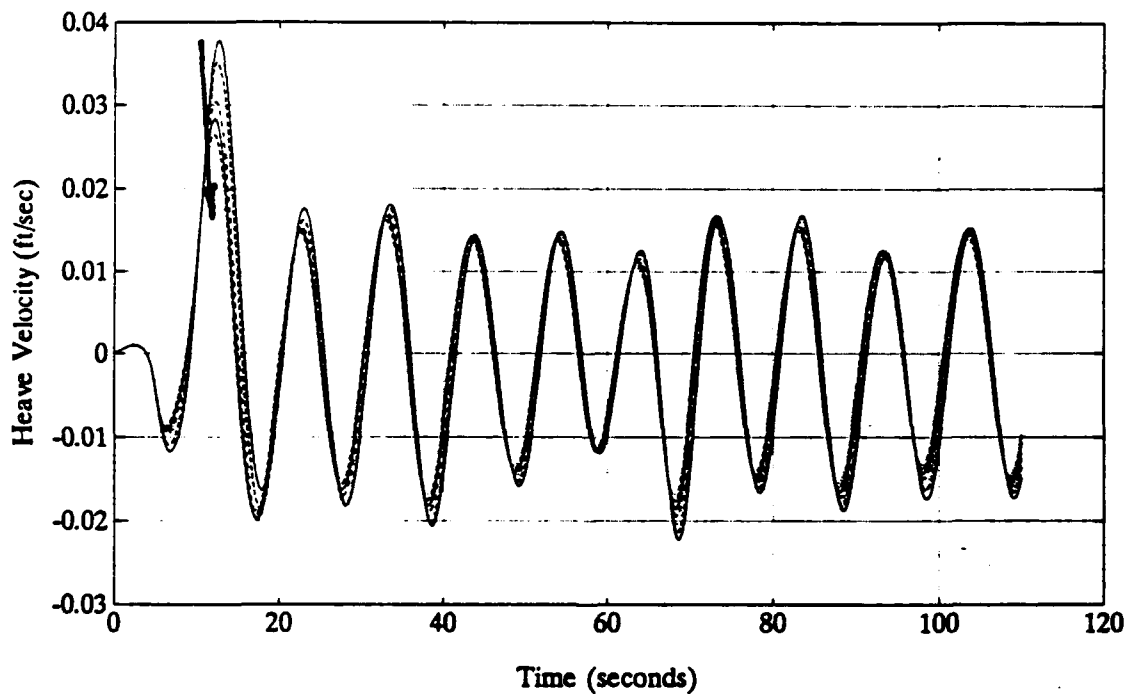
Figure 5.13 Parameter Sensitivity of Z_w on Heave Velocity

134
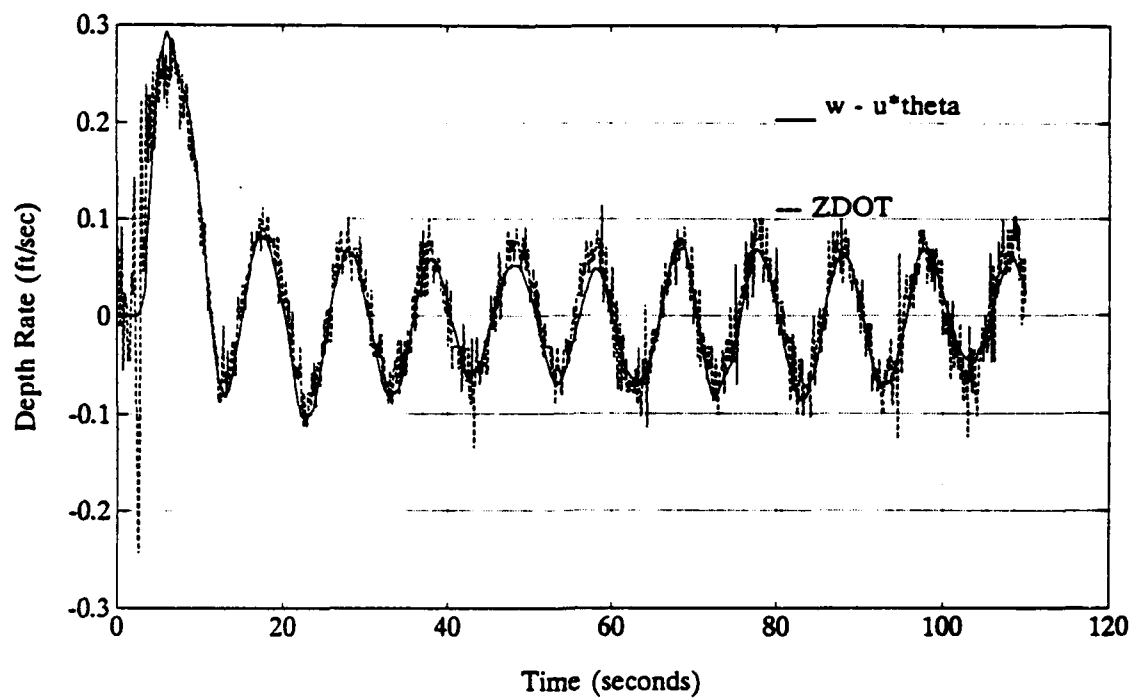
Figure 5.14 Comparison of Measured Depth Rate and Estimated Depth Rate

TABLE 5.6   PARAMETER SENSITIVITY OF M_q

PERCENT CHANGE	STD DEV $[\varepsilon_q]$	VARIANCE $[\varepsilon_q]$	STD DEV $[\varepsilon_q]$	VARIANCE $[\varepsilon_q]$
-60%	0.0196	3.84×10^{-4}	0.0180	3.23×10^{-4}
-40%	0.0148	2.19×10^{-4}	0.0162	2.61×10^{-4}
-20%	0.0122	1.48×10^{-4}	0.0153	2.33×10^{-4}
Nominal	0.0112	1.26×10^{-4}	0.0150	2.24×10^{-4}
+20%	0.0113	1.27×10^{-4}	0.0149	2.23×10^{-4}
+40%	0.0118	1.39×10^{-4}	0.0151	2.27×10^{-4}
+60%	0.0124	1.55×10^{-4}	0.0153	2.32×10^{-4}

TABLE 5.7   PARAMETER SENSITIVITY OF Z_δ

PERCENT CHANGE	STD DEV [ϵ_q]	VARIANCE [ϵ_q]	STD DEV [ϵ_q]	VARIANCE [ϵ_q]
-60%	0.0159	2.51×10^{-4}	0.0165	2.71×10^{-4}
-40%	0.0137	1.86×10^{-4}	0.0157	2.46×10^{-4}
-20%	0.0120	1.45×10^{-4}	0.0152	2.30×10^{-4}
Nominal	0.0112	1.26×10^{-4}	0.0150	2.24×10^{-4}
+20%	0.0114	1.30×10^{-4}	0.0150	2.26×10^{-4}
+40%	0.0126	1.57×10^{-4}	0.0154	2.38×10^{-4}
+60%	0.0144	2.08×10^{-4}	0.0161	2.59×10^{-4}

TABLE 5.8   PARAMETER SENSITIVITY OF Z_w

PERCENT CHANGE	STD DEV $[\varepsilon_q]$	VARIANCE $[\varepsilon_q]$	STD DEV $[\varepsilon_q]$	VARIANCE $[\varepsilon_q]$
-60%	0.0112	1.25×10^{-4}	0.0149	2.23×10^{-4}
-40%	0.0112	1.25×10^{-4}	0.0149	2.23×10^{-4}
-20%	0.0112	1.26×10^{-4}	0.0150	2.23×10^{-4}
Nominal	0.0112	1.26×10^{-4}	0.0150	2.24×10^{-4}
+20%	0.0112	1.26×10^{-4}	0.0150	2.24×10^{-4}
+40%	0.0113	1.27×10^{-4}	0.0150	2.24×10^{-4}
+60%	0.0113	1.27×10^{-4}	0.0150	2.24×10^{-4}

B. SLIDING MODE CONTROLLER DESIGN

The design if the sliding mode diving controller follows directly from the development of sliding mode theory in Chapter II. The diving controller is designed here in parallel with the procedure used on the steering controller with the only difference being the diving controller is a three state controller vice a two state controller. The applicable equations to describe the diving system are the heave, pitch and Euler relations for θ and $\dot{z}$. As with the steering system, the use of the heave equation in the diving system requires the heave velocity to be measured as an input to the diving controller. McDonald (1989) showed that a diving controller would function satisfactory without the input of heave velocity using only inputs of q pitch rate, θ pitch angle and Z depth. In order to keep the diving system controller as a simple as possible, the reduced order controller proven by McDonald (1989) is developed here for the NPS AUV II.

To begin the design of the diving controller, the SIMO subsystem equations must be identified to fit the form of Equation 2.1. the diving system equations of pitch rate and Euler relations for pitch angle and depth are written in state space form as:

139

$$\begin{Bmatrix} \dot{q} \\ \dot{\theta} \\ \dot{Z} \end{Bmatrix} = \begin{bmatrix} \dfrac{(M_q - mx_G)}{(I_y - M_{\dot{q}})} u_0 & \dfrac{-z_G W}{I_y - M_{\dot{q}}} & 0 \\ 1 & 0 & 0 \\ 0 & -u_0 & 0 \end{bmatrix} \begin{Bmatrix} q \\ \theta \\ Z \end{Bmatrix} + \begin{bmatrix} \dfrac{M_\delta}{(I_y - M_{\dot{q}})} u_0^2 \\ 0 \\ 0 \end{bmatrix} \delta_s$$

The equations are linearized about the nominal operating point of $u_0 - 1.5$ (ft/sec) and the state error vector is defined as:

$$\tilde{x} = \begin{Bmatrix} \tilde{q} \\ \tilde{\theta} \\ \tilde{z} \end{Bmatrix} = \begin{Bmatrix} q - q_{com} \\ \theta - \theta_{com} \\ Z - Z_{com} \end{Bmatrix}$$

with $u(t) = \delta_s$ a direct substitution can be made into Equation 2.5, the sliding mode control law.

The three terms which remain to be determined are the nonlinear switching term gain η, The boundary layer thickness ϕ and the **s** for the sliding surface definition. Following the method outlined in Chapter II, the **s** is defined as the right eigenvector of $(A - Bk)^T$, the transpose of the desired closed loop system dynamics, which corresponds to the zero eigenvalue. At this point in the process, it is necessary to choose the desired poles of the closed loop system dynamics again noting that one of the poles must be placed at the origin to allow the decomposition of the sliding mode control law. The open loop poles of the refined system are:

[0   -0.1817+0.4451i   -0.1817-0.4451i].

140

Therefore we already have a pole at the origin due to the direct integration of θ from q. The remaining poles are on the negative real axis and it is desired to move these poles to -0.5 + 0.4i and -0.5 - 0.4i, thereby increasing the response of the sliding surface dynamics. Using the linearized system equation, desired poles of [0   -0.5+0.4i   -0.5-0.4i] and standard pole placement techniques, the eigenvectors of the closed loop system dynamics transposed is:

$$\begin{bmatrix} 0.5261+0.6576i & 0.5261-0.6576i & -0.6943 \\ 0.0+0.5392i & 0.0-0.5392i & -0.6943 \\ 0 & 0 & 0.1898 \end{bmatrix}$$

with s defined as the right eigenvector corresponding to the zero eigenvalue,

$$s = \begin{bmatrix} -0.6943 \\ -0.6943 \\ 0.1898 \end{bmatrix} \quad \text{and} \quad s^T = [-0.6943 \quad -0.6943 \quad 0.1898] .$$

The remaining terms to define in the control law are the nonlinear switching term gain η and the boundary layer thickness ϕ. As shown in Chapter II, the nonlinear switching term gain must be greater than the bounded value of the unknown modeling errors. The system identification procedure used earlier in this chapter produced a plot of pitch acceleration error, Figure 5.7. This pitch acceleration error can be bounded by taking the absolute maximum value of the error and ensuring that η is larger than this value, thereby guaranteeing stability. Alternatively, a stochastic method can

141

be used to provide a confidence bound on the value of η required to have the pitch acceleration error contained within the bounds of η.

Once the minimum value of the nonlinear switching term gain is determined, a value of ϕ, the boundary layer thickness is estimated based on the desired amount of allowable state error on the system.

Taking the sliding mode control law and reducing it to only the nonlinear switching term yields:

$$u(t) = - [s^T B]^{-1} \eta_0^2 \tanh\left(\frac{s^T(\bar{X})}{\phi}\right)$$

Knowing the maximum amount of actuator response or movement u_{max} and solving the above equation for η gives a relation for the value of η which will cause the control actuator to saturate for a given value of state error.

$$\eta_0^2 = \frac{u_{max}}{[s^T B]^{-1} \tanh\left(\frac{s^T(\bar{X})}{\phi}\right)}$$

By holding ϕ fixed and varying the amount of state error a plot of η versus state error can be generated for a fixed value of ϕ. A family of these curves is generated in Figure 5.15 where $u_{max} = 0.4$ radians, the limit of plane deflection. The desired boundary layer thickness is chosen the same as in Chapter IV. Following this design procedure creates a sliding
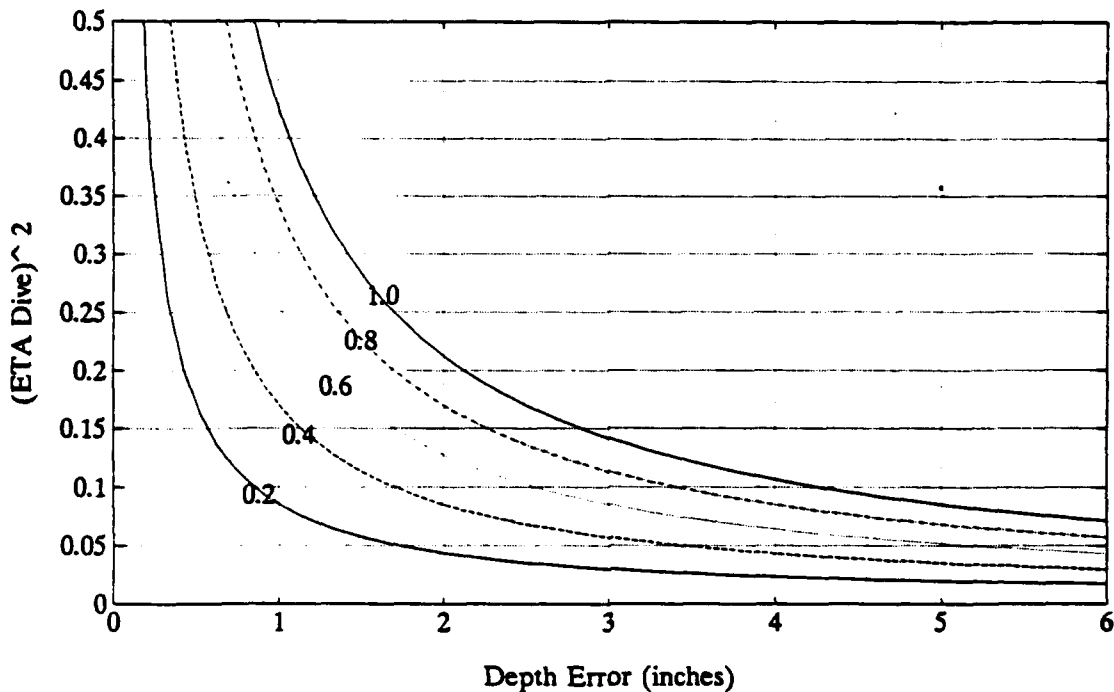
142

Figure 5.15 Plot Of η vs State Error For Various Values Of φ

mode control which is guaranteed to be stable and has the capability of controlling the amount of allowable steady state error.

F. DESIGN OF KALMAN STATE FILTER FOR THE DIVING SYSTEM

Following the discussion of Chapter IV, the Kalman State Filter can be used to reduce the sensor noise of the pitch rate gyro, the pitch angle gyro and depth cell. An additional advantage of the Kalman State Filter is that it is an optimal estimator and will also estimate w heave velocity. The design of the Kalman State Filter for the diving system follows the procedure outlined in Chapter II for a general Kalman filter. The system equations needed for the diving system Kalman State

143

Filter are the heave, pitch rate and Euler relations for pitch angle and depth. These three equations are written in state space form as follows:

$$\dot{x} = M^{-1}Ax + M^{-1}Bu + [\varepsilon_x]$$

where: $x = \begin{bmatrix} w \\ q \\ \theta \\ z \end{bmatrix}$ is the state vector, $[\varepsilon_x]$ = the modeling error

vector in the state equations or equivalently stated as the system noise vector and $u = \delta_s$ the commanded plane deflection.

$$M = \begin{bmatrix} (m - Z_w) & (-mx_G - Z_q) & 0 & 0 \\ (-mx_G - M_w) & (I_y - M_q) & 0 & 0 \\ 0 & 0 & 1 & 0 \\ 0 & 0 & 0 & 1 \end{bmatrix}$$ is the mass matrix

$$A = \begin{bmatrix} Z_w u_c & (Z_q + m)u_0 & 0 & 0 \\ M_w u_0 & (M_q - mx_G)u_0 & -z_G W & 0 \\ 0 & 1 & 0 & 0 \\ 1 & 0 & -u_0 & 0 \end{bmatrix}$$ is the steering system dynamics

$$B = \begin{bmatrix} Y_\delta u_0^2 \\ N_\delta u_0^2 \\ 0 \\ 0 \end{bmatrix}$$ is the system input matrix

The measurements available are q pitch rate, θ pitch angle and Z depth. This provides the following measurement equation:

$$y = \begin{bmatrix} 0 & 1 & 0 & 0 \\ 0 & 0 & 1 & 0 \\ 0 & 0 & 0 & 1 \end{bmatrix} \begin{Bmatrix} w \\ q \\ \theta \\ Z \end{Bmatrix} + \begin{Bmatrix} v_q \\ v_\theta \\ v_z \end{Bmatrix}$$

The plant noise covariance can be taken as the variance of the parameter identification error of Figure 5.7 and the measurement noise covariance can be taken as the square of the standard deviations of the individual measurements. The initial state estimate is set equal to the initial data point in the data record. This allows the initial estimation error covariance to be set equal to zero.

The filter results for pitch rate are shown in Figure 5.16, showing an improvement in the smoothness of the signal. The figure also shows the deviation in the estimated pitch rate from the measured pitch rate during the dive transient. This is as expected and would have had a closer match in this portion of the maneuver if the surface effect had not been present. Figure 5.17 shows the results for the pitch angle θ. The filter shows a small bias due to the initial orientation of the planes on the NPS AUV II. The planes operate off a position servo without position feedback. Therefore, if the planes are not perfectly aligned to the zero setting, the initial bias is carried in the plane command throughout the
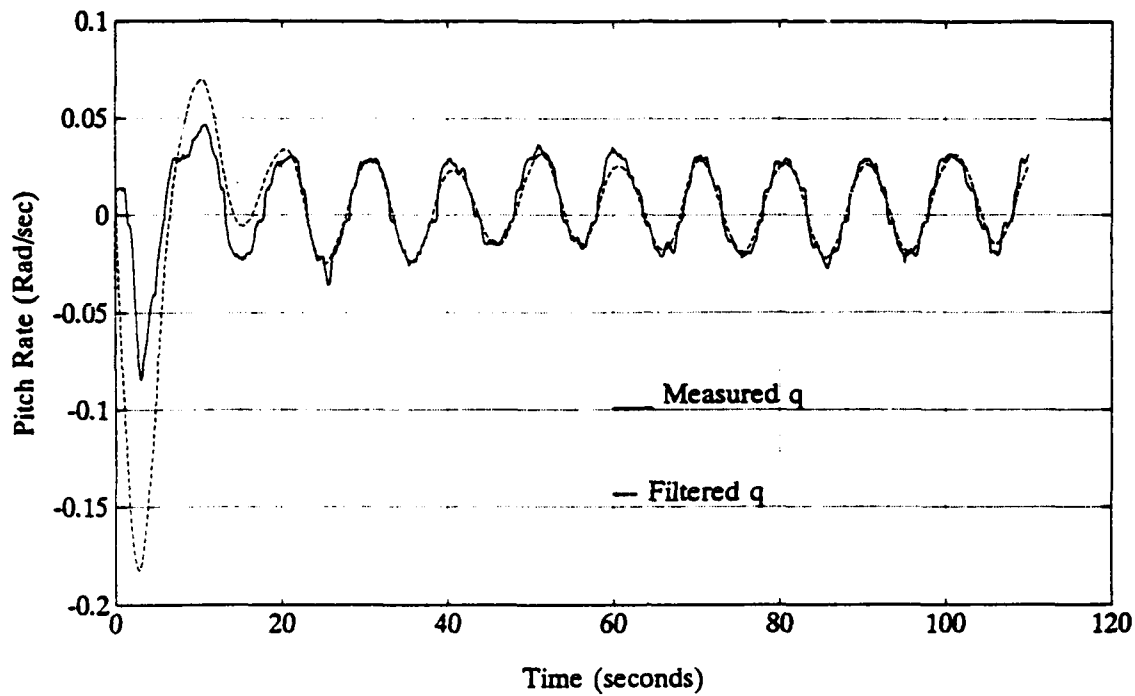
145

Figure 5.16 Kalman State Filter Results for q
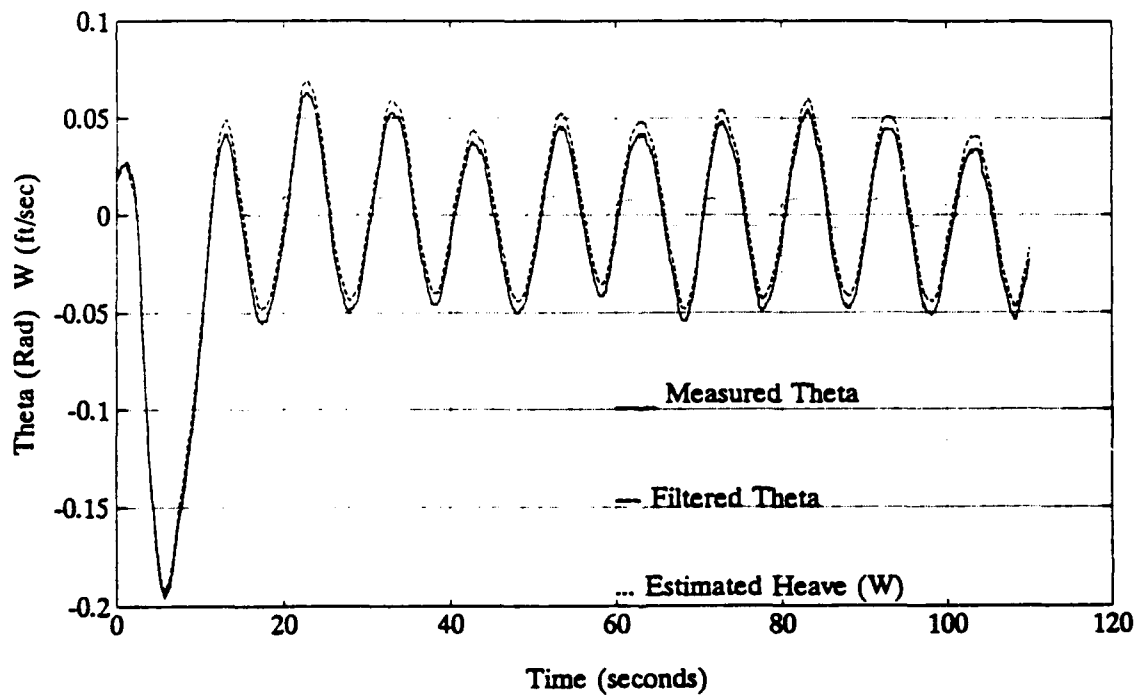
Figure 5.17 Kalman State Filter Results θ and w

146

mission. This initial bias is easily compensated for by the controller but when the record of dive plane commands are played back through the analytical model, the biases are included and affect the calculated position and orientation related variables. An optimal estimation of **w**, based on the system parameters is shown in Figure 5.17. This estimation of **w** is available to the navigation system to compute a dead reckoned position of vehicle depth. Figure 5.18 shows the results of the depth signals. It is seen that the measured and filtered signals are identical due to the low noise on the signal of the depth cell.
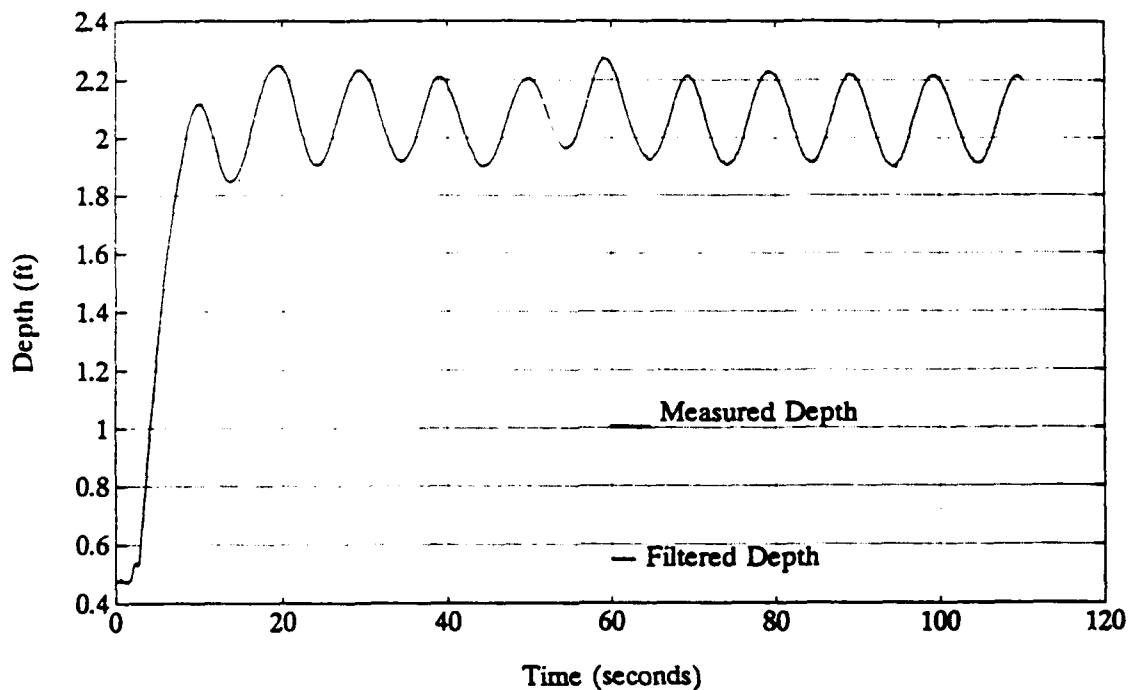
Figure 5.18 Kalman State Filter Results for Z

147

G. CLOSED LOOP SIMULATION OF THE SLIDING MODE DIVING CONTROLLER WITH FILTERED INPUTS

Figure 5.19 shows the block diagram of the closed loop diving simulation model incorporating the vehicle model, the injection of signal noise on the measured states of the vehicle model and the Kalman State Filter, to provide clean
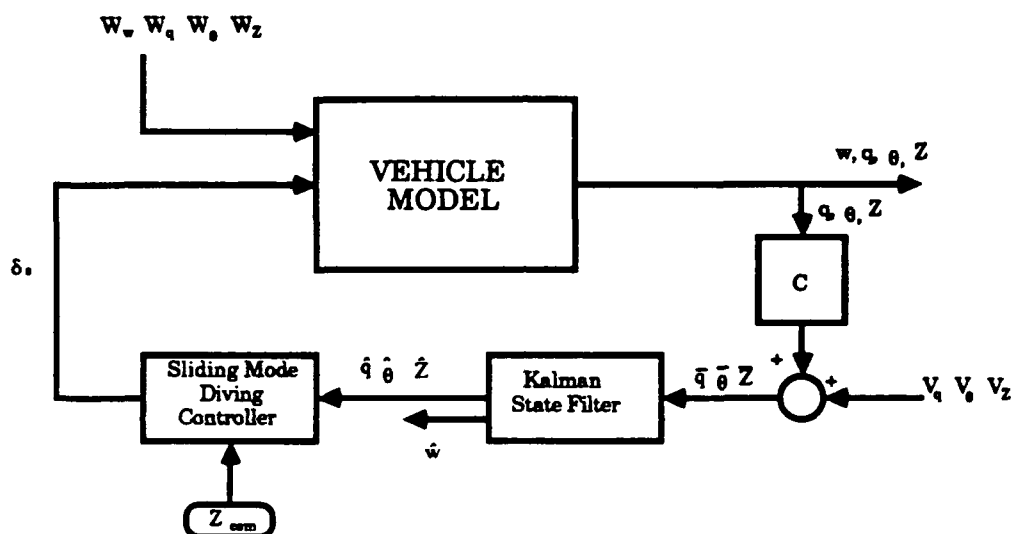
Figure 5.19 Block Diagram of Closed Loop Sliding Mode Diving Control With Kalman State Filter

signals to the sliding mode diving controller. Figure 5.20 shows the commanded depth and the vehicles noisy depth, indicating the control system is stable and tracks the commanded depth. Figure 5.21 shows the vehicles noisy pitch rate and the filtered pitch rate from the analytical model.

148
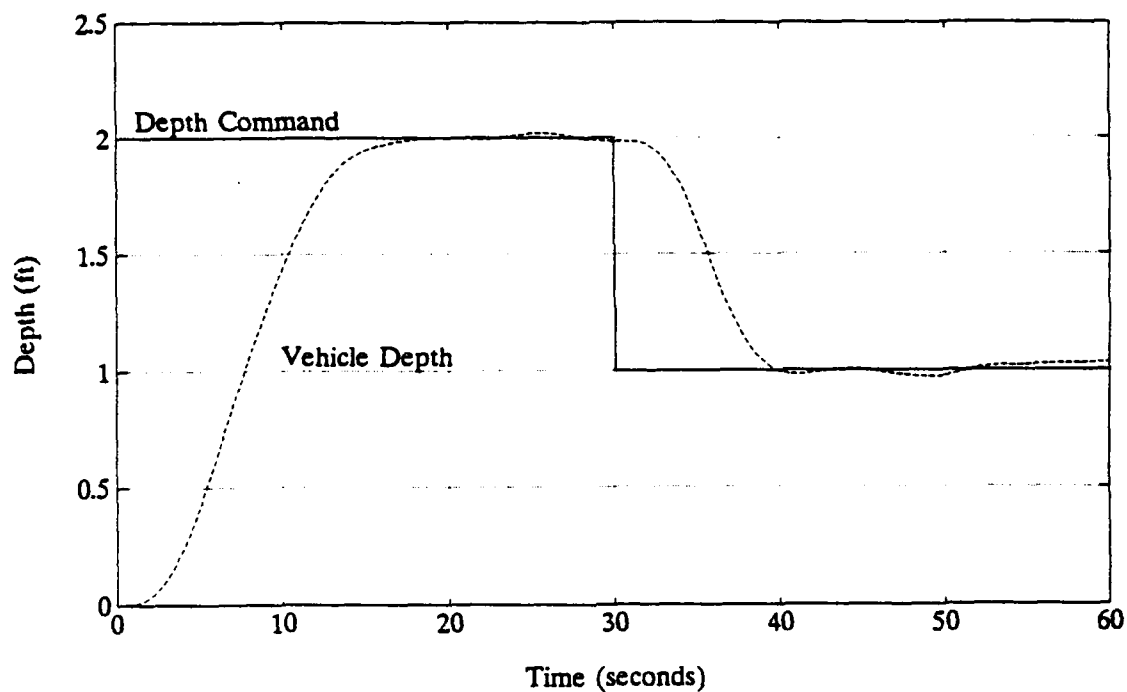
Figure 5.20 Depth Results of Closed Loop Simulation
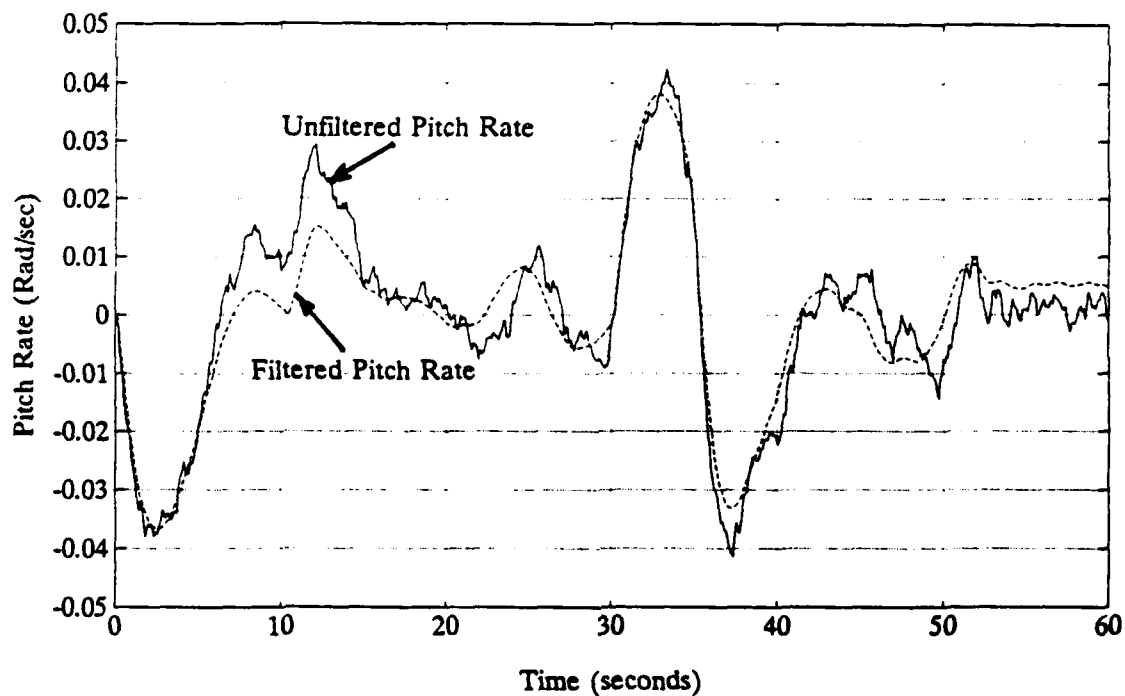
Figure 5.21 Pitch Rate Results of Closed Loop Simulation with Kalman State Filter

149

Figure 5.22 shows the filtered and unfiltered pitch angle signal from the closed loop simulation. The filtered and unfiltered pitch angles plot on top of each other indicating the Kalman State Filter is effective in filtering out the inputed signal noise without significant lags in the filtered pitch angle. Figure 5.23 shows the resulting plane command from the sliding mode control law from both filtered and unfiltered signals. The figure clearly shows that much of the chatter from the sensor noise can be removed from the control signal by applying the Kalman State Filter in the control loop. The response of the simulation with the input noise and Kalman State Filter included indicate adequate control of the system.
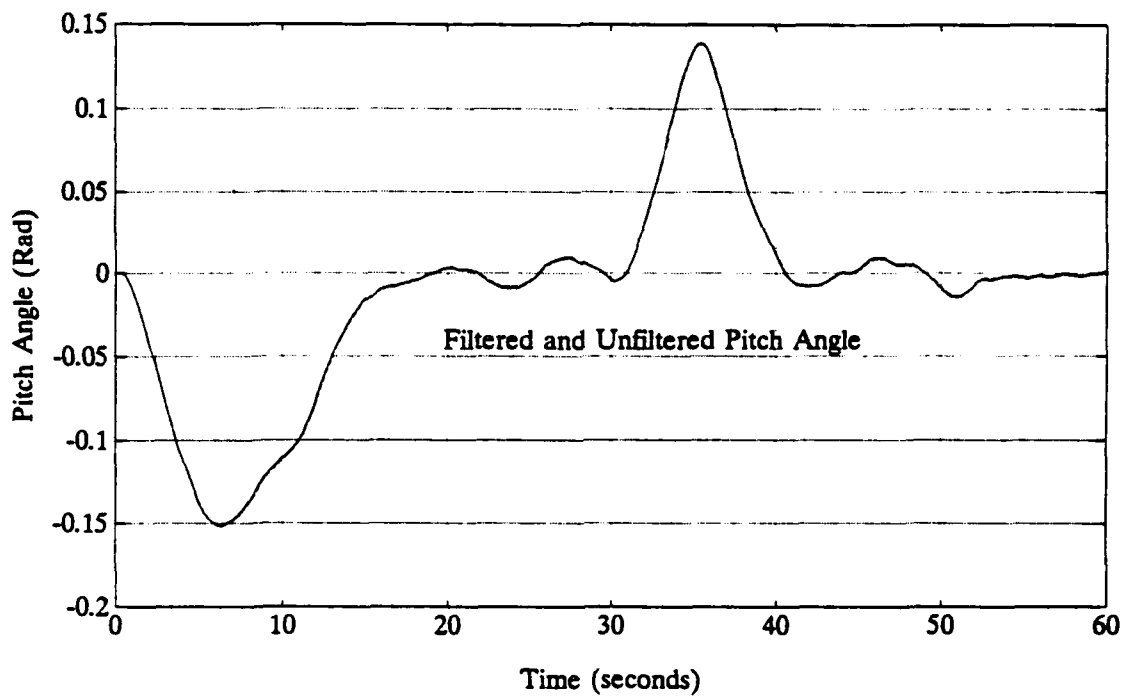
Figure 5.22 Pitch Angle Results of Closed Loop Simulation with Kalman State Filter
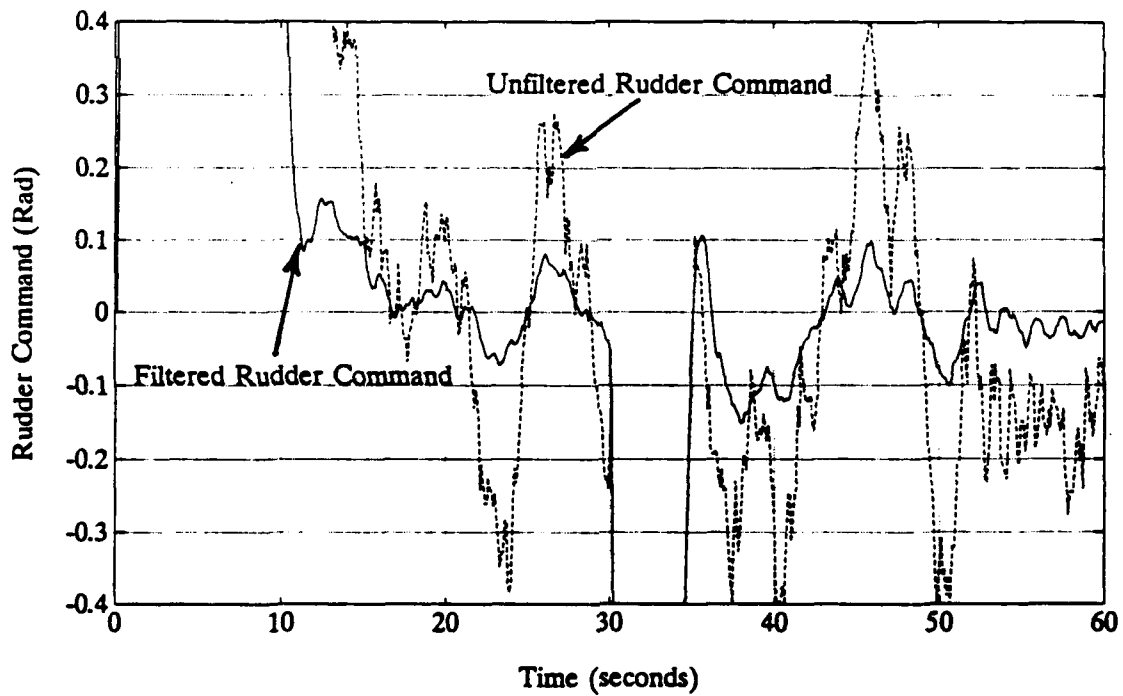
Figure 5.23 Rudder Angle Commands From Filtered and Unfiltered Input Signals

151

H. SUMMARY

This chapter shows that the same system identification technique can be used to identify the major important diving hydrodynamic coefficients. The identification technique can be used as an on-line fault monitor for the on board diagnostics system. The identified hydrodynamic coefficients are used in the design of a sliding mode control law and an optimal state estimator. The combination of optimal state estimator and sliding mode controller provides a robust control subsystem for the NPS AUV II's autopilot.

VI.   CONCLUSIONS AND RECOMMENDATIONS

A.   CONCLUSIONS

It has been shown that the Kalman Parameter Filter and a simple analytical model can provide accurate predictions of the NPS AUV II's response parameters. Once these parameters are identified they can be used by a fault monitor to detect changes in the vehicles operating characteristics. The Kalman Parameter Filter can be coded into the guidance/autopilot systems of the NPS AUV II to provide a real time estimate of the vehicles response parameters.

The use of a sliding mode controller has the advantage of added robustness in that the desired sliding surface dynamic characteristics can be designed into the linear portion of the controller and the nonlinear switching term can have a large gain to force the system to return to the sliding surface. The disadvantage of a large nonlinear switching term gain is that sensor noise is highly amplified and directed to the control actuator in the form of chatter.

The negative effects of the sliding mode controller can be reduced by two separate means: first a boundary layer thickness can be controlled by adjusting the slope of the hyperbolic tangent function of the nonlinear switching term, and secondly a Kalman State Filter can be used to filter the

input sensor noise. The Kalman State Filter has the added advantage that it can optimally estimate the unmeasured sway and heave velocities. The sway and heave velocity estimates may then be used to provide improved estimates of global vehicle location.

B. RECOMMENDATIONS

It is recommended that further study of the results of the Kalman Parameter Filter be conducted on the NPS AUV II with equipment faults programmed into the mission profile to verify the Kalman Parameter Filter can detect the existence of these faults. The filter results should be analyzed for various equipment failures in an attempt to develop an internal diagnostics system which can identify the exact nature of the fault and plan an alternative optimal backup operating mode to continue the planned mission.

The operation of the autopilot developed here should be tested on the NPS AUV II in the NPS swimming pool to verify the operation of the three independent sliding mode controllers. The improved dead reckoning navigation system should be tested to verify the predicted position of the vehicle to the actual position through an independent measurement.

APPENDIX A   SENSOR NOISE CHARACTERISTICS

SENSOR SIGNAL	STANDARD DEVIATION	VARIANCE
SPEED (u)	0.0273	7.426×10^{-4}
ROLL RATE (p)	0.0050	2.474×10^{-5}
PITCH RATE (q)	0.0050	2.538×10^{-5}
YAW RATE (r)	0.0023	5.375×10^{-6}
ROLL ANGLE (ϕ)	0.0035	1.127×10^{-5}
PITCH ANGLE (θ)	0.0017	3.045×10^{-6}
YAW ANGLE (ψ)	0.0004	2.012×10^{-7}
DEPTH (Z)	0.0025	6.068×10^{-6}

APPENDIX B   REFINED HYDRODYNAMIC COEFFICIENTS

Coefficient	Value	Coefficient	Value
X_{rr}	-0.00753	M_q	-0.01530
X_u	-0.00282	M_w	0.0
X_{vv}	-0.01743	$M_{\delta s}$	$-0.377*L*Z_{\delta s}$
$X_{\delta s \delta s}$	-0.01018	$M_{\delta b}$	$0.283*L*Z_{\delta b}$
$X_{\delta b \delta b}$	-0.01018	N_r	-0.00047
$X_{\delta r \delta r}$	-0.01018	N_v	-0.00178
X_{prop} (C_{po})	0.00778	N_r	-0.00390
Y_r	-0.00178	N_v	0.0
Y_v	-0.03430	$N_{\delta rs}$	$-0.377*L*Y_{\delta rs}$
Y_r	0.0	$N_{\delta rb}$	$0.283*L*Y_{\delta rb}$
Y_v	-0.10700	I_x (ft^4)	2.7
$Y_{\delta rs}$	0.01180	I_y (ft^4)	42.0
$Y_{\delta rb}$	0.01180	I_z (ft^4)	45.0
Z_q	-0.00253	X_{rs}	$-0.377*L$
Z_w	-0.09340	X_{rb}	$0.283*L$
Z_q	0.0	Weight (lbs)	435
Z_w	-0.78440	Length (ft)	7.3
$Z_{\delta s}$	-0.02110	ρ (slugs/ft^3)	1.94
$Z_{\delta b}$	-0.02110	X_G	0.0104
K_p	-0.00024	Z_G	0.0892
K_p	-0.00540	X_B	0.0104
M_q	-0.00625	C_{py}	0.5
M_w	-0.00253	C_{pz}	0.6

REFERENCES

Abkowitz,M.A., 1969, "Stability and Motion Control of Ocean Vehicles",M.I.T. Press.

Abkowitz,M.A., 1980, "Measurement of Hydrodynamic Characteristics from Ship Maneuvering Trials by System Identification", SNAME Transactions, Vol. 88, pp 283 - 318.

Astrom,K.J., Wittenmark,B., 1990, (2nd Ed), "Computer Controlled Systems Theory and Design", Prentice Hall, Englewood Cliffs, New Jersey.

Boncal, R.J., 1987, "A Study of Model Based Maneuvering Controls for Autonomous Underwater Vehicles," Master's Thesis, Naval Postgraduate School, Monterey, California, December.

DeBenito, C.D., 1990, "On-Board Real Time Failure Detection and Diagnosis of Automotive Systems", Trans. ASME Journal of Dynamic Systems, Measurement and Control, Vol.112, No.4, December, pp 769-773.

Dietz, W.E., Keich, E.L., Ali, M., 1989, "Jet and Rocket Engine Fault Diagonistics in Real Time", Journal of Neural Network Computing, Vol. 1, No. 1.

Dobeck,G.J.,Watkinson,K.W.,Freeman,E.H., 1982 "Navigation, Guidance, and Control of an Autonomous 30-Foot Model Submarine" Report No NCSC TR 370-82, Naval Coastal Systems Center, Panama City, Florida.

Fossen, T.I., 1991, "Nonlinear Modeling and Control of Underwater Vehicles", Dr. Ing. Thesis, Norwegian Institute of Technology, Trondheim.

Gertler, J., 1986, "Failure Detection and Isolation in Complex Process Plants - A Survey", IFAC Symposium on Microcomputer Applications in Process Control, Istanbul, Turkey.

Gertler,M., Hagen,G.R., 1967, "Standard Equations of Motion For Submarine Simulations", NSRDC Report No. 2510.

Gelb,A.,(Ed), 1988, "Applied Optimal Estimation",MIT Press, Cambridge, Massachusetts, (Original Printing 1974, 10th Printing 1988, ISBN 0-262-57048-3.

Good, M.R., 1989, "Design and Construction of the Second Generation AUV," Master's Thesis, Naval Postgraduate School, Monterey, California, December.

Healey, A.J., Good, M., 1992, "The NPS AUV II Autonomous Underwater Vehicle Testbed: Design and Experimental Verification" ASNE <u>Naval Engineers Journal</u>.

Healey, A.J., 1992, "Model Based Maneuvering Controls for Autonomous Underwater Vehicles" <u>ASME Transactions Journal of Dynamic Systems Measurement and Control</u>.

Himmelblau, D.M., 1978, "Fault Detection and Diagnostics in Chemical and Petrochemical Processes", Elsevier Scientific Publishing Company, New York.

Isermann, R., 1984, "Process Fault Detection based on Modeling and Estimation Methods", <u>Automatica</u>, Vol. 20, No. 4, pp 387-404.

Humphries, D., 1981, "Dynamics and Hydrodynamics of Ocean Vehicles", <u>IEEE OCEANS '81 Conference Proceedings</u> Vol. 1.,pp 88-91.

Lewis, D.J.,Lipscomb, J.M., Thompson, P.G., 1984, "The Simulation of Remotely Operated Underwater Vehicles", <u>Proceedings of ROV '84</u>, The Marine Technology Society, San Diego, California. pp 245-252.

Lewis, E.W. (Ed), 1989, "Principles of Naval Architecture", ISBN No. 0-939773-02-3, SNAME,

Lienard, D., "Multivariable Sliding Mode Control for AUV Autopilots," Engineer's Thesis, Naval Postgraduate School, Monterey, California, June 1990.

Slotine, J.J.E., Li, W., 1987, "Adaptive Manipulator Control. A Case Study", <u>Proceedings of 1987 IEEE Conference on Robotics and Automation</u>, Raleigh, North Carolina, pp 1392-1400.

Smith, N.S., Crane, J.W., and Summey, D.C., 1978, "SDV Simulator Hydrodynamic Coefficients", <u>NCSC Report No. TM-231-78</u>.

Warner, D.C., 1991 "Design, Simulation, and Experimental Verification of a Computer Model and Enhanced Position Estimator for the NPS AUV II," Engineer's Thesis, Naval Postgraduate School, Monterey, California, December.

Wilsky, A.S., 1976, "A Survey of Design Methods for Failure Detection in Dynamic Systems", <u>Automatica</u>, Vol. 12, pp 601-611

Yoerger, D.R., Slotine, J.J.E., 1985 "Robust Trajectory Control of Underwater Vehicles", _IEEE Journal of Oceanic Engineering_, Vol. 10, No. 4, October. pp 465-470.

Yoerger, D.R., Neuman, J.B., Slotine, J.J.E., 1986, "Supervisory Control Systems for the JASON ROV", _IEEE Journal of Oceanic Engineering_, Vol. 11, No. 3, pp 392-400

Yoerger, D.R., Cooke, J.G., Slotine, J.J.E., 1991, "The Influence of Thruster Dynamics on Underwater Vehicle Behavior and Their Incorporation into Control System Design", _IEEE Journal of Oceanic Engineering_, Vol. 15, No. 3, pp 167-178.

Young, D.B., 1969, "Model Investigation of the Stability and Control Characteristics of the Contract Design for the Deep Submergence Rescue Vehicle (DSRV)", _Report No. 3030. David Taylor Research Center_, Bethesda, Maryland.

INITIAL DISTRIBUTION LIST

No. of Copies

1. Defense Technical Information Center   2
   Cameron Station
   Alexandria, Virginia 22304-6145

2. Library, Code 52   2
   Naval Postgraduate School
   Monterey, California, 93943-5002

3. Dr. A.J. Healey, Code ME   1
   AUV Project
   Department of Mechanical Engineering
   Naval Postgraduate School
   Monterey, California 93940

4. Prof. Fotis Papoulias, Code ME/Pa   1
   Department of Mechanical Engineering
   Naval Postgraduate School
   Monterey, California 93940

5. Fredric G. Bahrke   1
   579 B Wilkes Lane
   Monterey, California 93940

6. Fred Concillieri   1
   Naval Underwater Systems Center
   Newport, Rhode Island 02841-5047

7. Robert Wilson   1
   Head, Systems Engineering Branch
   David Taylor Research Center
   Carderock, Bethesda, Maryland 20084-5000

8. Dan Steiger, Marine Systems Group   1
   Naval Research Laboratory
   Washington, D.C. 20032

9. Mr. Kirk Dye   1
   Naval Coastal Systems Center
   Panama City, Florida 32407-5000

160

10. Technical Library   1
    Naval Surface Warfare Center
    Silver Spring, Maryland 20901

11. Radm. Evans, Code SEA-92   1
    Naval Sea Systems Command
    Washington, D.C. 20362

12. NPS Naval Engineering   1
    Code 34
    Monterey, California 93943-5100